IMAGING OF BL LAC OBJECTS

A THESIS SUBMITTED TO THE

UNIVERSITY OF OXFORD

IN PARTIAL FULFILLMENT OF THE

REQUIREMENTS FOR THE DEGREE OF

DOCTOR OF PHILOSOPHY

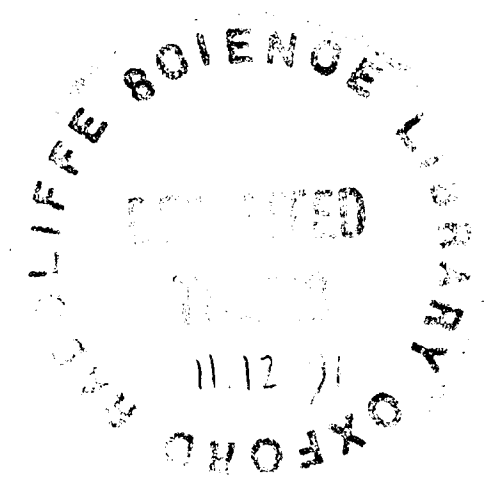

by

Roberto G. Abraham

Wolfson College

September 1991

Table of Contents

Abstract

The investigation of the host galaxies of BL Lac objects (BL Lacs) is a promising new field made practical in recent years by advances in detector technology and improved telescope siting. By better understanding the nature of these host galaxies we can test the standard beaming and lensing models for BL Lacs.

This thesis describes the techniques that we have developed for studying the host galaxies of BL Lac objects, and presents the results of a survey of BL Lac host galaxies that we have undertaken with the 4.2m William Herschel Telescope. This survey successfully resolved many new host galaxies, determined the morphology of three BL Lac host galaxies for the first time, and confirmed the morphology of an additional three objects. One BL Lac object, PKS1413+135, displayed a number of surprising properties, and was consequently studied in greater detail at multiple wavelengths. These observations are also presented in this thesis. We conclude with a description of Monte-Carlo simulations that we have undertaken in order to better determine the uncertainty in the results from our survey, and to assess the promise of future telescope/instrumentation combinations for host galaxy imaging.

CHAPTER 1

BL LACERTAE OBJECTS

INTRODUCTION

The purpose of this chapter is to describe the general properties of BL Lacertae objects (BL Lacs), and to present the models currently being put forward to explain them. Section 1.1 outlines the important observations, and contrasts the properties of BL Lacs with those of other Active Galactic Nuclei (AGN). Section 1.2 presents the physical problems that conventional models for AGN encounter when extrapolated to explain the behaviour of BL Lacs. Section 1.3 describes how some of these problems are mitigated by simple beaming models for these objects, and Section 1.4 describes how these beaming models can be expanded upon to explain the unusual redshift distribution of BL Lacs. Section 1.5 outlines the selection effects inherent in obtaining samples of BL Lacs. Section 1.6 describes what little we know about the host galaxies of BL Lac objects, and illustrates how host galaxy imaging surveys such as the one described in this thesis can play an important role in testing models for BL Lacs. Section 1.7 concludes with an outline of this thesis.

1.1 CANONICAL PROPERTIES OF BL LACS

Recent years have seen important progress in our understanding of BL Lac objects. Up until 1968, BL Lacertae was believed to be a fairly commonplace variable star. In the intervening years we have learned that BL Lacs and similar objects are among the most exotic of extragalactic objects, exhibiting many properties characteristic of radio-loud quasars (compact radio core, extended diffuse radio emission, starlike appearance optically), while remaining intriguingly different, with very strong multiwaveband variability in both flux and polarization and a lack of emission lines. This "feast or famine" twist to their behaviour often stretches the standard physical models for Active Galactic Nuclei (AGN) to their limits. They are, however, comparatively rare, with only 100 or so known to exist, and their redshift distribution is strongly skewed towards lower redshifts ($z \leq 0.2$) relative to the quasar distribution.

1.1.1 BL Lac spectra

Figure 1.1 (taken from the review in Woltjer [1990]) illustrates typical optical spectra for a quasar and two Seyfert galaxies. By way of contrast, Figure 1.2 illustrates the virtually featureless spectrum of a typical BL Lac (in this case B2 1308+326). Few BL Lacs have known redshifts: in the standard Burbidge and Hewitt [1989] compendium of BL Lac objects, only 36 out of 85 objects possessed published redshifts. Any detected lines are typically weak absorption or narrow emission lines originating in the host galaxy (Filippenko *et al.* [1986]; Stickel *et al.* [1989, 1990]; Falomo [1989,1991]), although very weak broad-line features are detected in a few objects during weak continuum states (eg. Falomo *et al.* [1989]). The featureless optical/IR continuum of most BL Lac objects is consistent with a power-law of spectral index $0.5 < \alpha < 2.5$, except for the nearest objects such as PKS0521-365 (Falomo *et al.* [1989]) where distortions in the power law

consistent with host galaxy contributions are sometimes found. At higher redshifts, there is little evidence for the bumps or other distortions of the continuum often seen in quasars (and usually attributed to dust emission). The infrared continuum typically joins directly onto the radio continuum, which eventually turns over at a frequency consistent with synchrotron self-absorption. All of these points are illustrated in the multiwaveband spectrum of the BL Lac PKS0735+178, shown in Figure 1.3 (taken from Madejski and Schwartz [1989]).

The characteristic shape of the spectrum strongly implies that the entire radio through infrared spectrum is synchrotron in origin (Woltjer [1990]). The most successful models for this emission (Blandford and Koñigl [1979]; Marscher and Gear [1985]) postulate that the synchrotron source is a shocked relativistic jet propagating at a small angle to the observer's the line of sight. The jet motion is required in order to explain the rapid variability in both flux and polarization seen in BL Lacs (these observations and the beaming model are both discussed further below). The limited X-ray information to date suggests that BL Lacs often (but certainly not always, as seen in Figure 1.3) exhibit a significant self-compton component in the X-ray spectrum. In an important observation, Worrall [1989] has noted that BL Lacs exhibit a mean soft X-ray spectral index twice as steep as that of Optically Violently Variable quasars (OVVs) and High Polarization Quasars (HPQs), suggesting that the BL Lacs are physically distinct from the OVV/HPQs (despite the fact that they are often grouped together with the OVVs and HPQs in the so-called "Blazar" category of AGN). This is illustrated in Figure 1.4. Additional support for the distinction between OVV/HPQs and BL Lacs is given in Section 1.1.4.

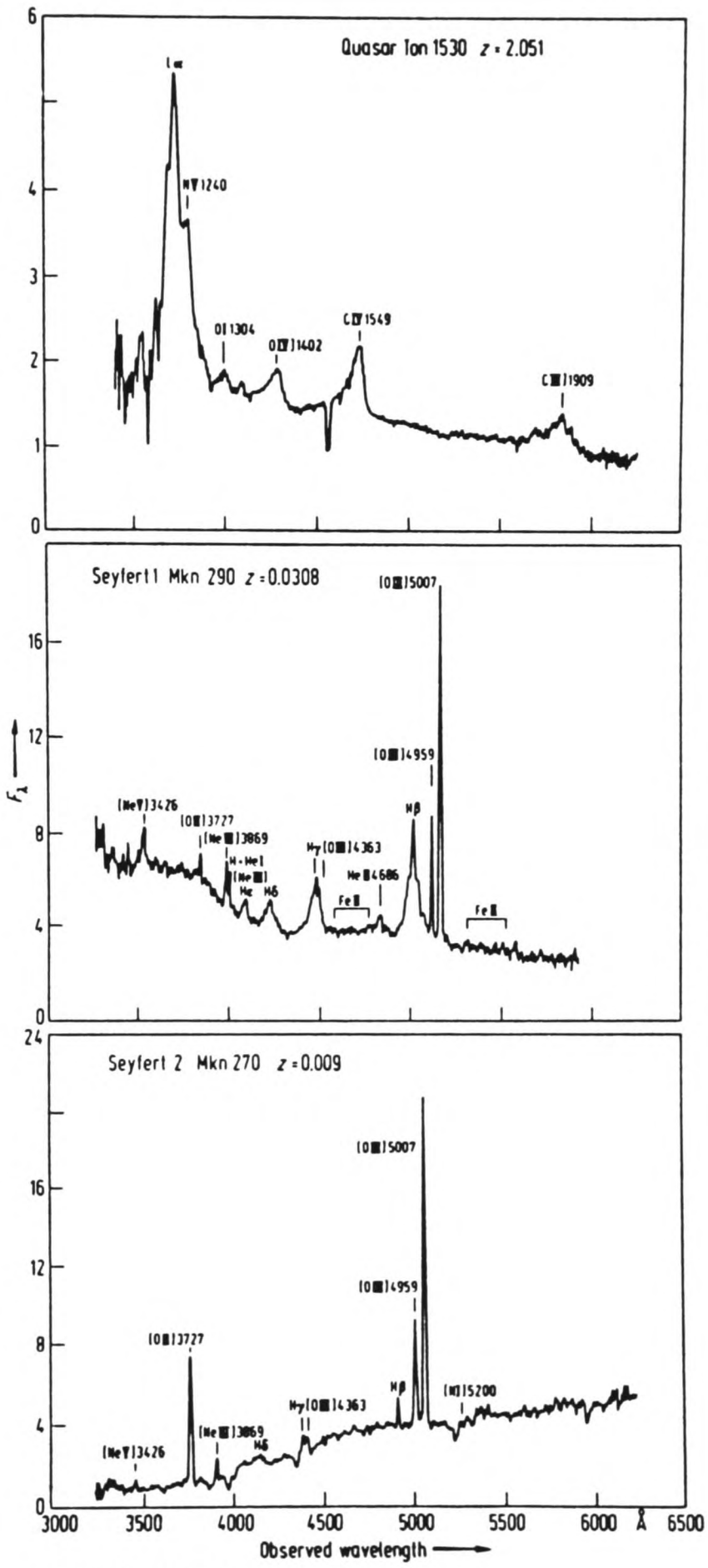

Fig. 1. Spectra of three AGNs

Figure 1.1 Typical AGN spectra (taken from from Blandford, Netzer, and Woltjer [1990]).

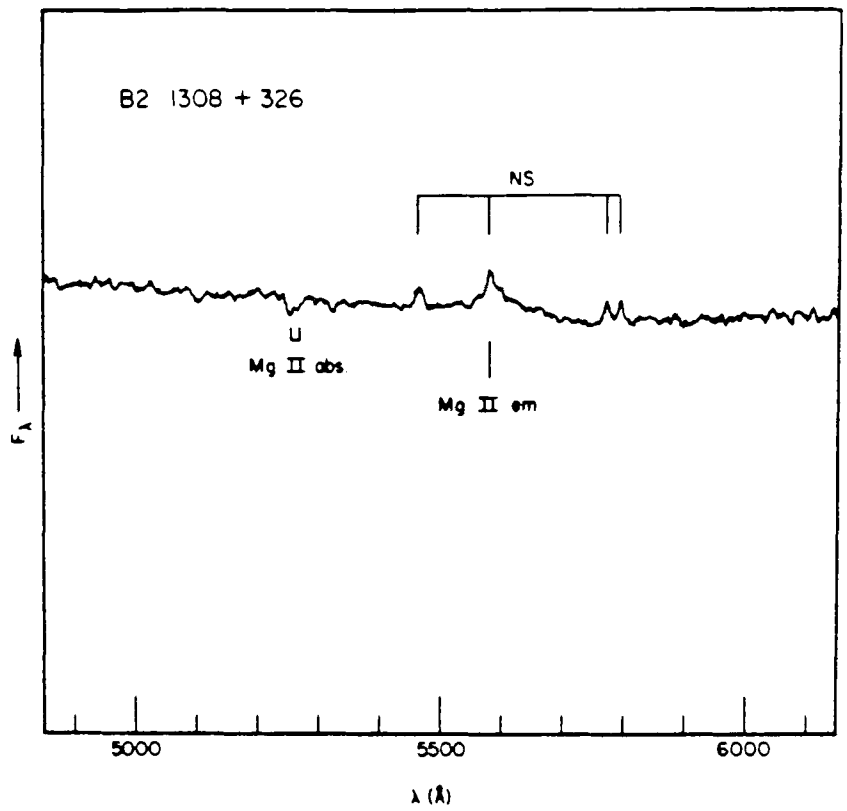

Fig. 1 - A portion of the spectrum of B2 1308+326. NS marks the positions of partially uncancelled night-sky lines. The lower boarder represents the zero flux level.

Figure 1.2 Spectrum of B2 1308+326. Taken from Miller *et al.* [1978].

1.1.2 Variability and polarization

BL Lacs exhibit variability on timescales from hours to months (in this sense they resemble the OVV/HPQ quasars). The standard light-crossing time arguments would therefore suggest that the energy source for BL Lacs is at most light-hours in size, strongly constraining physical mechanisms for these objects.

There is some evidence for a decrease in variability timescale with increasing frequency, with a variability timescale of hours common in the X-ray regime (McHardy [1990]; Tagliaferri [1989]), days or weeks in the optical regime, and months in the radio. Even at optical wavelengths, however, variability on a timescale of hours is not unknown, as shown in Figure 1.5 (taken from Wagner [1991]). Coordinated multiwave-

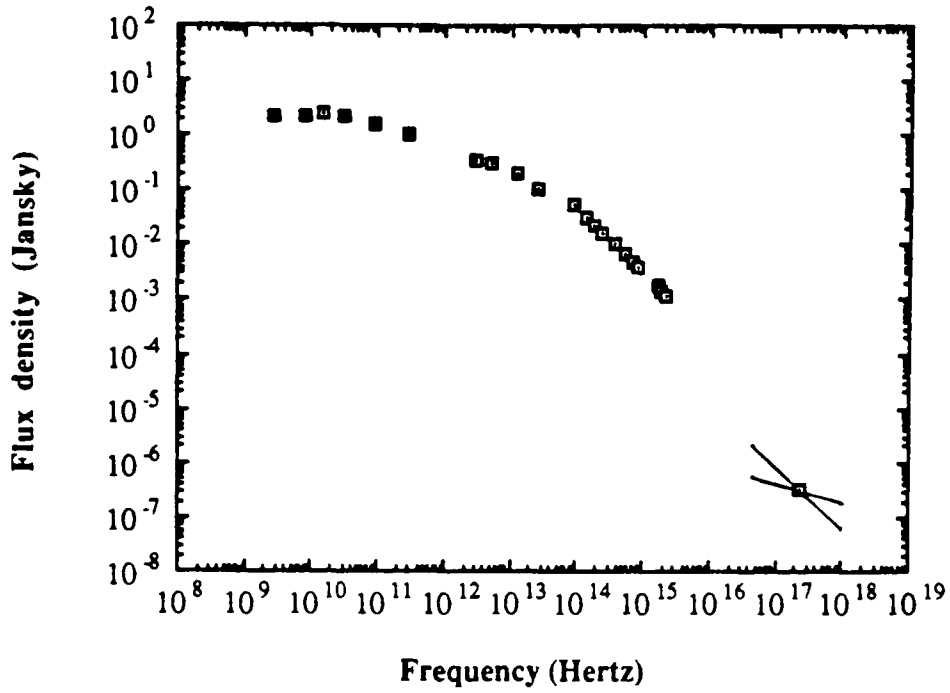

Figure 5. Overall electromagnetic spectrum of PKS 0735+178. The IRAS data are from Impey and Neugebauer (1988); X-ray spectrum is from Madejski and Schwartz (1988). Remaining data are from Bregman *et al.* (1984).

Figure 1.3 Multiwaveband spectrum of PKS0735+178, taken from Madejski and Schwartz [1989].

band studies (eg. Wagner [1991] and McHardy *et al.* [1990]) generally find correlated radio/infrared/optical variability with lags and dispersions consistent with the predictions of shocked synchrotron-emitting bent jet models (eg. Marscher and Gear [1985]; Marscher [1991]). BL Lacs exhibit substantial (typically 5-15%) optical/infrared and radio polarization, adding credence to this interpretation. Polarization variability timescales (in both amplitude and position angle) range from days to weeks in the optical (Angel and Stockman [1980]) to months in the radio (Hughes, Aller, and Aller [1985]).

1.1.3 Optical and radio morphology

BL Lacs are quasi-stellar at optical wavelengths, although many of the nearer examples exhibit definite "fuzz" associated with the presence of an underlying host galaxy.

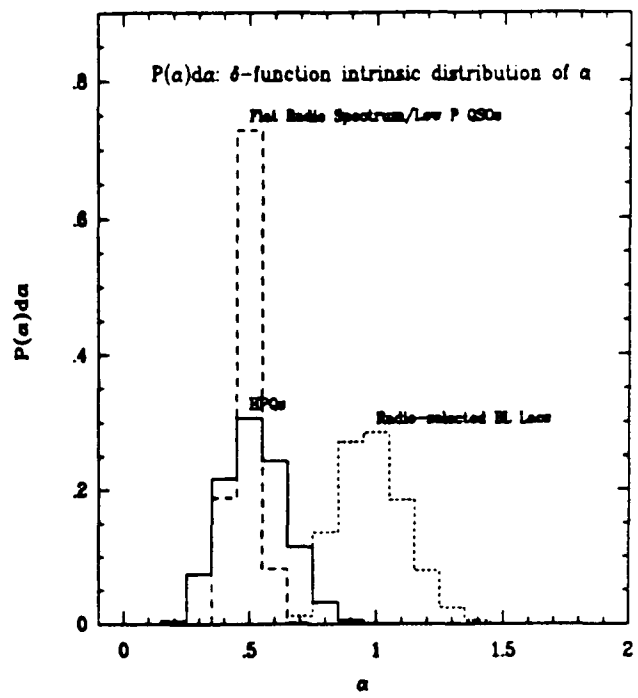

Figure 1: The likelihood of α for the special case of each sample having a delta-function intrinsic distribution of α. Note the separation of the BL Lac objects and the HPQs.

Figure 1.4 Distribution of X-ray spectral indices for OVV/HPQs and BL Lacs (taken from Worrall [1989]). Note that all objects (including OVV/HPQs) were radio selected.

The optical properties of these host galaxies are the central theme of this thesis, and will be discussed at greater length in section 1.6 below and in the following chapters.

Radio maps of BL Lacs invariably exhibit powerful, compact, flat-spectrum radio cores. Around half of the well-studied objects exhibit low level extended emission (eg. Ulvestad and Antonucci [1986]) on scales up to hundreds of kiloparsecs. There is a wide range in the morphology of this extended emission, but it is generally consistent with weak lobe emission seen "head on" along the beaming axis, and it is in this context that we will have more to say about extended emission in section 1.4 below (on unified schemes). Arcsecond scale radio jets are rarely seen, although VLBI observations of one-sided milliarcsecond jets are not unusual (eg. Eckart *et al.* [1987]). Superluminal motion

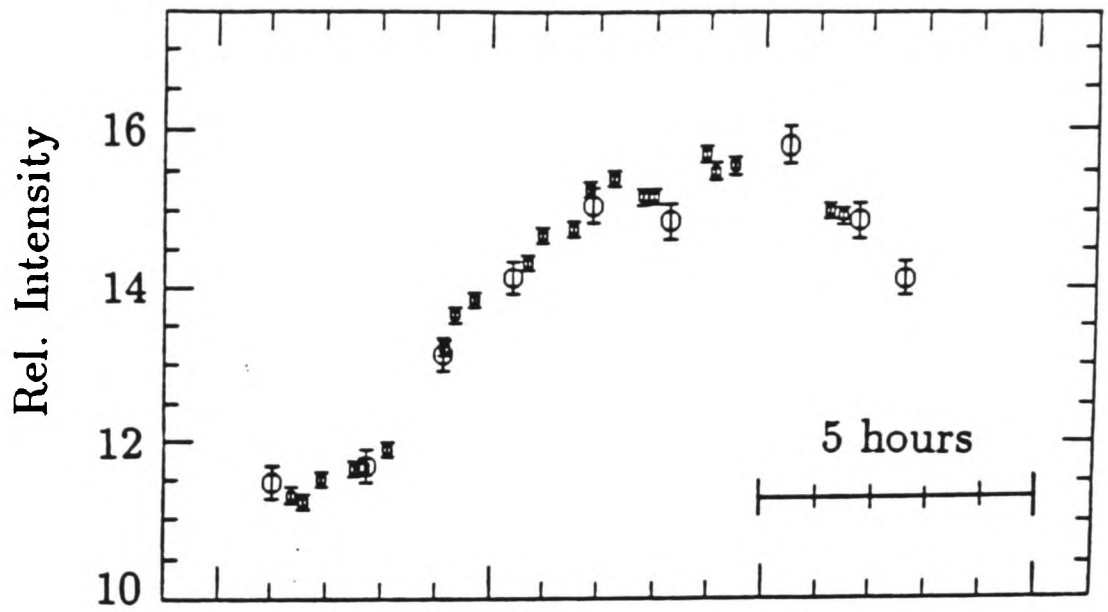

Fig. 1. Comparison of the measurements of 0716+714 performed at the two telescopes. Circles represent measurements obtained with the 0.7m telescope at Heidelberg - Kõnigstuhl (mean exposure-time 15 min), boxes indicate measurements with the 2.2 m telescope at Calar Alto (exposure-time about 100 sec). Both data sets were normalized to the same reference star such that the mean ratio during the whole campaign equals unity. During this particular night of J.D. 2447927, the 40 % change in flux is well covered by both telescopes. The lightcurves agree with another within the errors, confirming the reality of even low-amplitude modulations on top of the all-over behaviour.

Figure 1.5 Time series illustrating optical hours-timescale variability in the BL Lac 0716+714. Taken from Wagner [1991].

has been detected in at least five BL Lacs (Zensus [1989]; McHardy *et al.* [1990]). Zensus [1989] suggests that there is a trend for relativistic jets in BL Lacs to be propagating at lower apparent speeds ($\sim 4c$) than is the case for quasars, and for BL Lac radio cores to be more compact than is the case for quasars.

1.1.4 Redshift distribution

The redshift distribution for a complete sample of radio-selected BL Lac objects in the Kuhr *et al.* [1981] 1 Jy catalogue is shown in Figure 1.6 below (taken from Browne [1989]). For comparison, this figure also illustrates corresponding distributions for flat-spectrum quasars in the same catalogue, and for Fanaroff and Riley type I radio galaxies from the 3C catalogue. It is immediately apparent that the BL Lac redshift distribution is strongly skewed towards low redshifts, and is nothing like the distribution for the flat spectrum quasars. Indeed, around 25% of the BL Lacs in the catalogue are in the $0.0 < z < 0.1$ bin, while *none* of the flat-spectrum quasars are in this bin. The fact that the OVV/HPQ quasars follow the flat-spectrum quasar redshift distribution (they are included in this group in the figure) lends added evidence to the conclusion that BL Lacs are distinct from the OVV and HPQ quasars.

1.2 THE FAILURE OF SYNCHROTRON MODELS

The characteristic power-law spectral slope and high polarized flux from BL Lacs strongly suggests that synchrotron mechanisms are responsible for the observed flux (an excellent review of synchrotron mechanisms in this context appears in Hughes and Miller [1991]). There is, however, a severe problem (first described in Hoyle, Burbidge, and Sargent [1966] for quasars) which occurs when simple synchrotron models are applied to rapidly varying, highly luminous sources, such as BL Lacs. The problem, which has come to be known as the "Compton Catastrophe", is as follows: in any synchrotron source, there will be a self-compton contribution from the emitted low-energy photons being scattered up to X-ray energies by the relativistic synchrotron electrons. As the en-

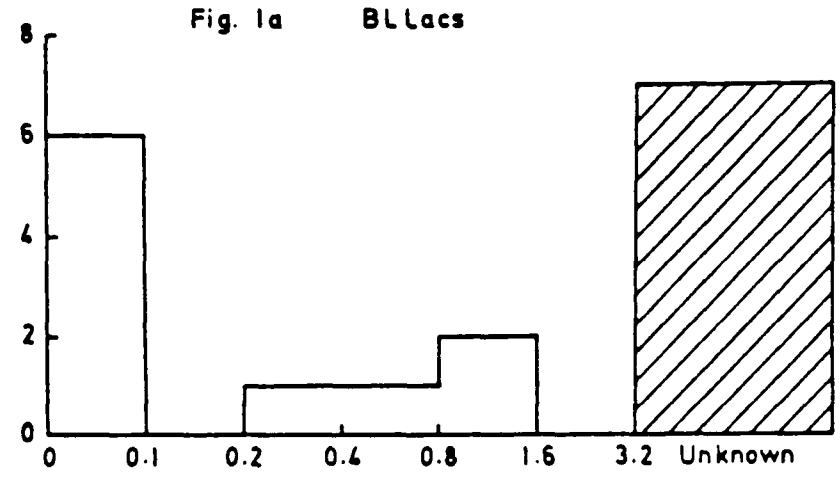

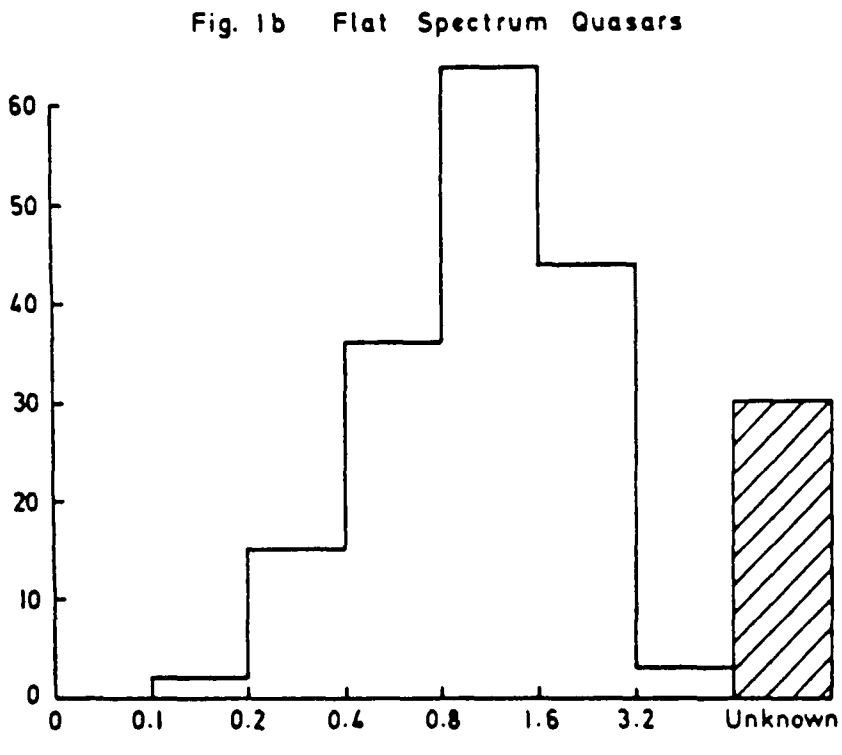

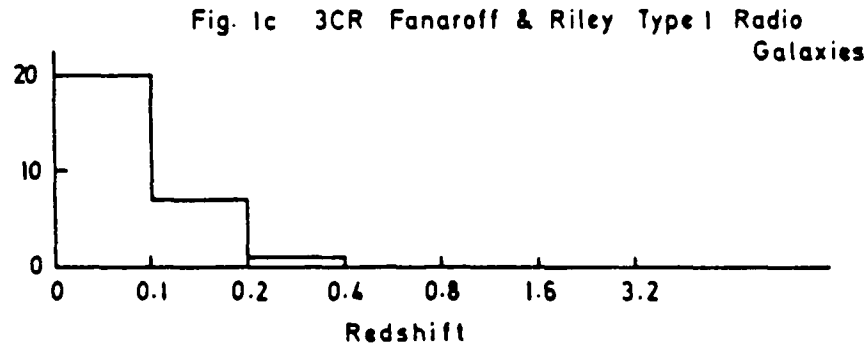

Figure 1. Redshift distributions for a) BL Lac objects from the Kuhr et al. 1 Jy catalogue, b) flat radio spectrum quasars from the Kuhr et al. 1 Jy catalogue and c) low luminosity (Fanaroff & Riley type) radio galaxies from 3CR.

Figure 1.6 Redshift distributions (taken from Browne [1989]) of BL Lacs, flat spectrum quasars, and FR I radio galaxies.

ergy density of the radiation field in the synchrotron source is increased, this self-compton contribution becomes increasingly dominant, until eventually the scattering electrons lose so much energy that the synchrotron mechanism shuts down. There is therefore a maximum energy density for synchrotron sources, corresponding to a maximum brightness temperature (cf. Hughes and Miller [1991]) around 10^{12} K. (The brightness temperature is defined as the temperature of a black body which, at a particular frequency, would produce the observed flux density.)

The small size of the energy generating region in BL Lacs (as implied by their rapid variability), along with their intrinsically very high luminosity, requires that an enormous amount of energy be generated in a tiny (several A.U.) region in these objects. One finds that the maximum brightness temperature allowed by synchrotron mechanisms is exceeded by several orders of magnitude in many BL Lacs. We are left, then, in a difficult situation: the spectral properties of BL Lacs are consistent with those of synchrotron sources, except for the basic fact that synchrotron sources cannot exist at the required power density levels.

For the solution to this dilemma we take advantage of a relativistic sleight of hand, in a solution that most would dismiss as unbelievably contrived were it not for the fact that relativistic jets are seen by radio astronomers every day.

1.3 SIMPLE BEAMING MODELS

1.3.1 Beaming models

Beaming models postulate that what we observe in a BL Lac is a relativistic jet being oriented at a close angle θ to the line of sight (Blandford and Rees [1978]), according

to the geometry illustrated in Figure 1.7. If we denote rest-frame (source) quantities by primed symbols, and observer-frame quantities by unprimed symbols, then the following relativistic transformations for the time interval Δt, frequency ν, transverse speed (in units of of c) β, and spectral intensity I apply:

$$\Delta t = \delta^{-1} \Delta t' \qquad [1.1]$$

$$\nu = \delta \nu' \qquad [1.2]$$

$$\beta_{\mathbf{apparent}} = \beta \sin\theta / (1 - \beta \cos\theta) \qquad [1.3]$$

$$I_\nu(\nu) = \delta^3 I'_{\nu'}(\nu') \qquad [1.4]$$

where we adopt the standard notation for the Doppler factor δ and the Lorentz factor γ:

$$\delta = \gamma^{-1}(1 - \beta \cos\theta)^{-1} \qquad [1.5]$$

$$\gamma = 1/\sqrt{1 - \beta^2} \qquad [1.6]$$

According to this model, then, not only the apparent superluminal speed of VLBI knots in jets, but also the observed rapid variability (and hence small calculated size) and enormous source luminosity of BL Lacs are artifacts of a relativistic jet observed at a small angle to the beaming axis. In the source frame the brightness temperature limit implied by the Compton Catastrophe is not exceeded. While admittedly an elegant argument in its own right, we emphasize that what makes the above reasoning compelling is the observational VLBI evidence for the existence of relativistic jets. Given the existence of jets, it seems natural to suppose that at least some of these may be observed with the required geometry, particularly in light of the favorable selection effects provided by the greatly increased flux for objects in this geometry.

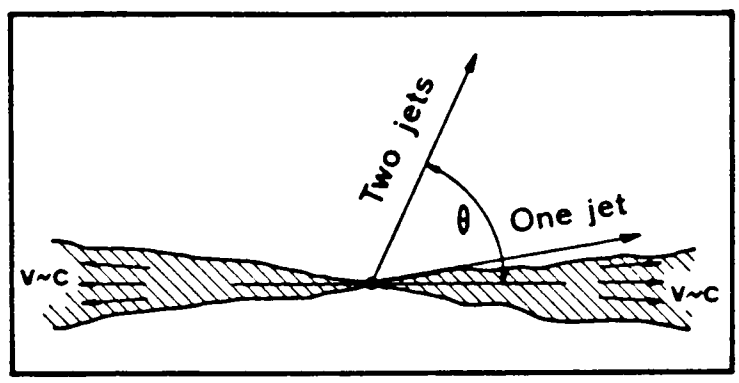

Fig. 5.2. Beaming of jets due to relativistic aberration. When the source is observed from a small angle θ, only one bright jet is seen. Two, comparably bright jets can be seen when $\theta \sim \pi/2$.

Figure 1.7 The beaming geometry described in the text. Taken from Blandford [1991].

1.4 BL LAC REDSHIFT DISTRIBUTIONS

While beaming models clearly simplify the energetic problems inherent in synchrotron models for BL Lacs, it is important to realise that in the simple beaming model we have so far presented for BL Lacs, their strange redshift distribution remains a problem. Two solutions to this problem have appeared in the literature: the beaming model of Browne [1983], and the lensing model of Ostriker and Vietri [1985,1990].

1.4.1 FR I Radio Galaxies and BL Lacs

In an important paper, Browne [1983] has argued that the anomalous redshift dis-

tribution of BL Lac objects would be explained if their parent population is made up of Fanaroff and Riley type I radio galaxies. Fanaroff and Riley type I (FR I) radio galaxies are comparatively weak radio sources ($P_{178\mathrm{MHz}} < 5 \times 10^2 5\mathrm{W\ Hz^{-1}}$), with edge darkened large scale radio structures, and often possess two sided jets that start off one sided and develop the second structure after about 10% of the length of the jet (Muxlow and Garrington [1991]). The host galaxies of FR I radio galaxies tend to be optically brighter and significantly more clustered than the hosts of FR II radio galaxies (Owen and Laing [1989], Prestage and Peacock [1988], Lilly and Prestage [1987]). Most importantly, the FR I radio galaxies have been shown to be cosmologically non-evolving (Wall, Pearson, and Longair [1980]), so associating them with the BL Lacs could account for the latter's unusual redshift distribution.

The redshift distribution of FR I radio galaxies is shown in Figure 1.6, and is in good agreement with the BL Lac redshift distribution shown in the same figure. The crucial test of this hypothesis is to look for agreement between the orientation independent properties of BL Lacs and those of FR I radio galaxies, and this comparison is made in the next two figures (taken from Ulrich [1989]). Figure 1.8 compares the intrinsic radio power in the extended components of the B2 bright sample of radio galaxies (mostly made up of FR Is) to the extended emission surrounding BL Lacs, and Figure 1.9 compares the few known BL Lac host galaxy absolute magnitudes (complete as of 1989) to the absolute magnitudes of the hosts from the B2 survey. The distribution of orientation independent properties of BL Lacs and FR I radio galaxies is clearly quite similar, in good agreement with the predictions of the Browne [1983] model.

A simple calculation of the space densities of nearby BL Lacs and FR I radio galaxies based upon the extended radio emission of the samples (Browne 1989) suggests that this beaming model is consistent with the population statistics provided that the average jet Lorentz factor γ is around 10. This is in reasonably good agreement with the

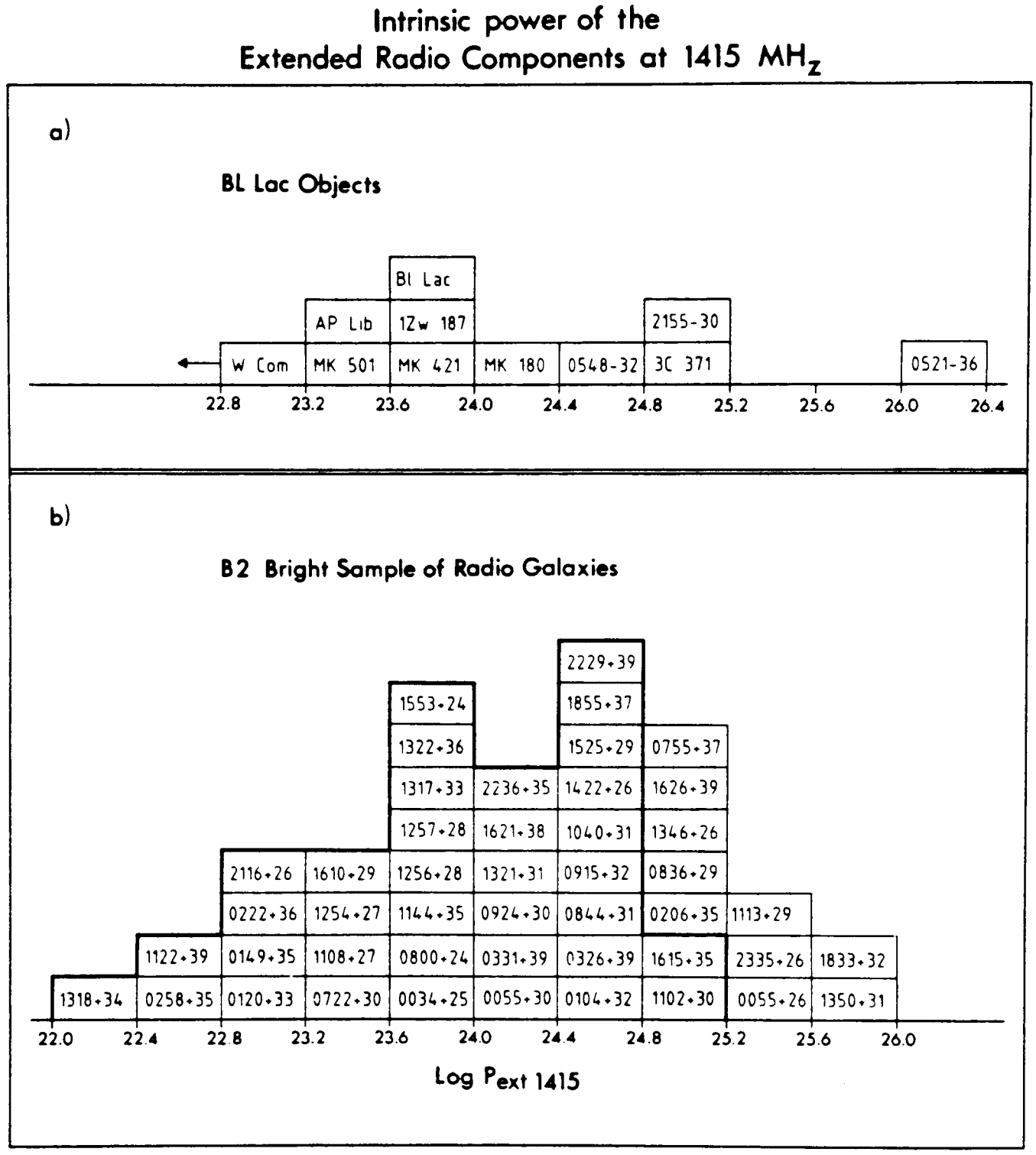

Figure 2 - The distribution of the absolute radio power of the extended radio components of BL Lac objects (top) and of the B2 bright sample of radio galaxies (bottom) (H=50, q_0=0.5). Frequency: 1.4 GHz. Thin line: the ten B2 radio galaxies with intrinsic radio power of the extended component larger than 10^{25} WHz^{-1}.

Figure 1.8 A comparison of the power in the extended radio components of BL Lacs with the extended radio components of objects in the B2 Bright Sample (taken from Ulrich [1989]).

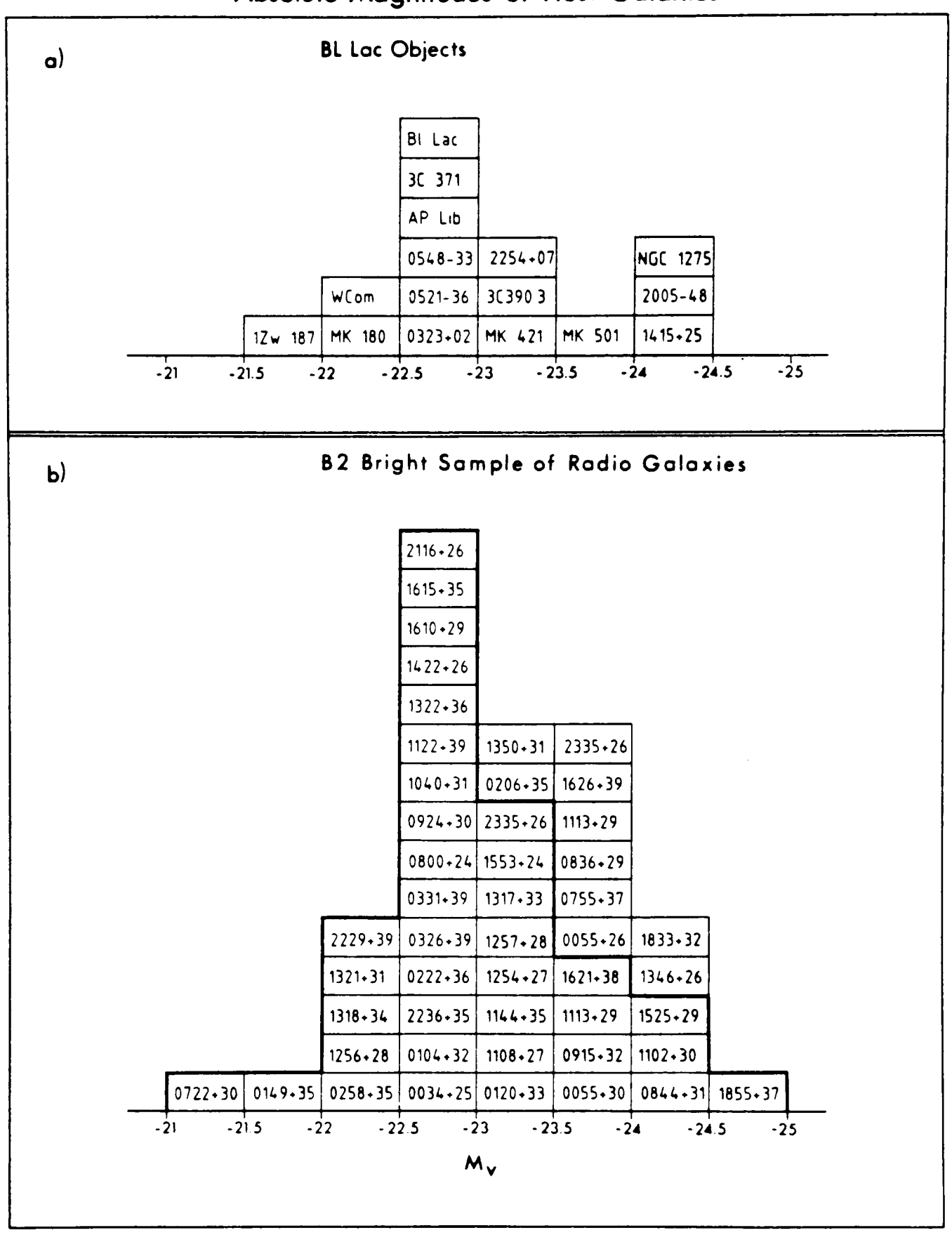

Figure 1 - a) top. The distribution of the absolute V magnitudes of the host galaxies in nearby BL Lac objects. b) bottom. The absolute V magnitudes of the radio galaxies in the B2 bright sample. Thin line: the ten B2 radio galaxies with intrinsic power of the extended radio component larger than 10^{25} WHz^{-1} (H=50, q_o=0.5).

Figure 1.9 A comparison of the absolute magnitudes of BL Lac hosts with the absolute magnitudes of galaxies from the B2 Bright Sample (taken from Ulrich [1989]).

$\gamma = 5$ required to boost the core power of radio galaxies to that of BL Lacs. Detailed calculations of the luminosity function of BL Lacs based upon radio, optical, and X-ray constraints have thus far proven inconclusive: adopting the FR I radio galaxies as the parent population of BL Lacs may (Padovani and Urry [1990,1991]; Morris *et al.* [1991]), or may not (Wolter *et al.* [1991]), be consistent with the strange redshift distribution exhibited by BL Lacs.

It is worth noting that the beaming model for BL Lacs described here bears similarities to, but is completely distinct from, other more ambitious unified scheme models (eg. Barthel [1990]; Orr and Browne [1982]) which attempt to unify a wider range of radio-loud AGN. The strange redshift distribution exhibited by BL Lacs requires that these objects be treated separately from other AGN in beaming models.

1.4.2 Gravitational lens models

Another popular model put forward to explain the redshift distribution of BL Lacs is the gravitational microlensing model of Ostriker and Vietri [1985,1990]. In this model, BL Lacs are distant ($z > 1$) OVV/HPQ quasars (which are themselves possibly beamed) being gravitationally microlensed by a nearby foreground galaxy. This model predicts three peaks in the redshift distribution of BL Lacs, one at low ($z \sim 0.1$) redshift (corresponding to the observed overdensity in nearby BL Lacs), and two at redshifts near the distant OVV/HPQ.

In addition to accounting for the local overdensity of BL Lacs, the model also accounts for their lack of emission lines, since the broad-line region is too big to be lensed. In addition, the model makes several testable predictions, the strongest of which are:

(1) Anomalous redshifts should sometimes be seen in bright BL Lac point sources (i.e. absorption or emission line redshifts in the core should sometimes be different from those detected from the image of the underlying lensing galaxy).

(2) The probability of microlensing increases as the fourth power of the velocity dispersion, so most lensing galaxies should be ellipticals.

(3) The BL Lac point source should not be centred on the image of the underlying lensing galaxy. The size of this predicted decentring should typically be several arcseconds for lensing galaxies at intermediate ($z \sim 0.2$) redshifts (Ostriker and Vietri 1985, Narayan and Schneider 1985). Testing this de-centring prediction is an important part of this thesis, and is described in the following chapters.

Ostriker and Vietri cite several examples of BL Lacs with apparently anomalous redshifts, the most compelling of which are AO 0235+164 and PKS0537-441. In a recent paper, however, Narayan and Schneider [1990] point out that in the microlensing model of Ostriker and Vietri both of these objects should be gravitationally macrolensed as well (with consequent multiple images of the central point source that are not seen in the observations), unless the lensing galaxies are extremely underdense. Furthermore, in Chapter 2 of this thesis we examine the basis upon which PKS0537-441 has been put forward as a lensing candidate (Stickel *et al.* [1991]), and suggest that the evidence for this is in fact very weak. Gear [1991] has also pointed out that multiwaveband monitoring of the the spectra of BL Lacs and OVV quasars implies that the continuum emitting regions of OVV quasars are much too large to be lensed by stars.

In a similar microlensing model, Nottale [1986] has suggested that the flux variability in BL Lacs can be explained by microlensing of distant AGN (a highly variable OVV/HPQ background source is not needed in this model as most of the variability is due to stochastic nature of the microlensing). The variability timescale (in seconds) given by this model is:

$$\tau = \frac{5 \cdot 10^{14}\mathrm{m}}{v_{\perp}} \sqrt{\frac{M}{M_{\odot}}} \qquad [1.7]$$

where $v_{\perp}$ is the transverse velocity of the microlensing star. It is difficult, if not impossi-

ble, to reconcile such a model with the observations, since the hours timescale variability seen in some BL Lacs implies transverse velocities near c for the lensing stars, even if they are of very low mass.

1.5 X-RAY VS. RADIO SELECTION EFFECTS

A major impediment to our understanding of BL Lacs is the paucity in the number of objects available for study. Until very recently the discovery rate for new BL Lac objects has not been keeping pace with the corresponding discovery rate for quasars. The discovery of larger numbers of BL Lacs would obviously hasten further progress in our understanding, but continuations of traditional search techniques (usually relying on radio selection by examining strong, high frequency radio sources and then looking for featureless optical spectra in optical counterparts) have led to the discovery of few additional objects. Polarization surveys have thus far proved fruitless (Jannuzi & Green [1989]). It has recently become clear, however, that X-ray selection techniques are highly efficient, and the application of these techniques has lead to an effective doubling in the number of known BL Lac objects in the last two years (Stocke *et al.* [1989], Maccacaro *et al.* [1989]). At some doubt, however, is the critical issue of whether the X-ray selected BL Lacs and the radio selected BL Lacs are drawn from the same population of objects.

X-ray selected BL Lacs appear to differ from radio selected BL Lacs in a number of ways (Figures 1.10 and 1.11). X-ray selected objects seem to be less variable, less polarized, have flatter overall spectra, and have larger starlight fractions than do radio selected BL Lacs (Maraschi *et al.* [1986]; Ghisellini *et al.* [1986]; Stocke *et al.* [1989]; Schwartz *et al.* [1989]). Authors differ in their assessments of the degree to which these

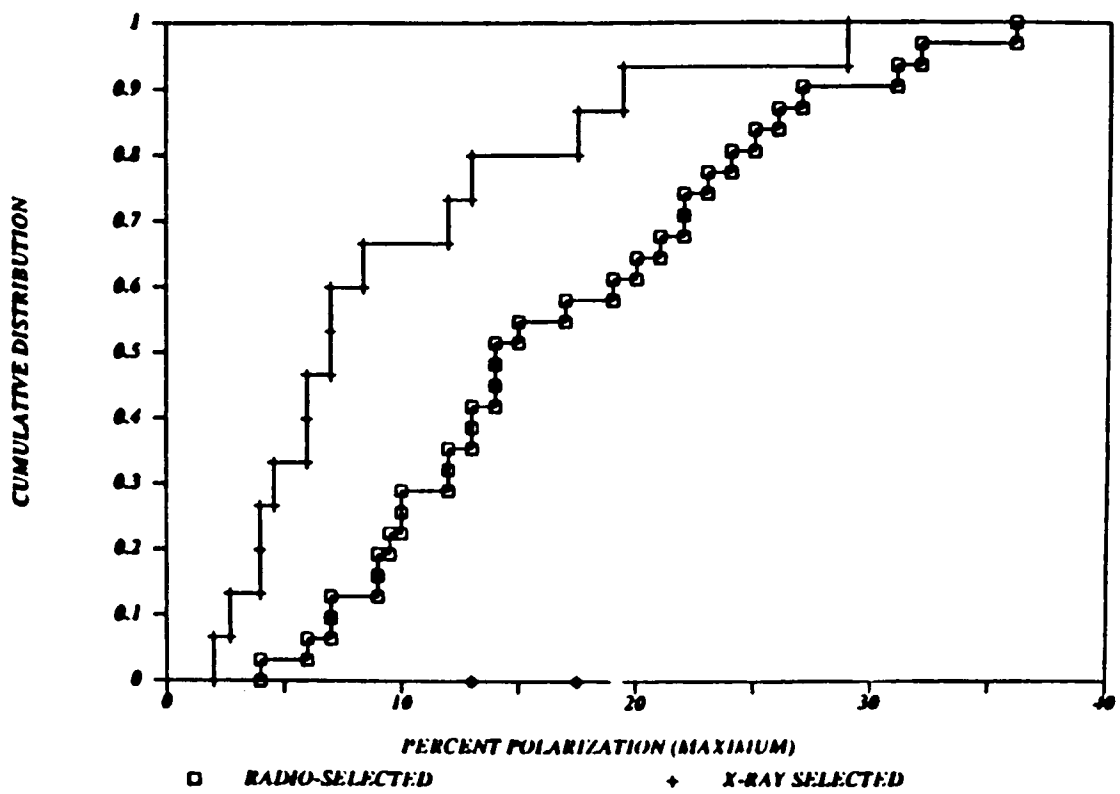

Figure 3 Estimated cumulative distribution functions for the maximum polarization observed from 31 radio selected BL Lacs (squares; Angel and Stockman 1980) and the 15 HEAO-1 X-ray selected BL Lacs (plus signs). There is only a 0.3% chance that the two observed distributions are drawn from the same parent population.

Figure 1.10 Comparison of maximum polarizations for samples of X-ray selected and radio-selected BL Lacs. Bear in mind that the radio selected objects have been much more heavily observed than their X-ray selected counterparts. Taken from Schwartz *et al.* [1989].

differences are indicative of different populations, as opposed to selection effects resulting from sampling a single parent population with a spread of properties, as suggested by similarities in the extended radio emission exhibited by both classes of objects (Polatidis [1989]). Discriminating between these two possibilities is critical if we hope to use the increased numbers of BL Lacs supplied by the X-ray selected objects in a meaningful way. A comparison of the types of hosts underlying X-ray and radio selected BL Lacs

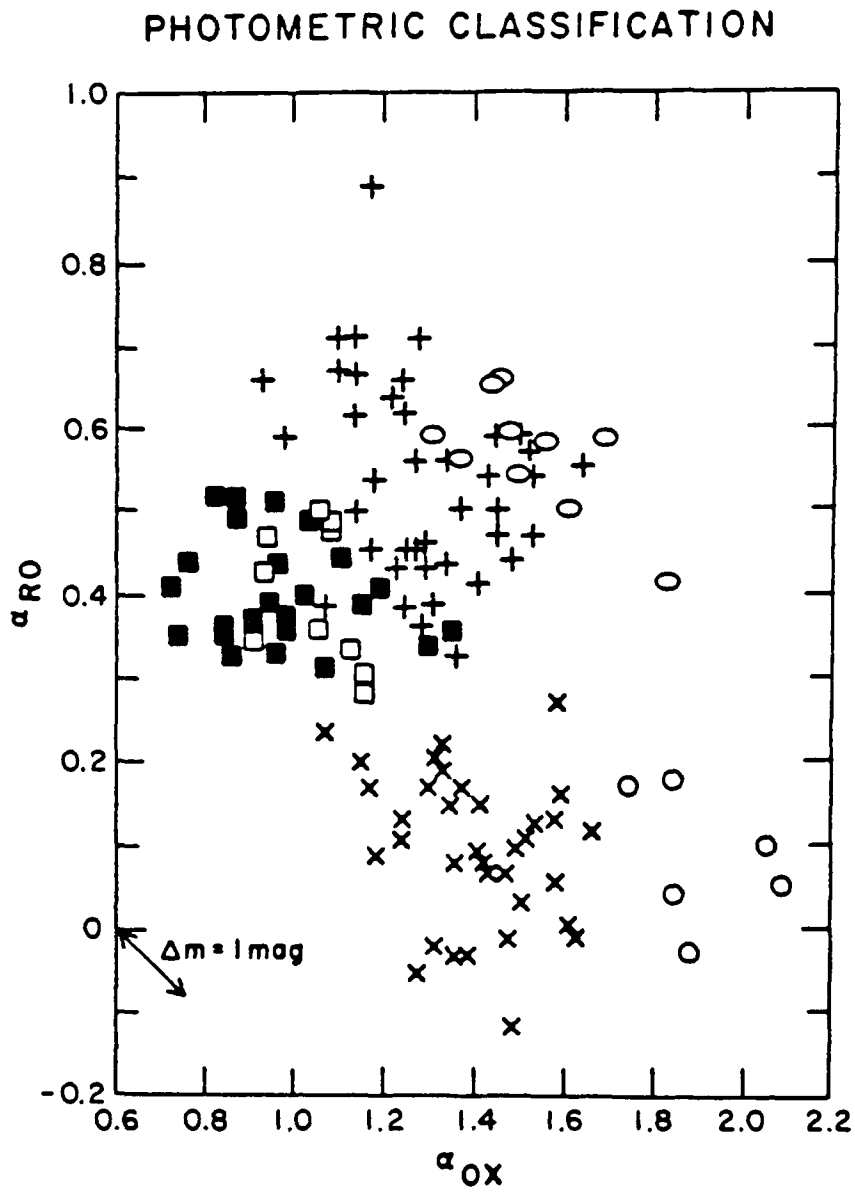

Figure 2: The overall energy distributions for several classes of active extragalactic object. The axes, α_{ox} and α_{ro}, are the two point optical-to-x-ray and radio-to-optical spectral indices (Stocke et al, 1985). The boxes are x-ray selected BL Lacs (EMSS + HEA01-A2; filled boxes $f_x > 10^{-12}$ ergs/s/cm^2; open boxes $f_x < 10^{-12}$); the ellipses are radio selected BL Lacs; the plus signs are x-ray selected radio-loud AGN, the crosses are x-ray selected radio-quiet AGN. The circles are the "normal" galaxies. For the radio-quiet AGN only those objects detected with the VLA ($f_r \geq$ 1mJy) are shown; approximately 275 more radio-quiet AGN have VLA upper limits of ~1 mJy, which place them in the same area of this Figure as the crosses.

Figure 1.11 Energy distributions for various classes of AGN. Taken from Stocke [1989].

would enable us to determine if the hosts come from the same population, and would go a long way towards clearing up the issue of whether the X-ray selected and radio selected BL Lacs are the same types of objects.

1.6 BL LAC HOST GALAXIES

Because host galaxy morphology (like extended radio emission) is independent of orientation, comparing the host galaxies of BL Lacs to those of the putative FR I parent population allows a strong test of beaming models. Similarly, the decentring of the continuum source from the image of the lensing galaxy in the Ostriker and Vietri lensing model is a directly testable property. Unfortunately, we know very little about the host galaxies of BL Lacs, and most of what we do know has already been summarised in Figure 1.8. The absolute magnitudes of BL Lacs are clearly rather similar to those of B2 Bright Sample radio galaxies given in Ulrich [1989] and reproduced in this figure, but what exactly are we comparing the BL Lac hosts to? It is clearly important to understand what sort of galaxies comprise the B2 Bright Sample.

The 48 B2 radio galaxies comprising the Bright Sample were chosen according to the following criteria (Fanti *et al.* 1973, Colla *et al.* [1975]):

(1) Bright apparent magnitude ($m_{\mathrm{Zwicky}} > 15.4.$).

(2) Absolute radio luminosity at 408 MHz > 0.25 Jy.

(3) Elliptical or S0 morphology (classification was based by inspection of POSS plates or from published morphologies).

(4) Declination $24° < \delta < 40°$.

It is important to recognize that this is a subset of the complete sample described in Fanti *et al.* [1973] and Colla *et al.* [1975], and that this subset explicitly does not include the spirals found in the survey (the properties of the optically brightest 15 of these spirals are given in Fanti [1973], with an additional 10 given in Colla [1975]). This almost certainly does not affect the conclusions given in Ulrich [1989], because the radio structure in these spirals was not found to extend beyond the optical size of the galaxies (and is therefore probably due to supernovae emission and nuclear Seyfert activity), unlike the diffuse radio structure in the Elliptical/S0 galaxies, which were found to extend out to hundreds of kiloparsecs. More interesting is the fact that no distinction was made between Ellipticals and S0s in compiling the Bright Sample, and indeed making such a distinction was not possible given the low resolution of the optical data used to classify the sample images. This point is not made in Ulrich [1989], wherein it is *assumed* that these galaxies are all ellipticals. Given the significant dynamical differences between ellipticals and S0s, and the possible ramifications these may have on the formation and propagation of jets, it is clear that this is an important limitation. At present *we do not know the relative fraction of Ellipticals to S0s in the B2 Bright Sample*, so the agreement between the distributions shown in Figure 1.8 is consistent with the existence of S0 BL Lac hosts.

This point has not been commonly realized. Most recent reviews of AGN (eg. Woltjer [1991]) imply that the hosts of BL Lacs are well known to be ellipticals, while in fact only a handful of BL Lacs have securely classified hosts. We consider a "securely classified host" to be one where the host morphology is determined by modelling the BL Lac as a point source with various underlying galaxy models in order to determine whether or not a particular galaxy model reproduces the observations with reasonable statistical confidence. Given this criterion, it is certainly true that the nearest 1/3 of the 15 BL Lacs whose hosts had published absolute magnitudes (Ulrich [1989]) prior to the survey described in the thesis are bright ellipticals. In this category we can certainly

place **MKN180** ($z = 0.046$; Ulrich [1978], Miller *et al.* [1978]), **BL Lac** ($z = 0.070$; Kinman [1975], Miller *et al.* [1977]), **AP Lib** ($z = 0.049$; Westerlund *et al.* [1982], Baxter *et al.* [1987]), **MKN421** ($z = 0.031$; Ulrich *et al.* [1975]), and **MKN501** ($z = 0.038$; Hickson *et al.* [1982]).

It is also true that the majority of the remaining $\sim$ 10 BL Lac hosts which have published absolute magnitudes have absolute magnitudes that are based upon an *assumed* elliptical morphology. At redshifts greater than about $z = 0.05$ it is difficult to determine the morphology of galaxies buried beneath bright cores without excellent seeing and careful model fitting. Only one fairly distant object, 1E1415+2557 ($z = 0.237$; Halpern *et al.* 1986) was classified as a disc (on the basis of model fits to data taken with the Palomar 1.5m in good seeing). Prior to our undertaking the survey described in this thesis, then, we possessed reliable BL Lac host identifications and absolute magnitudes for fewer than ten objects. None of these objects had been carefully analysed for the decentring predicted by the lensing model.

1.7 OUTLINE OF THE THESIS

It is clear that important tests of the standard models for BL Lacs can be undertaken by imaging surveys of BL Lacs. This thesis describes such a survey that we have undertaken with the William Herschel Telescope.

The plan of this thesis is as follows: Chapter 2 describes the analysis techniques that we have developed in order to extract host galaxy information from CCD images of BL Lacs, and Chapter 3 describes the results of applying these techniques to the objects in our survey. Chapter 4 focuses on our results for a particularly interesting BL Lac

object, PKS1413+135, and describes follow-up observations that we have undertaken to learn more about this object. Chapter 5 describes Monte-Carlo simulations of BL Lac hosts that we have constructed in order to quantify the sources of error in our survey, and in order to determine what possibilities for future work in BL Lac imaging are opened up by forthcoming improvements in telescopes and detectors. Chapter 6 summarizes our conclusions.

Chapter Two

HOST GALAXY ANALYSIS TECHNIQUES

INTRODUCTION

Prior to our survey, less than one quarter of the hundred or so known BL Lacs showed any evidence for an underlying host galaxy. Only 7 of these host galaxies were morphologically classified.

Why has it proven so difficult to detect and analyse the morphologies of BL Lac host galaxies? In this chapter we show how the necessary observations are not only made difficult by cosmological effects, but also by the more mundane effects of seeing, core contamination, and sparse data sampling. Section 2.1 of this chapter describes the effects of each of these on observations of BL Lac hosts, and outlines possible reduction techniques that can be used to mitigate these effects. Section 2.2 then goes from the general to the specific, and describes the reduction techniques we have chosen to implement in our survey.

2.1 OBSERVATIONAL LIMITATIONS

2.1.1 Cosmological dimming and K-corrections

Imaging observations that are intended to detect faint objects are generally background-limited, and are critically dependent on the surface brightnesses of the objects. In a Newtonian universe, this surface brightness remains constant with distance d, because the inverse square law loss in apparent luminosity l is compensated for by the $1/d^2$ decrease in observed metric area. In a General Relativistic Friedmann universe (Weinberg [1972], Weedman [1986]), the situation becomes more complex. The rate of photon emission and emitted photon energy are both larger in the emitting object's rest frame by a factor of $(1+z)$, so the observed flux f is related to the rest frame luminosity L according to:

$$f = \frac{L}{4\pi d^2 (1+z)^2} \qquad [2.1]$$

where d is now the proper distance, and is given (for $q_o > 0$) by:

$$d = \frac{q_o z + (q_o - 1)(\sqrt{1+2q_o z} - 1)}{q_o^2 H_o c^{-1}(1+z)} \qquad [2.2]$$

(Throughout this work we will assume that $H_o = 50$, and $q_o = \frac{1}{2}$.)

Similarly, a "ruler" used to measure a size in the rest frame occupies a fixed fraction of the universe at any epoch, so the standard ruler used to make a rest frame measurement at a redshift z differs from our standard ruler by a factor of $(1+z)$. The angular size of an object with a rest frame size D, observed at a proper distance d, is therefore given by $(1+z)D/d$. The surface brightness, Σ, is defined as a flux per unit angular area, and therefore decreases with redshift according to:

$$\begin{aligned} \Sigma(z) &= \frac{L}{4\pi d^2 (1+z)^2} \left[\frac{(1+z)D}{d}\right]^{-2} \\ &= \frac{\Sigma(0)}{(1+z)^4} \end{aligned} \qquad [2.3]$$

If we denote the surface brightness in mag/arcsec^2 by μ, this corresponds to an increase of:

$$\mu(z) = \mu(0) + 10\log(1+z). \qquad [2.4]$$

Another consequence of General Relativity upon the efficacy of observations at high redshifts is the "K-effect", which accounts for the fact that the filter response function in an observer's frame corresponds to a blueshifted and narrowed filter response function in the object's rest frame. Unlike the $(1+z)^4$ surface-brightness dimming, the K-effect poses no limitation in principle, since an observer wishing to measure a particular rest-frame colour could simply choose an appropriate filter whose response function would correspond to the desired colour in the rest-frame. It does, however, often pose limitations in practise, due to the unavailability of appropriate filters and/or lack of knowledge about redshifts. The K-effect is usually accounted for by using tabulated K-corrections, calculated (in magnitudes) by:

$$K(z) = 2.5 \cdot \log(1+z) + 2.5 \cdot \log \frac{\int_0^\infty F(\lambda\ )S(\lambda)d\lambda}{\int_0^\infty F(\lambda_o/(1+z))S(\lambda)d\lambda} \qquad [2.5]$$

where $F(\lambda)$ is the filter response function, and $S(\lambda)$ is the spectral energy distribution (SED). The first term in the K-correction equation accounts for the narrowing of the filter bandpass, and the second accounts for the shifting of the response function. Because the Kitt Peak (Mould) filter set used to observe the objects described in this thesis differs significantly from the standard Johnson filters used by many researchers, equation [2.5] was calculated numerically to generate the K-corrections used in this survey (a table of K-corrections corresponding to disc and elliptical galaxy SEDs is given in Chapter 5).

The effects of cosmological dimming and the K-effect are quite severe, together amounting to a $\sim (1+z)^5$ dimming in the monochromatic surface brightness for a distant galaxy. Figure 2.1 (taken from Hammer [1990]) illustrates this effect for a typical elliptical galaxy; it is clear that in most cases general relativistic effects constitute the primary

limiting factors in detecting faint underlying host galaxies at redshifts approaching $z = 0.5$.

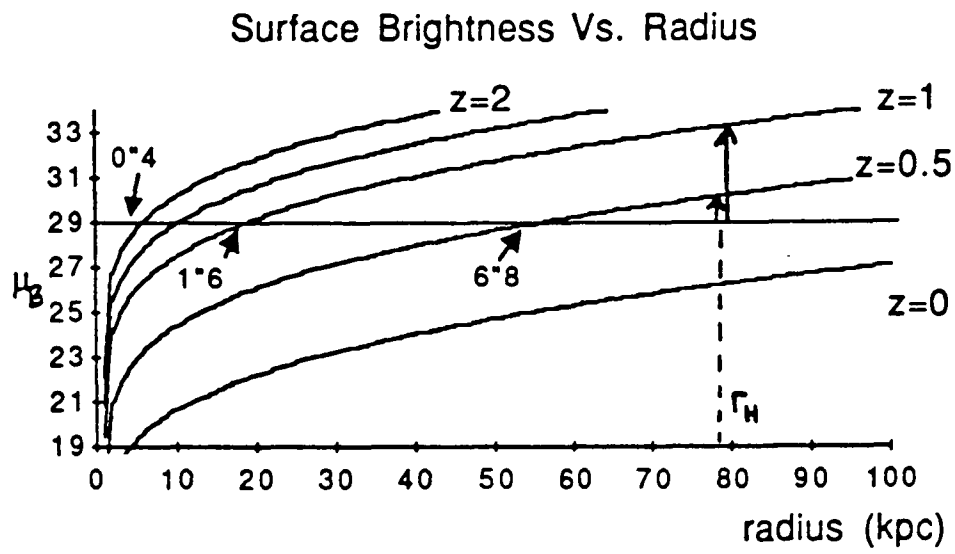

Figure 3: Surface-brightness profile of a bright elliptical (M_B=-23.3, r_{eff}=10 kpc and $\mu_B(0)$=12.3 mag. arcsec^{-2}, for H_0=50) from z=0 to z=2, for which surface brightness and k dimming act (given by Ellis et al, 1982 and Rocca-Volmerange and Guiderdoni, 1988). Its surface-brightness is assumed to follow a $r^{1/4}$ law (de Vaucouleurs, 1948), its radius at low-z being delimited inside the μ_B=26.5 mag. arcsec^{-2} contour (Holmberg, 1958). A detection limit of μ_B=29 mag. arcsec^{-2} is assumed. It shows the size in kpc which will be detectable if such a galaxy is redshifted to z>0 , without assuming evolution). To detect such a galaxy up to its Holmberg radius (78 kpc) needs a luminosity evolution of 1.5 mag at z=0.5, 4.5 mag at z=1 (see arrows), 6 mag at z=1.5 and 7.3 mag at z=2. The apparent diameter of a redshifted bright elliptical is also noticed: since z≥2 it would appear as a point like source except if there was strong evolution.

Figure 2.1 B-band Surface brightness profile of a giant elliptical (taken from Hammer [1990]) as a function of redshift.

2.1.2 Seeing effects

Seeing degradation affects observations of distant host galaxies in two ways. Seeing not only distorts the shapes of the underlying hosts, but also contaminates these hosts

with light from the central point source. This first effect is discussed here, while the second effect is analysed in the next section.

Seeing distortion of images can be modelled as a convolution of an un-degraded image, $i(x, y)$, with a point spread function $P(x, y)$. The degraded image $I(x, y)$ is given by:

$$I(x,y) = \int_{-\infty}^{\infty} \int_{-\infty}^{\infty} i(\alpha,\beta)P(x-\alpha, y-\beta)d\alpha\, d\beta \qquad [2.6]$$

The effects of seeing can to some extent be mitigated by deconvolution procedures intended to invert [2.6], provided that the point spread function (PSF) of the final image is well understood. Because of the unfortunate abberations in the optics of the Hubble Space Telescope, much progress has recently been made in deconvolving PSFs from images, but it is not yet possible to invert [2.6] without distorting $i(x, y)$ at low light levels, rendering direct deconvolution ineffective for morphological classification of distant host galaxies. A more tractable approach (adopted by us, and described in section 2.2) is to assume a particular a parametric form for $i(x, y)$ as the sum of a point source and a galaxy model, and then fit $I(x, y)$ to the observed image. This method works well, provided the adopted galaxy model is a reasonable representation of the true galaxy morphology.

2.1.3 Core contamination

Observation of underlying hosts is of course made much more difficult if the BL Lac core is so bright that it dominates the light from the host galaxy. This effect is primarily responsible for the small numbers of photographically detected BL Lac hosts. With the advent of linear CCD detectors, however, it has become possible to "subtract off" the central point source, provided that an accurate model for this central source is adopted. This model is often a scaled version of the PSF used in order to model the effects of seeing.

Many authors (eg. Weistrop *et al.* [1981], Stockton and Ridgeway [1991]) adopt a core-subtraction technique that is independent of subsequent host galaxy modelling. The core model is numerical, and is defined to be the scaled image of a sky-subtracted field star on the CCD frame. The core contribution to the BL Lac is determined by maximizing the scaling factor subject to the constraint that the residual image is non-negative and monotonically increasing towards its center. This technique has the advantage of being simple and does not assume that any underlying fuzz is a galaxy with a particular shape (aside from being monotonically brighter towards its center). On the other hand, this technique clearly over-estimates the contribution of the central core and often requires smoothing of resulting image in order to remove the effects of the added noise in the image (the scaled noise from the field star image is added quadratically to the noise from the BL Lac image). Furthermore, if any modelling of the underlying host is required, an analytic point-spread function must *still* be defined in order to use [2.6] to determine the morphology of the underlying host. We therefore decided to incorporate core modelling and galaxy modelling into a single operation, with the core contribution being simply another free parameter in the fits.

We cannot emphasize strongly enough the need for an accurate model of the PSF at low surface brightnesses before attempting any core modelling or subtraction. A PSF with slightly inaccurate wings often gives reasonable results when convolved with a galaxy to simulate the effects of seeing, but using the same PSF can lead to inaccurate results if it is scaled and subtracted to remove a point source from an AGN host galaxy. The necessity for accurate PSF information was met in our observations by making sure that each observed BL Lac had at least one reasonably bright comparison star in the same field, from which we determined the PSF by least squares fitting an adopted model. After experimentation with many different models for the surface brightness profiles of stars on WHT CCD frames, a PSF model given by the sum of a gaussian and two exponentials

was chosen. For observations made under poorer seeing conditions (FWHM $\geq$ 1.3), the second exponential component in this model was found to be unnecessary.

We note that seeing-degraded stars are often modelled as gaussians in image reduction software (eg. STARLINK's Kappa). This approximation is sufficiently good to allow reasonable estimation of the full-width at half-maximum (FWHM) of stellar images, but does not allow a good description of the outer wings of stellar profiles (as pointed out in Moffat [1969] and Schweizer [1979]). The sum of two gaussians, a model used in the past by a number of authors (e.g. Falomo *et al.* [1991]) to model PSF stars imaged by other telescopes, also gave much poorer results than our adopted model (as illustrated in Figure 2.2 below), although the sum of three or more gaussians apparently gives quite good results (Bendinelli [1990]). For our purposes (ie. modelling underlying galaxies) the only important feature of PSF models is that they accurately reproduce our CCD data, since we are not concerned with the physics by which the PSF is generated in the atmosphere (for which an excellent, albeit complicated, model can be found in Woolf [1982]).

As a cautionary example illustrating the possible effects of inaccurate core modelling, we show in Figure 2.3 several contour plots obtained by Stickel and coworkers (Stickel *et al.* [1988, 1991]) in 1.2" seeing of the BL Lac PKS0537-441 (z=0.894). These authors claim that the BL Lac is resolved, and since it is unlikely a host could have been detected have at z=0.894, conclude that PKS0537-441 is an example of a foreground galaxy lensing a distant OVV quasar. The authors adopt a simple lorentzian model for the core, and after subtracting this contribution, find that the putative foreground galaxy is well modelled by a disk (i.e. an exponential profile). Their core model is illustrated in frame (b) of Figure 2.3, and has a width of 5.2" at R=26.25 mag/arcsec^2. Figure 2.4 illustrates a field star, of similar brightness, imaged by us with the WHT under slightly *better* seeing conditions (1.1"). This star has a width of 9" at R=24.5 mag/arcsec^2, and an extrapolated width of at least 12" at R=26.2 mag/arcsec^2, almost identical to the

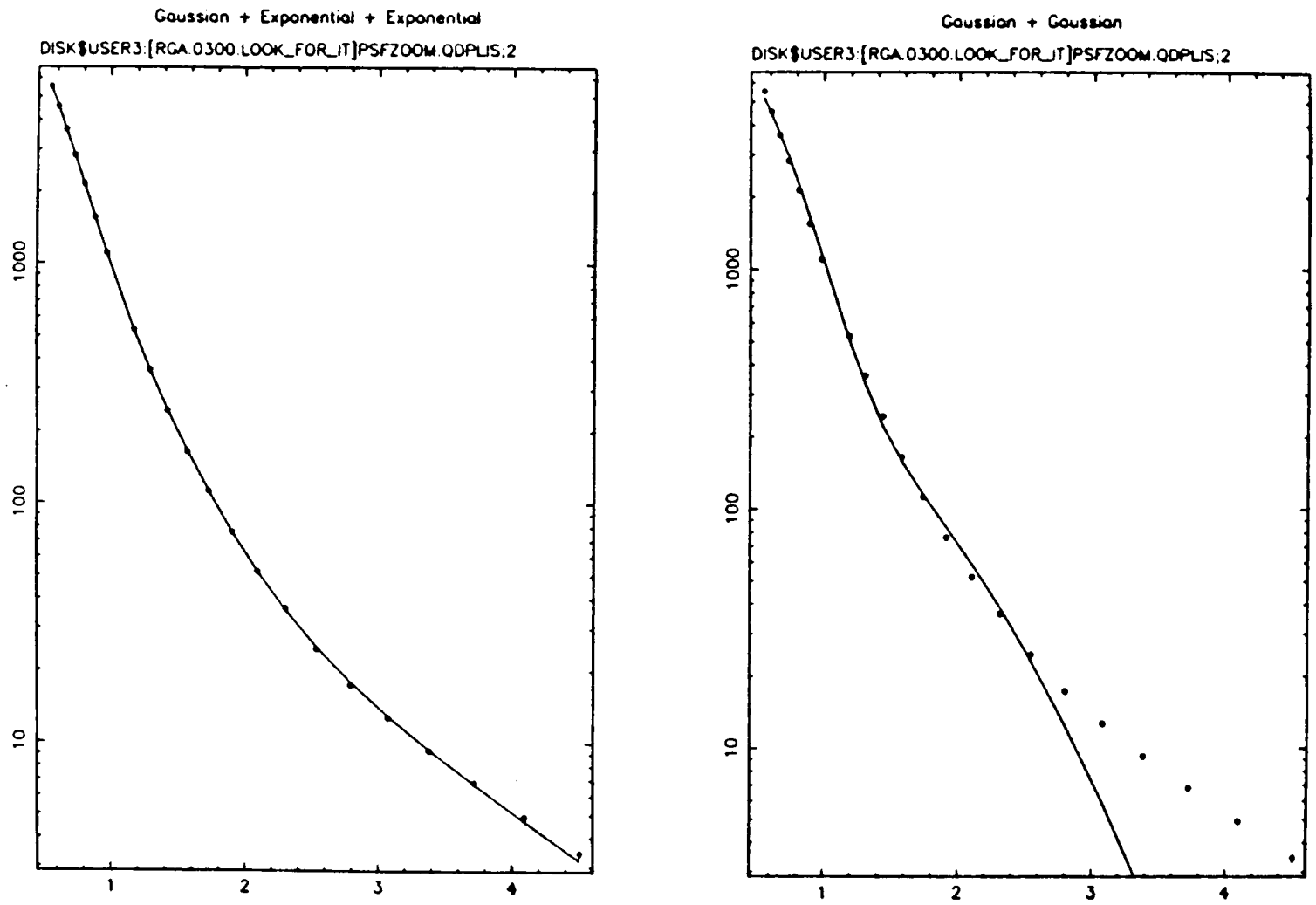

Figure 2.2 A field star imaged by the WHT (points), fit by our PSF model (left), and a PSF modelled by the sum of two gaussians (right).

width as the "resolved" PKS0537-441! Furthermore, the contribution of the WHT PSF star at low light levels is very well approximated by an exponential, the same model determined by Stickel *et al.* to be the best fit model to their underlying galaxy. It is possible that the WHT PSF may differ in overall shape from the PSF of the telescope used by Stickel *et al.* (the 2.2m on La Silla), but in view of the close resemblance between the BL Lac and a carefully modelled WHT PSF star, the conclusion that PKS0537-441 is resolved (and therefore lensed) appears somewhat questionable.

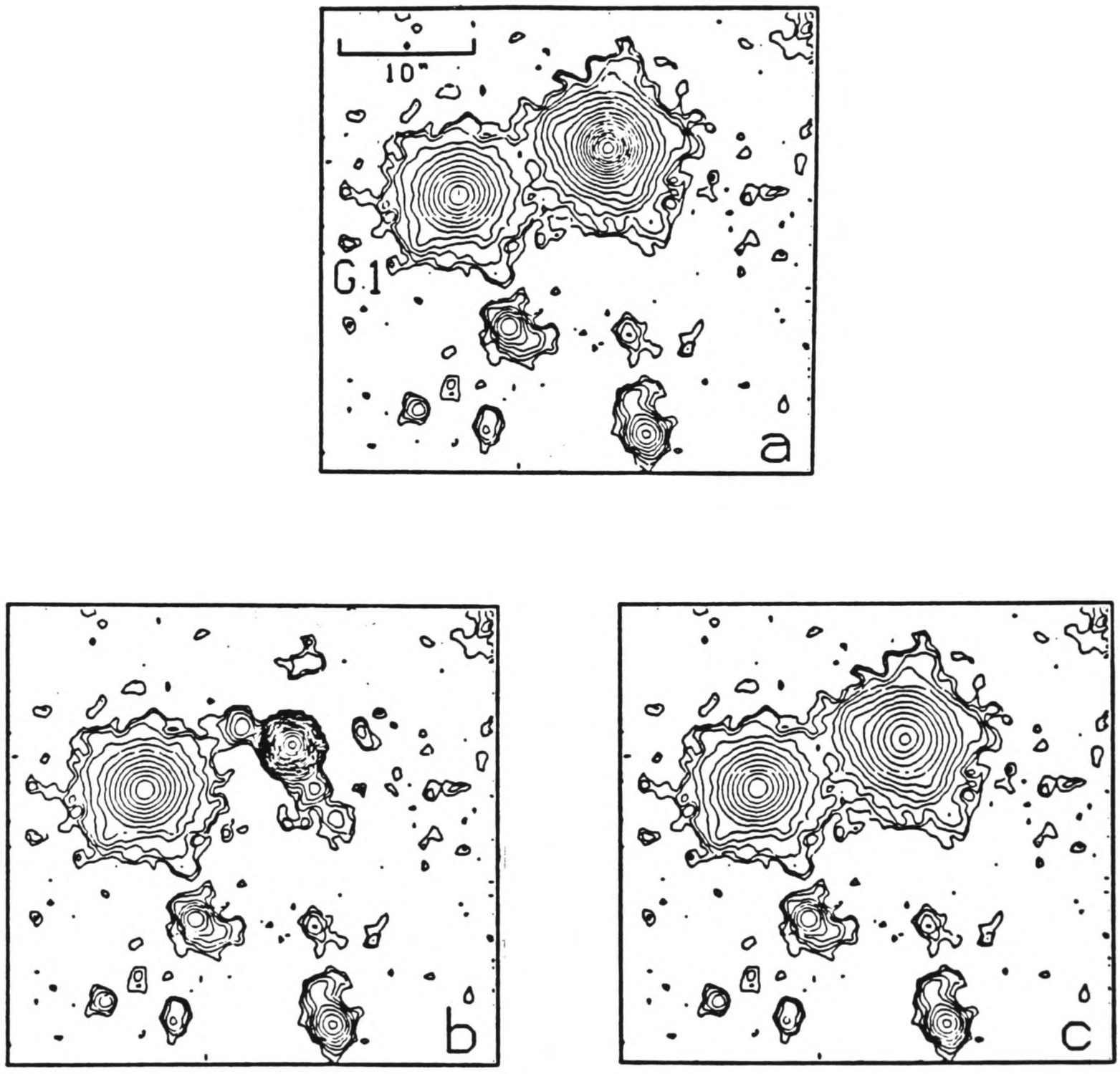

Figure 2.3 Subsections from CCD frames of PKS0537-441 taken from Stickel *et al.* (1991). Lowest contour is 26 magnitude per arcsec^2, with contour spacing of 0.5 mag/arcsec^2. (a) PKS0537-441 is north of centre and on the right. (b) PKS0537-441 with foreground disc galaxy model subtracted, leaving the stellar core. (c) PKS0537-441 with stellar core subtracted, leaving the foreground galaxy.

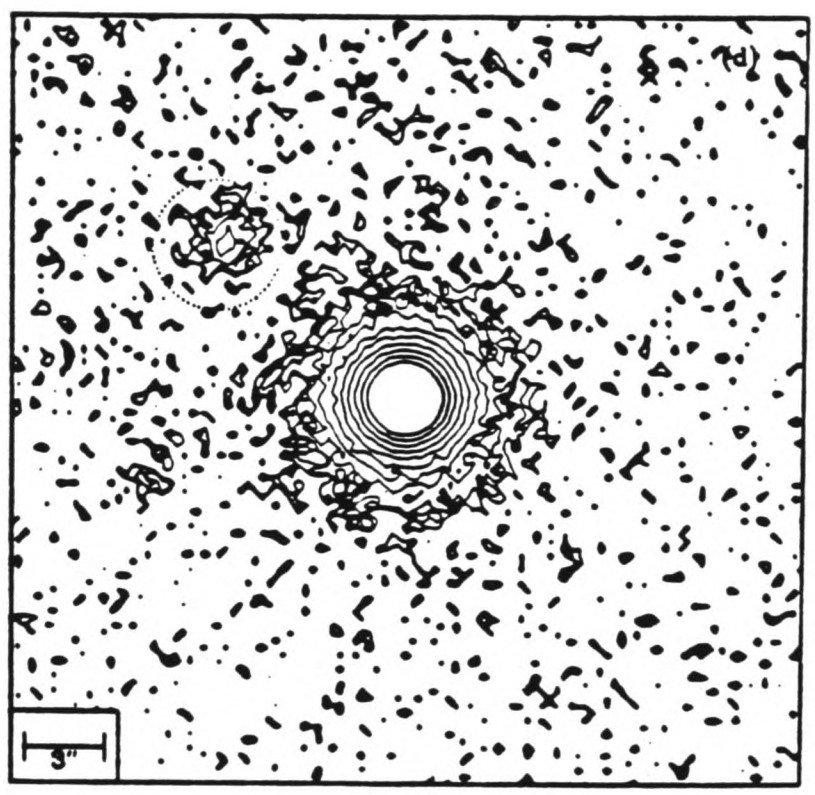

Figure 2.4 Field star, of similar brightness to PKS0537-441, imaged with the WHT under 1.1 arcsec seeing. Lowest contour corresponds to R=24.5 mag/arcsec^2.

2.2 MODELLING

Despite the difficulties described in the previous section, the detection of BL Lac hosts out to moderately high ($z \sim 0.4$) redshifts is often possible under good seeing conditions. Because of the low light levels involved, however, host galaxy *classification* is much more difficult than it is for nearby galaxies, and it is no longer possible to classify

hosts without detailled modelling.

Our modelling of BL Lacs proceeded in two steps. Firstly, we extracted surface brightness profiles for the BL Lac images by fitting ellipses to the image isophotes. We then fit various seeing-degraded galaxy + bright core models to these profiles, in order to try and determine if there was any evidence for an underlying host, and if so, to try to determine its morphology. A typical result illustrating this analysis procedure is shown in Figure 2.5, where we show a contour map of the BL Lac 4U1444+43, its corresponding surface brightness profile, and the results of fitting this profile by elliptical and disc host galaxy models.

In principle, model fitting could have proceeded directly from the two-dimensional image, without the need for reducing the image to a radial surface brightness profile. This was indeed attempted, but the amount of computer time required proved prohibitive. Instead, we obtained the profiles using the PROF program developed by Robert Jedzrejewski while at the Institute of Astronomy, Cambridge, and at the Space Telescope Science Institute. This program was written as a complement to the GASP surface photometry package developed by Mike Cawson at Cambridge. The algorithms used by the profile extraction software, and possible errors resulting from it, are discussed in section 2.2.1 below. The procedures adopted to perform the subsequent model fits are described in section 2.2.2 below.

2.2.1 Isophote fitting and profile extraction

Perhaps the easiest way to extract a surface brightness profile for a galaxy is simply to take a cut along the major axis of the object. This is wasteful in terms of signal-to-noise, however, and one looks for some sort of azimuthal averaging scheme. Early work generally averaged the points in circular annuli about the centre of the image, but this may not be appropriate if the image isophotes are not perfect circles. Most of our images

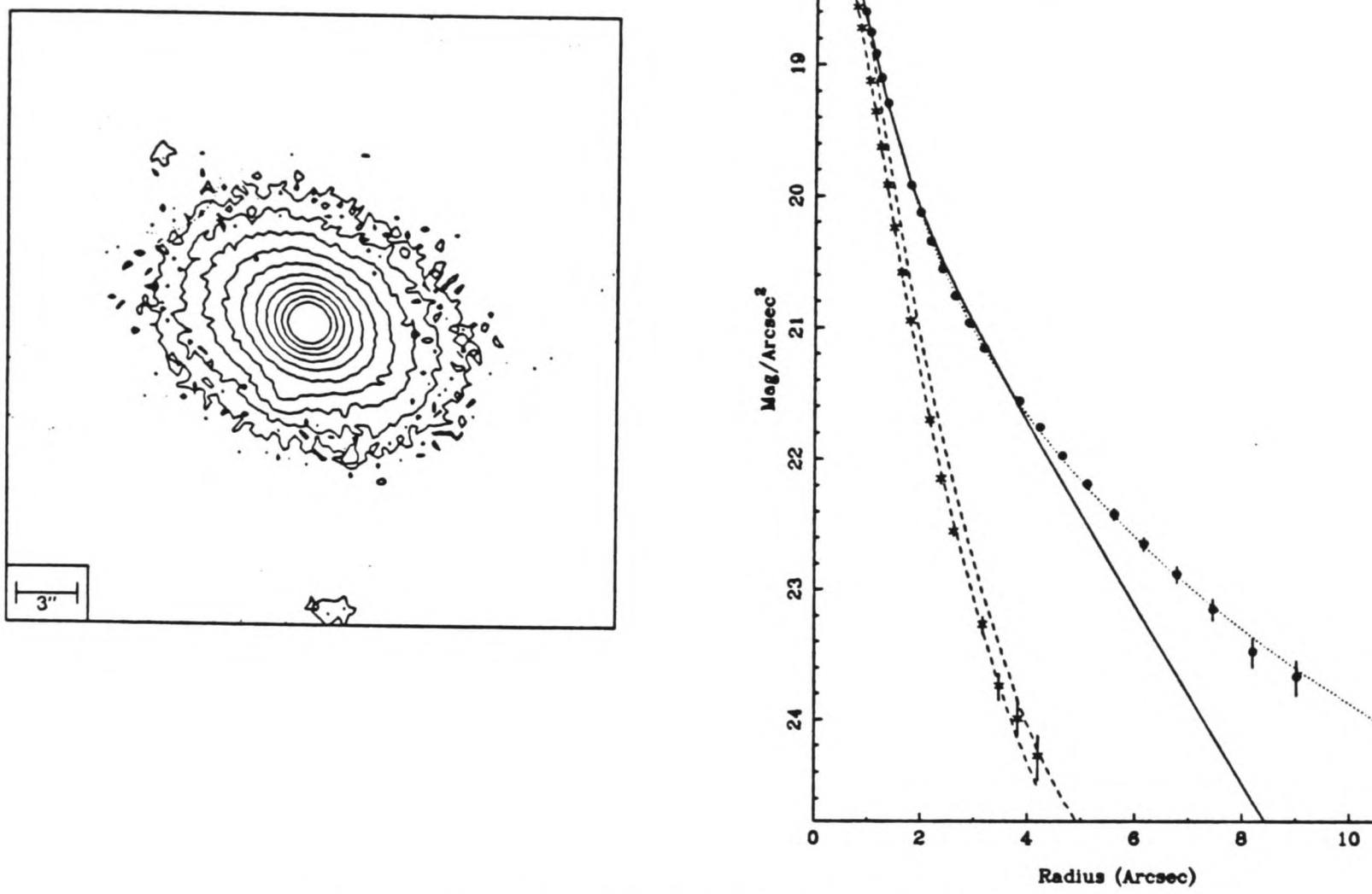

Figure 2.5 CCD contour image (left) and corresponding surface brightness profile (right) for the BL Lac 4U1444+43. Best fitting disc (solid line) and elliptical (dotted line) models are superimposed on the BL Lac profile. The asterisks and the two dashed lines are, respectively, the measured PSF surface brightness profile, a fit to this profile, and a scaled-up PSF model for comparison with the BL Lac profile.

are well fit by circular isophotes, but significant deviations from circularity can occur for larger sources, when the underlying galaxy dominates the image at large radii. We therefore decided, like a number of other authors, to fit elliptical isophotes to the images instead.

Elliptical isophotes are chosen because they are easy to fit, and are an excellent representation of the isophotes of elliptical galaxies. The surface brightness profile is typically given by plotting the isophotal brightness as a function of semi-major axis distance, with the least squares fitting procedure essentially performing a weighted average of the intensity along a given isophote, greatly improving the signal to noise. Areas of the image that are contaminated by overlapping images are interactively "masked" prior to the fitting, and are not included in the subsequent analysis.

The PROF elliptical isophote fitting program has been used by a number of other authors for similar purposes (e.g. Fraix-Burnet *et al.* [1991]). The algorithm used by this program (Jedzrejewski [1987]) is conceptually simple. The program first fixes the semi-major axis a of the desired isophote, and then guesses values for the ellipticity ϵ, position angle Φ, and x and y positions of the center of the isophote. The intensity values given by sampling the true data around this ellipse are then fitted to the model:

$$I = I_o + A_1 \sin(E) + B_1 \cos(E) + A_2 \sin(2E) + B_2 \cos(2E) \qquad [2.7]$$

where E is the eccentric anomaly (equivalent to angle θ for small ellipticities). If the chosen ellipse is a good representation of an isophote, A_1, B_1, A_2, and B_2 are close to zero, and I_o is the surface brightness at the chosen semi-major axis length. If any of the A's or B's are significantly different from zero, the trial ellipse does not describe an isophote. If we define I' to be the derivative of the intensity along the semi-major axis (evaluated at the semi-major axis length), and Δx_a and Δy_a to be position shifts along the major and minor axes, then for small errors in the parameters the fit can be improved by altering the ellipse parameters according to:

$$\Delta x_a = \frac{-B_1}{I'} \qquad [2.8]$$

$$\Delta y_b = \frac{-A_1(1-\epsilon)}{I'} \qquad [2.9]$$

$$\Delta\epsilon = \frac{-2B_2(1-\epsilon)}{aI'} \qquad [2.10]$$

$$\Delta\Phi = \frac{2A_2(1-\epsilon)}{aI'[(1-\epsilon)^2-1]} \qquad [2.11]$$

The procedure is then repeated with the new ellipse parameters, until either a good fit to $I = I_o$ is eventually achieved, or until the iteration limit is reached (at which point we conclude that no elliptical isophote adequately fits the data). The program then fixes a new semi-major axis length, and the procedure is repeated until a complete profile is built up.

The resulting surface brightness profiles have errors assigned to individual points by directly sampling the spread of pixel values around a given elliptical isophote. We expect the relative sizes of the error bars on the profiles to be roughly correct using this procedure, but numerical errors and the smoothing inherent in any interpolation make the correct absolute size of the errors uncertain. This does not affect the results of our analysis because we are comparing the *relative* goodness of fit in our data to various models. This important point is discussed further in the next section.

The PROF program was originally written to extract surface brightness profiles from comparatively large galaxies whose surface brightness gradients are much shallower than the objects we analyze, and it relies on a fast bilinear interpolation scheme to estimate intermediate pixel values. Experiments we have performed on simulated BL Lacs suggest that a slight improvement in the accuracy of the results could be obtained by adopting a more accurate interpolation routine in the program, but at a great cost in execution time. We therefore decided to retain the bilinear interpolation routine, but to improve upon the resulting accuracy by expanding each image using an accurate but slow multinomial algorithm, prior to running it through the profile fitting software. Tests on simulations indicate that this procedure achieves accuracy comparable to that obtained by incorporating a slower interpolation routine in the profile fitting software, but it is

much faster because the slowest interpolations need only be done once.

Because we were very concerned with obtaining accurate intensities, we only retained points where PROF indicated that ellipses were accurate fits to the data. We define a "good-fitting" isophote to be one where the first four coefficients of the fourier series describing the residuals around the best-fitting ellipse were all less than 4% of the standard deviation around the isophote. We were typically able to extract profiles down to $\sim 1-2\%$ of the sky background level. We could of course extract fainter isophotes by relaxing our criteria for good-fitting ellipses, but it was felt that the resulting gain in depth would be offset by the possibility of fitting our galaxy models to low-level morphological disturbances in the hosts (which are unaccounted for in our analytical galaxy models), very faint contaminating foreground objects, or spurious structure due to imperfect flat fielding.

2.2.2 Host galaxy classification

The surface brightness profiles of the BL Lac and host galaxy were modelled as:

i) a scaled PSF derived from a star in the CCD frame.

ii) a scaled PSF plus a seeing-degraded de Vaucouleurs $r^{1/4}$ law (representing an elliptical host), given by:

$$\Sigma(r) = \Sigma_e \exp\{-7.67[(r/r_e)^{1/4} - 1]\} \qquad [2.12]$$

where Σ_e is the surface brightness at the effective radius, r_e.

iii) a scaled PSF plus a seeing-degraded exponential law (representing a disc host), given by:

$$\Sigma(r) = \Sigma_s \exp(-r/r_s) \qquad [2.13]$$

where Σ_s is the central surface brightness, and r_s is the exponential radius.

Circularly symmetric versions of the PSF were two-dimensionally convolved with galaxy models in order to simulate the seeing degradations (cf. equation [2.6]). Sky backgrounds were sampled in regions near the BL Lac and comparison star, and the modal background values were incorporated as fixed parameters in the fits. Standard deviations of the modal sky values in the sampled regions were added in quadrature to the errors assigned by the profile extraction software in order to account for uncertainty in background values.

Best fit-models were obtained by incorporating the models above into a subroutine, which was then linked into the program QDP (written by Allyn Tennant of the Marshall Space Flight Center) as a user defined function. QDP does the fitting using a modified version of the CURFIT subroutine given in Bevington [1969].

Classification into a given morphological type was based upon the results of an F-test on the relative χ^2 values returned by the fits. The F-test is designed to test for statistically different *variances* in distributions, and is the standard statistical test for determining the necessity of additional terms in a fit. The first step in performing an F-test is to define a quantity, f, given by the ratio of the weighted variances in the two fits:

$$f = \frac{\chi_a^2/\nu_a}{\chi_b^2/\nu_b} \qquad [2.14]$$

where ν_a and ν_b are the degrees of freedom in models a and b. The F-test therefore has the additional advantage of being insensitive to a constant multiplicative factor in defining the error bars in the fitted point, since any such factors are constant coefficients of χ^2, and cancel out in the numerator and denominator of [2.14]. The *relative* goodness of fit between the two models is the important quantity in an F-test. The quantity f given in [2.14] can be shown (Bevington [1969]) to be distributed according to the F-distribution,

given by:

$$P_f(f,\nu_1,\nu_2) = \frac{\Gamma[(\nu_1+\nu_2)/2]}{\Gamma(\nu_1/2)\Gamma(\nu_2/2)}\left(\frac{\nu_1}{\nu_2}\right)^{\nu_1/2}\frac{f^{\frac{\nu_1-1}{2}}}{(1+f(\nu_1/\nu_2))^{\frac{\nu_1+\nu_2}{2}}} \qquad [2.15]$$

The F-test is given by the integral of this quantity:

$$P_F(F,\nu_1,\nu_2) = \int_F^\infty P_f(f,\nu_1,\nu_2)df \qquad [2.16]$$

which gives the probability of observing a given value of F from a random set of data points fitted by the correct model.

An F-test was first performed comparing the relative χ^2 values of the PSF BL Lac model to the PSF + host BL Lac models. A successful host detection at this stage corresponded to an F-test result indicating statistically significant improvement in the fit, resulting from the inclusion of host components, at a 90% confidence level. At this stage the statistically significant "detection" of a host underlying B20912+297 was rejected because its reference star was much fainter than the BL Lac, and we could not be certain that this "detection" was not an artifact resulting from extrapolating the PSF model for the BL Lac well beyond the limited reference star data.

If a host was detected, a second F-test was performed comparing the relative χ^2 values of the two host models to each other. The host was classified as a disc or an elliptical if this test indicated that one model was significantly better than the other at a 90% confidence level. If the F-tests indicated equally good fits, we classified the host morphology as "unknown". In order to test the reliability of our results for fainter hosts, we applied our analysis technique to a number of synthetic BL Lac models (described in Chapter 5). These simulations indicated that we could reliably differentiate between disc and elliptical hosts out to redshifts of $z > 0.3$ for hosts with $M_V \sim -22$.

In obtaining best fit models for the BL Lacs, the galaxy model surface brightnesses and scale lengths were allowed to vary independently. No à priori attempt was made to restrict the fitted parameters to "astrophysically reasonable" ranges. In those cases where

hosts were detected and the redshift of the object was known, however, the parameters for the best fitting models did fall into a range consistent with the parameters of normal bright galaxies (our criteria for "normal bright galaxies" are discussed at length in the next chapter). The parameters for the rejected host model were generally outside this range. We view this as a useful check on the consistency of our results, but emphasize that our classifications for BL Lac hosts are based entirely on the relative χ^2 of the fits, and not on our preconceptions about reasonable values for the fitted parameters.

Where a host was detected but disc and elliptical models gave equally good fits (i.e. those hosts classified as having "unknown" morphology), one or both of the fitted models usually gave parameters consistent with realistic underlying galaxies. The low signal to noise level of most of these detections implies that many of these "unknown" morphology hosts are probably quite distant ($z \approx 0.4$), and we consider conclusions drawn from these objects to be much less secure than those obtained from the other objects.

We emphasize that our modelling does not address the much more difficult question of whether or not the (deVaucouleurs law and exponential law) models universally chosen by workers in the field to characterize the galaxies underlying QSO adequately describe the true morphology of the hosts. Answering this question is complicated not only by the need for absolute errors on each point in the luminosity profile, but also by the fact that the analytic formulae used to model galaxy profiles are generalizations that are rarely followed perfectly, even by nearby galaxies. We have therefore had to *assume* that distant disk hosts are well described by exponential surface brightness profiles, and that distant elliptical hosts are well described by deVaucouleurs law profiles. This is certainly true for most nearby galaxies, but may not be true for more distant ones. While this assumption seems a safe one, we must await future very high resolution observations for confirmation (these will hopefully be able to address host morphology in a more model independent way, by for example clearly resolving spiral arms). Furthermore, the underlying hosts

of quasars sometime exhibit morphological disturbances (often attributed to tidal events or mergers) which can alter their luminosity profiles; a similar situation may or may not occur with BL Lacs. Our masking of obviously disturbed regions prior to fitting the profiles, and our requirement that all surface brightness points correspond to good fitting ellipses, should minimize the effects of any such disturbances.

Chapter Three

AN IMAGING SURVEY OF BL LAC HOST GALAXIES

INTRODUCTION

This chapter describes the results of an imaging survey of 23 BL Lacertae objects that we have undertaken with the William Herschel Telescope in a search for underlying host galaxies. Fourteen of these objects are resolved in our survey. We have determined the morphology of three of these galaxies for the first time, and have confirmed the morphology of an additional three. All of the observed underlying hosts are centred on their bright cores, and two of the newly classified hosts are disc systems. These results are in disagreement with the predictions of standard beaming and lensing models for these objects. We have calculated absolute magnitudes for observed hosts with known redshifts and find them to be consistent with the results obtained by previous authors, despite the unexpected morphology exhibited by some of the underlying hosts. By making a number of assumptions, we have estimated redshifts for resolved (but unclassified) hosts whose redshifts were unknown.

Section 3.1 of this thesis gives details about the observations made during the course of this survey. The surface brightness profiles and model fits resulting from these observations are given in Section 3.2. The surface brightness profiles are discussed and interpreted in sections 3.3 through 3.6. Finally, a brief summary is presented in section 3.7.

3.1 OBSERVATIONS

Observations were made during 10-12 April 1989 and 29-30 November 1989 using the William Herschel Telescope (operating at f/4 via the Taurus optical system) and a 400x590 GEC P8603 CCD detector (readout noise of 5-10 ADU, ~1 electron/ADU, dark count <1 ADU/pixel/hour). The image scale was 0.27 arcseconds per pixel. All objects were imaged through a Kitt Peak R-band filter.

An initial short exposure was made with the telescope centred on the published BL Lac object position in order to identify the object. After this initial exposure, the telescope was moved, if necessary, in order to accommodate a reasonably bright comparison star in the field of view. The final image for each object is the sum of several (typically ~5) coadded integrations, with integration times for individual frames chosen to avoid saturation of the BL Lac or comparison star. Guiding was sufficiently accurate to allow most frames to be coadded directly, with re-registration being necessary only for a few objects. Flux calibrations for both runs were performed by observing standard stars several times during each night. Conditions were photometric, with excellent seeing, for most objects. Slight systematic variations in the object fluxes were detected in some of the individual frames for OQ530, while a much larger effect was found in all of the individual frames for ON325, leading us to suspect that these objects were observed through a thin layer of haze. We have corrected for this effect in OQ530 by normalizing the affected frames, and conclusions about the morphology of the host underlying OQ530 are unaffected (star images on the frames are undistorted, and flat-fielding is barely affected). We cannot, however, exclude the possibility of systematic errors of up to half a magnitude in our photometry of this object. We were unable to correct for the much larger variations in the ON325 frames, and our analysis of this object is therefore rather

limited.

With the exception of bright, well-studied BL Lacs such as MKN501 and AP Lib (which were included as "controls" to verify our photometry), total exposure times were between 1000 and 2000 seconds per object. Individual frames were debiased and flat-fielded in the standard manner prior to being coadded, using twilight sky exposures as flat fields for all BL Lacs observed in the April run. For several BL Lacs observed during the November run, we improved our flat fielding by displacing the telescope by a few arcseconds between individual exposures, and then median-compared the resulting CCD frames to generate a flat. This typically reduced the level of residual background "structure" resulting from imperfect flat fielding from around 1% of the background level to less than 0.5%).

A log of observations is given in Table 3.1.

3.2 RESULTS

Surface brightness profiles for the BL Lac and comparison star were obtained using the procedure outlined in the previous chapter. Surface brightness profiles for resolved BL Lacs, and the corresponding best fit models, are illustrated in Figure 3.1(a). Detailed model fitting results and best fit parameters are given in Table 3.2. Obvious obscuring objects on the frames (nearby stars or galaxies or defects on the CCD) were masked prior to the analysis by setting their pixels to a preassigned negative value which instructs the software to ignore the masked pixels. The extent to which such masking was necessary for individual BL Lacs is shown in Figure 3.1.

Of the 23 BL Lacs in our sample, eight possessed known redshifts: MKN501

Table 3.1 Record of Observations

Name	RA [1950]	Dec	m_{total}	Date	Exposure [s]	Seeing [Arcsec]
PKS0019+058	00 19 54	05 52 31	< 21	29/11/89	1500	0.8
0300+470	03 00 10	47 04 34	16.3	29/11/89	400	0.8
PKS0422+004	04 22 12	00 29 17	15.4	29/11/89	570	0.6
0503-043	05 03 23	-04 23 16	< 21	29/11/89	1250	0.9
PKS0735+178	07 35 14	17 49 09	16.3	12/4/89	1600	1.1
B20752+258	07 52 35	25 50 37	17.3	12/4/89	1400	1.9
PKS0754+100	07 54 23	10 04 40	16.2	11/4/89	1400	0.9
PKS0808+019	08 08 51	01 55 50	16.2	12/4/89	1700	1.4
PKS0829+046	08 29 11	04 39 51	15.3	11/4/89	1825	1.0
0836+182	08 36 40	18 13 25	16.9	29/11/89	660	0.9
B20912+297	09 12 54	29 45 56	15.7	11/4/89	1500	1.1
4U1057-21	10 57 44	10 05 42	16.1	12/4/89	1600	2.2
MKN180	11 33 30	70 25 00	13.6	11/4/89	500	1.0
ON325	12 15 21	30 23 40	16.7	10/4/89	1500	1.1
1E1402+042	14 02 21	04 16 20	16.5	11/4/89	1600	0.7
PKS1413+135	14 13 34	13 34 18	18.6	11/4/89	1500	0.9
OQ530	14 18 06	54 36 57	15.0	10/4/89	1500	0.9
4U1444+43	14 26 36	42 53 46	15.5	12/4/89	500	1.1
PKS1514+197	15 14 41	19 43 11	16.8	10/4/89	2500	1.1
AP Lib	15 14 45	-24 11 22	14.2	11/4/89	500	1.2
MKN501	16 52 12	39 50 26	12.5	12/4/89	100	0.7
PKS1717+178	17 17 00	17 48 09	17.3	11/4/89	1600	0.7
2335+031	23 35 34	03 10 01	17.8	29/11/89	1430	1.0

Note: Magnitudes listed in column four were obtained by synthetic aperture photometry on the R-band CCD frames. Aperture diameters were between 10" and 20", and do not enclose all of MKN501, MKN180, or AP Lib. The seventh column records the full-width at half-maximum of field stars on the CCD frame.

Table 3.2 Summary of Model Fits

Name	$\frac{\chi^2_{PSF}}{\chi^2_{ELL}}$	$\frac{\chi^2_{DISC}}{\chi^2_{ELL}}$	Σ_e $[\frac{mag}{arcsec^2}]$	r_e ["]	$m_{elliptical}$	Σ_s $[\frac{mag}{arcsec^2}]$	r_s ["]	m_{disc}	COMMENTS:
PKS0019+058	(see Notes)		-	-	-	-	-	-	Too faint for profile fits.
0300+470	0.93	1.04	-	-	-	-	-	-	Unresolved.
PKS0422+004	15.4	0.74	23.0	1.98	18.6	20.6	0.93	19.1	Resolved.
0503-043	(see Notes)		-	-	-	-	-	-	Too faint for profile fits.
PKS0735+178	0.4	0.49	-	-	-	-	-	-	Unresolved; z=0.424.
B20752	1.71	0.86	-	-	-	-	-	-	Unresolved.
PKS0754+100	(see Notes)		-	-	-	-	-	-	Resolved; models poor.
PKS0808+019	0.78	1.02	-	-	-	-	-	-	Unresolved.
PKS0829+046	26.7	0.74	25.7	22.9	16.7	21.1	2.72	17.3	Resolved; faint PSF star.
0836+182	4.5	0.84	27.9	100	17.0	22.3	7.1	16.7	Resolved.
B20912+297	(see Notes)		-	-	-	-	-	-	Faint PSF star.
4U1057-21	55	0.93	26.3	39.4	16.5	21.4	3.8	17.1	$\epsilon \approx 0.2$. Poor seeing.
MKN180	1478	19.0	21.7	7.10	14.3	18.5	2.16	14.9	Elliptical; $\epsilon \approx 0.1$.
ON 325	(see Notes)		-	-	-	-	-	-	Resolved;Unphotometric.
1E1402+0416	(see Notes)		-	-	-	-	-	-	Unresolved;v.faint PSF.
PKS1413+135	108	0.12	24.0	5.3	18.0	20.9	1.71	18.4	Disc; $\epsilon \approx 0.6$.
OQ530	46.4	0.57	24.7	18.7	16.6	20.3	2.64	16.8	Disc; $\epsilon \approx 0.3$.
4U1444+43	2844	31.8	21.89	4.20	15.9	18.86	1.44	16.4	Elliptical; $\epsilon \approx 0.3$.
PKS1514+197	1.35	1.19	-	-	-	-	-	-	Unresolved.
AP Lib	1107	13.7	21.6	5.66	14.6	18.17	1.56	15.3	Elliptical; $\epsilon \approx 0.0$.
MKN501	134	12.6	20.59	9.3	12.7	16.6	1.7	13.7	Elliptical; $\epsilon \approx 0.25$.
PKS1717+178	3.07	1.01	29.7	52.3	22.1	23.9	1.85	22.1	Resolved.
2335+031	(see Notes)		-	-	-	-	-	-	Resolved;models poor.

Notes: Host magnitudes in columns 6 and 9 were obtained by integrating models to R=25 mag/arcsec^2. Ellipticity values (ϵ) are recorded in the final column.

(z=0.0337), MKN180 (z=0.0458), AP Lib (z=0.0486), 4U1444+43 (z=0.129), OQ530 (z=0.152), 4U1057-21 (z=0.184), PKS1413+135 (z=0.26), and PKS0735+178 (z=0.424). With the exception of PKS0735+178, all of these were resolved by our survey. Only the hosts underlying MKN501, MKN180, AP Lib, and OQ530 were morphologically classified prior to our survey (all as large ellipticals). We confirm the classifications for MKN501, AP Lib, and MKN180, reclassify OQ530 as a disc, and newly classify the hosts underlying a further two (4U1444+43 as an elliptical, and PKS1413+135 as a disc). The two classified disc hosts in this survey are at moderately large redshifts, but were observed under excellent seeing (0.9"), and are at redshifts where we can securely differentiate ellipticals from discs (compare, for example OQ530 and 4U1444+33, which are at similar redshifts).

Of the remaining 15 (presumably most distant) objects in our sample, we were able to resolve an additional seven, none of which we were able to morphologically classify.

Figure 3.1(b) records the position shifts and ellipticities of the best-fitting isophotes for the BL Lacs and PSF stars, as a function of semi-major axis length. The ellipticity points allow an estimation of the ellipticity of the underlying host, while the position shift points test for decentring of the pointlike core of the object (which dominates the inner isophotes) from the underlying galaxy (which dominates the outer isophotes). None of the objects in our sample exhibit evidence for decentring, although our method is probably not sensitive to very small decentring on scales of less than 0.5 arcseconds.

While our morphological classifications are based purely upon χ^2 results from the model fits, we emphasize that these classifications are consistent with the immediate impression given by inspection of both the images and surface brightness profiles. The high ellipticity in PKS1413+135 is suggestive of a disc host. Similarly, simple morphological classifications can be made by inspection of the profiles for the some of the more extended hosts (e.g. AP Lib, 4U1444+43, OQ530, PKS1413+135), since the fit to the PSF models

allows a determination of the limiting radius inside which the signal from the central point source is dominant (typically $\sim$ 3"). The expected morphological classification is clear from the remainder of the profile, with deVaucouleurs law ellipticals turning up at large radii, while those objects classified as discs have profiles that remain straight, or even turn slightly down. These simple classifications agree perfectly with the detailed fit results.

The previous classification of OQ530 as an elliptical (Stickel *et al.* [1991]) was not based upon fitting a point source + convolved galaxy model to the BL Lac, but rather on an unconvolved fit of galaxy models to the outer portion ($r > 5$ arcsec) of the visible host galaxy (which extends out to $r \sim 9$"). By adopting the effective radius given in Stickel *et al.* [1991]), we also obtain a good fit to an elliptical galaxy profile in these outermost regions (although a disc model gives a similarly good fit), but the resulting seeing-convolved elliptical galaxy model *alone* exceeds the surface brightness of the observed BL Lac (combined galaxy+core) between 2" $< r <$ 5", clearly ruling out this model. The point source in OQ530 appears to have been $\sim$ 0.5 mag brighter during Stickel *et al.* 's observation of OQ530, possibly masking this effect. In our opinion, successful morphological classification of objects at these redshifts crucially depends upon careful modelling of the point spread function, and upon its subsequent incorporation into model fits.

3.3 DISCUSSION

The most remarkable aspect of our survey is the discovery of disc hosts underlying three BL Lacs. Previously, Halpern *et al.* [1986] claimed to have resolved an underlying

disc host in 1415.6+2557, but this isolated observation did not receive sufficient attention to seriously question the validity of simple beaming models. More recently, Stickel *et al.* [1988] have reported the existence of a disc host in the lens candidate 0537-441 (but see the reservations we express about these observations in the previous chapter), and Falomo *et al.* [1991] has reported the discovery of pointed isophotes in H2356-309 (4U0009-33), suggestive of a weak disc underlying the dominant elliptical structure in this object. In the next chapter we describe in more detail our discovery of the disc system underlying PKS1413+135 (also included here as part of our larger survey), adding additional weight to the conclusion that some BL Lacs reside in disc galaxies. The discovery of the additional underlying disc galaxies reported in this chapter increases the total number of known disc hosts to four out of the 20 or so classified BL Lac hosts. While the presence of BL Lac disc hosts is not consistent with the simplest beaming models, the underlying discs we observe are centred on their bright BL Lac cores, and therefore pose a problem for lensing models as well.

With the exception of PKS1413+135, our current images are not of sufficient quality to allow us to separate the central point core from the bulge component of disc BL Lac hosts. For PKS1413+135, we were successful in doing this (M^{c}Hardy *et al.* [1991]), and have classified this object as an S0b-c galaxy under the DDO system. Further imaging is needed to determine the exact classifications of the other disc hosts. There is some precedent for at least moderately strong radio sources being associated with S0 galaxies (eg.3C120 and 3C31, discussed further in the next chapter), and unified scheme models would therefore seem compatible with these hosts, provided examples of collimated beaming in other S0 systems could be found. Unified schemes would have more difficulty if these objects turned out to be late type spirals. We note, however, that disc hosts are also found amongst radio-quiet QSO, leading to unification schemes linking radio-quiet QSO with Seyferts (Weedman [1986]). It is possible that our observations are

indicative of a closer than expected relationship between BL Lac objects and radio quiet QSO, but the small sample of known BL Lac discs makes comparison difficult. Thus far it appears that the radio-quiet QSO discs are somewhat smaller and bluer than BL Lac discs (Hutchings, Crampton, and Campbell [1984]).

3.4 ABSOLUTE MAGNITUDES

Absolute magnitudes for BL Lac hosts with known redshifts examined in this survey are given in Table 3.3, assuming $H_o = 50$ km s^{-1} Mpc^{-1}, $q_o = \frac{1}{2}$, as throughout this thesis. In computing these values, we first transformed our Kitt Peak R-band colours to the Johnson V-band by assuming the underlying hosts exhibited a typical old-star spectral energy distribution corresponding to the data in Pickles [1985] and Weedman [1986]. We have adopted an old-star spectrum for all objects, including discs, because the two best-studied discs (1415+259 and PKS1413+135) both exhibit colours more typical of old stellar populations. Numerical integrations over interpolations of the tabulated values for the spectral energy distribution, modulated by the filter response functions, were used to determine the K-corrected colours between observed R-band (integrated to $\mu_R = 25$ using fitted host parameters) and rest-frame V-band (integrated to $\mu_V^{\rm rest} = 26$, assuming no rest-frame V − R colour gradient in the profiles). We have assumed a typical underlying host ellipticity of 0.2 where we could not measure it directly.

Our derived absolute magnitudes agree well with previously published results for the three control objects included in our sample. Our results differ by less than 0.1 magnitude with published results for MKN501 and AP Lib. For MKN180, the best previously available absolute magnitude determination (Ulrich [1989]) could only restrict

Table 3.3 Absolute Magnitudes of Host Galaxies

Name	z	Type	F	$m(\mu_V^{rest} = 26)$	M_V	COMMENTS:
4U1057-21	0.186	Unknown	N/A	≈ 16.0	≈ -24.0	Observed under poor conditions.
MKN180	0.0458	Elliptical	99.9%	14.2	-22.8	$-23.0 < M_V < -21.8$;Ulrich 198
PKS1413+135	0.26	Disc	99.8%	18.3	-23.3	
OQ530	0.152	Disc	91.0%	16.8	-23.2	
4U1444+43	0.129	Elliptical	99.9%	15.7	-23.9	
AP Lib	0.049	Elliptical	99.9%	14.3	-22.8	$M_V = -22.8$; Ulrich 1989
MKN501	0.034	Elliptical	99.9%	12.7	-23.6	$M_V = -23.6$; Ulrich 1989

Note: Column 4 is the F-test confidence level for the chosen model. Column 5 records the R band magnitude of the chosen model, integrated out to a radius corresponding to V=26 mag/arcsec^2 in the object's rest frame. The absolute magnitudes in column 6 have been corrected for extinction (Burstein and Heiles 1978).

the host magnitude to within the -21.8 to -23.0 range, consistent with our measurement of -22.8.

For the six morphologically classified objects with redshifts in our sample, we obtain $< M_V >= -23.3$, slightly brighter than the value of $< M_V >= -22.5$ obtained by Ulrich [1989] in her review of the best available data in the literature for the absolute magnitudes of BL Lac host galaxies, and in good agreement with the value of -22.9 reported in Stickel *et al.* [1991]. This seems consistent with the selection effects inherent in our observations of more distant objects. The disc underlying 1415+297 (Halpern *et al.* [1986] is among the brightest of BL Lac hosts, while the remaining discs reported in this

thesis lie near the centre of the luminosity distribution for BL Lac hosts. It is clear that many more redshifts for BL Lacs are required to determine whether disc and elliptical hosts have different luminosity functions.

The absolute magnitudes determined by this survey remain consistent with the hypothesis that the BL Lac parent population is made up of FR type I radio galaxies, although the discovery of disc hosts is a serious challenge to this model. One possibility is that a hitherto undiscovered population of disc FR type I radio galaxies exists. An imaging survey designed to compare optical properties of FR I and FR II radio galaxies with $z \leq 0.2$ was recently completed by Owen and Laing [1989]. They fitted images to a deVaucouleurs $r^{\frac{1}{4}}$ law to test for ordinary ellipticals, and to a power law to determine if the galaxies could be better characterized as cD galaxies. They found that while FR I optical light profiles tended to be flatter than FR II profiles, most FR I galaxies were still better fitted by $r^{\frac{1}{4}}$ laws. No attempt was made to fit disc models to galaxies in their survey, but exponential discs would probably be better fitted to $r^{1/4}$ laws rather than to the even more slowly decaying cD profiles. We consider the possibility of some disc FR I radio galaxies to remain open.

3.5 ESTIMATION OF REDSHIFTS

The lack of redshifts for many of the objects described in this thesis prevents us from deriving absolute magnitudes for most objects. We can, however, crudely estimate their redshifts of the hosts by matching the image parameters returned by our fits to the redshifted properties of normal galaxies. We emphasize that any absolute magnitude calculated from this estimation is fixed to be representative of the class used to make the

estimate, and should not be used to test against theoretical models. We do, however, hope that these estimates will help observers in selecting instruments and exposure times for future observations of these objects.

A problem in estimating redshifts lies in deciding exactly what a "normal" BL Lac host looks like. Owen and Laing [1989] have demonstrated that FR I galaxies, the parent population in the most widely accepted unification model, display a range of optical properties. The FR I galaxies described by Owen and Laing seem optically rather similar in luminosity and morphology to the brightest cluster galaxies studied by a number of observers. We have therefore chosen to adopt them as our "reference" set of elliptical galaxies for comparison with our BL Lac elliptical host models. A reference set of galaxies for disc model hosts is more difficult to come by, and after some experimentation we decided simply to define a galaxy that was an amalgamation of the properties of the known BL Lac disc systems, and to use that in the redshift estimates.

3.5.1 Elliptical hosts

We estimate the redshifts of the elliptical hosts by assuming that their central surface brightnesses and effective radii are correlated according to the relationship given by Hoessel and Schneider for brightest galaxies in Abell clusters. The Hoessel and Schneider [1985] relationship gives reasonable agreement when used to predict parameters for the (mostly control) BL Lacs in our sample with known redshifts and elliptical hosts: MKN180 (predicted z=0.059, true z=0.046), MKN501 (predicted z=0.022, true z=0.034), and AP Lib (predicted z=0.067, true z=0.049), and 4U1444+43 (predicted z=0.106, true z=0.129). These predicted redshifts are consistent with the ~0.75 mag dispersion in the central surface brightnesses of the Hoessel and Schneider relationship. Assuming $q_o = \frac{1}{2}$, for our sample of ellipticals to obey the Hoessel and Schneider relationship we must numerically solve the following for z:

$$\Sigma_e = 18.82 - 0.365 + 3.02\log[r_e \frac{(1+z) - \sqrt{1+z}}{3.44 \cdot 10^{-4} \cdot H_o \cdot (1+z)^2}] + 10\log(1+z) + K(z) \quad [3.1]$$

where Σ_e is the observed surface brightness at the effective radius in magnitudes/arcsec^2, r_e is the observed effective radius in arcseconds, and the second term on the right hand side is the adopted correction between the Thuan and Gunn r-band used by Hoessel and Schneider and Kitt Peak R-band. The resulting predicted redshifts and absolute magnitudes for the ellipticals in our sample, as well as for those objects with unknown morphologies, are shown in Table 3.4. Note that the Hoessel and Schneider relationship is calibrated using $H_o = 60$ km s^{-1} Mpc^{-1}, and that this value was used in solving the equation above to estimate the redshifts. The effective radii and absolute magnitudes as given in Table 3.4 have been converted to the $H_o = 50$ km s^{-1} Mpc^{-1}, $q_o = \frac{1}{2}$ system used throughout this thesis.

Table 3.4 Estimated Absolute Magnitudes for Host Galaxies With Unknown Morphology

Name	z Elliptical	z Disc	M_V Elliptical	M_V Disc	COMMENTS:
PKS0422+004	0.31	0.15	−23.6	−20.8	
PKS0829+046	0.25	0.23	−24.8	−23.9	
0836+182	0.28	0.27	−24.8	−25.0	Both models doubtful.
PKS1717+178	No Solution	0.43	N/A	−21.2	

Note: Columns 2 and 3 give estimated redshifts based upon assumed morphologies (see text). Columns 4 and 5 give the corresponding absolute magnitudes.

3.5.2 Disc hosts

Little is known about the detailed morphological characteristics of BL Lac disc hosts, and any procedure we adopt to estimate their redshifts is bound to be imprecise. At redshifts large enough to make the newly discovered discs as faint as we observe them, these systems would have to be quite large, with exponential radii of order 10kpc. Such radii are consistent with the range of sizes exhibited by the discs underlying 1415.6+2557 (17 kpc), PKS1413+295 (9 kpc), and OQ530 (9 kpc). A simple redshift estimate can be made by assuming a fixed rest-frame size and calculating the redshift at which this would be observed at the apparent size. By adopting an intermediate scale size of 12kpc, for the known discs we would have estimated z=0.48 for PKS1413+135 (true z=0.26), z=0.22 for OQ530 (true z=0.15), and z=0.15 for 1415+297 (true z=0.24).

We can obtain another estimate by assuming that BL Lac disc hosts exhibit the constant central surface brightness $\mu_B = 21.65$ found by Freeman [1970] in a sample of nearby spirals. By further assuming an old star colour correction (consistent with the old-star colours exhibited by PKS1413+135 and 1415+297) of 1.5, we can estimate the redshift at which the $(1+z)^4$ monochromatic flux-dimming and K-correction reduces this central surface brightness to the observed level. This procedure appears, on the whole, to give similar results to the one outlined earlier. Using this procedure we would have estimated z=0.19 for PKS1413+135 (true z=0.26), z=0.10 for OQ530 (true z=0.15), and z=0.28 for 1415+297 (true z=0.24). In any case, the true redshifts tend to be bracketed by the values given by the two procedures, and the values given in Table 3.4 for the redshifts of the disc hosts are the averages of the two estimates.

3.6 SELECTION EFFECTS IN THE SAMPLE

It is difficult to obtain samples of BL Lac hosts that are complete in any meaningful statistical sense. Few hosts are known, and most published lists of BL Lacs are mixtures of objects selected at different wavelengths. The vast majority of the objects in this sample were radio-selected, and during the course of our observations we became aware of a similar survey being undertaken by Stickel and colleagues of radio selected BL Lacs in the 1Jy Galaxy Catalogue (Kühr and Schmidt [1990]). We tried to minimize overlap with their observations; most of our objects were therefore not in the 1Jy Catalogue, and we expect our results to be biased towards BL Lacs that are relatively weak in the radio.

As discussed in Section 1.5, it has recently become clear that X-ray selection is an highly efficient tool for discovering BL Lacs (Maccacaro *et al.* [1989]; Schwartz *et al.* [1989]). It is not clear whether X-ray-selected and radio-selected BL Lacs come from the same population of objects (Morris [1991]; Polatidis [1989]). We plan to extend our present imaging program to include a number of X-ray-selected BL Lacs in order to directly test whether the host populations of these objects are the same.

3.7 CONCLUSIONS

Our survey of 23 BL Lac objects has resolved many new BL Lac hosts, and we have morphologically classified three of these objects for the first time. No strong evidence for decentring between the BL Lacs and underlying hosts was found in any of these objects. Surprisingly, we have discovered two disc host galaxies, the existence of which is not consistent with standard models for these objects. The ramifications of these

observations are still not clear, but the similarity of the absolute magnitudes of these hosts to the FR I radio galaxies suggests that our observations could be indicative of a population of disc BL Lac host galaxies with collimated beaming.

Figure 3.1 Caption

(a) Surface brightness profiles. Points marked by asterisks are the star profile, dots are the BL Lac profile. The dashed line is the best fitting PSF star model (also shown as a best-fit to the BL Lac profile to illustrate how well it fits the BL Lac). The solid line is the disc + PSF core model, and the dotted line is the elliptical (de Vaucouleurs law) + PSF core model.

(b) Ellipticities and position shifts. Dots represent BL Lac data points, asterisks represent PSF star points. The top curve illustrates the ellipticity of the isophotes as function of semi-major axis radius, while the lower curve records the position shifts of the centres of the isophotes.

(c) and (d) Isophotal contour maps of subsections of the CCD frames, showing the resolved BL Lac objects, and their corresponding PSF stars. Lowest contour levels are at 5σ for AP Lib, MKN501, MKN180, and 4U1444+43, and at 1.5σ for all other objects. Successive contour levels are displayed logarithmically, and increase in units of 0.5 magnitude/arcsec^2. The areas inside the dotted circles enclose interfering objects excluded from the profile fitting analysis. All objects are centred in these figures, with the exception of the reference stars for PKS0422+004, MKN 180, and PKS1413+135, which were near the edges of the CCD frames and are displayed slightly displaced.

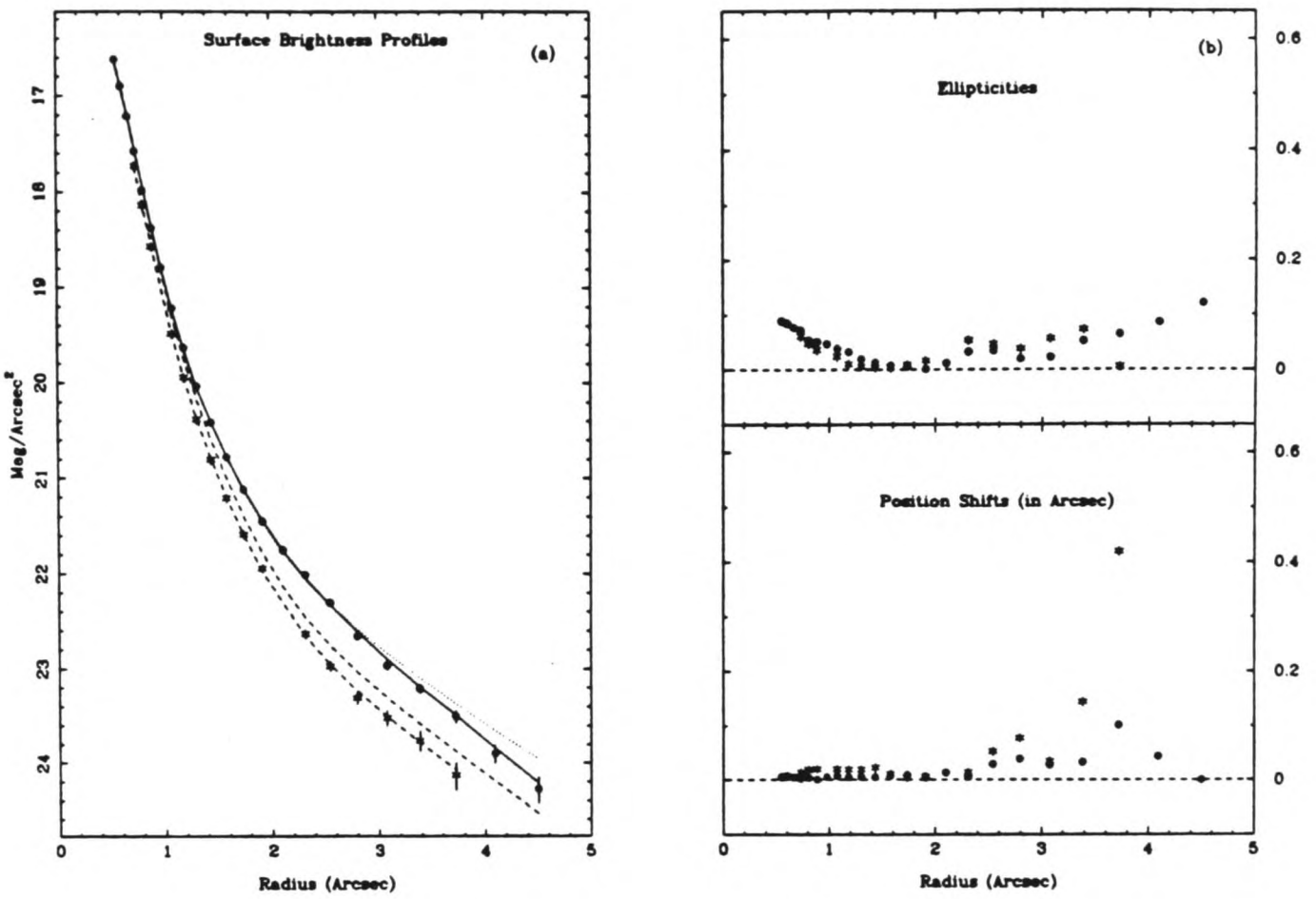
PKS0422+004
Surface Brightness Profiles
(a)
Mag/Arcsec²
Radius (Arcsec)
(b)
Ellipticities
Position Shifts (in Arcsec)
Radius (Arcsec)
BL Lac Object
(c)
3"
PSF Reference Star
(d)
3"

Figure 3.1

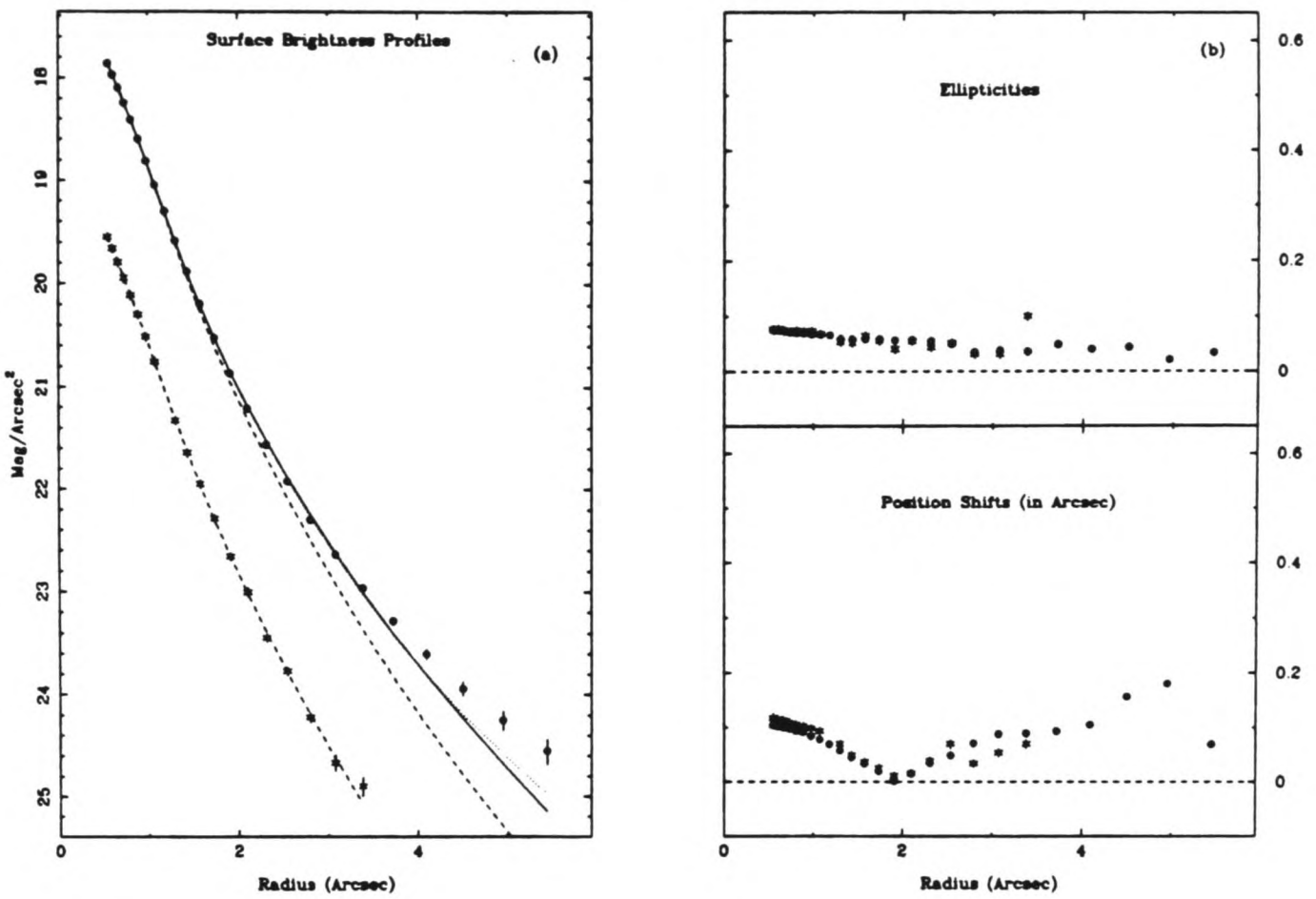

Figure 3.1 (continued)

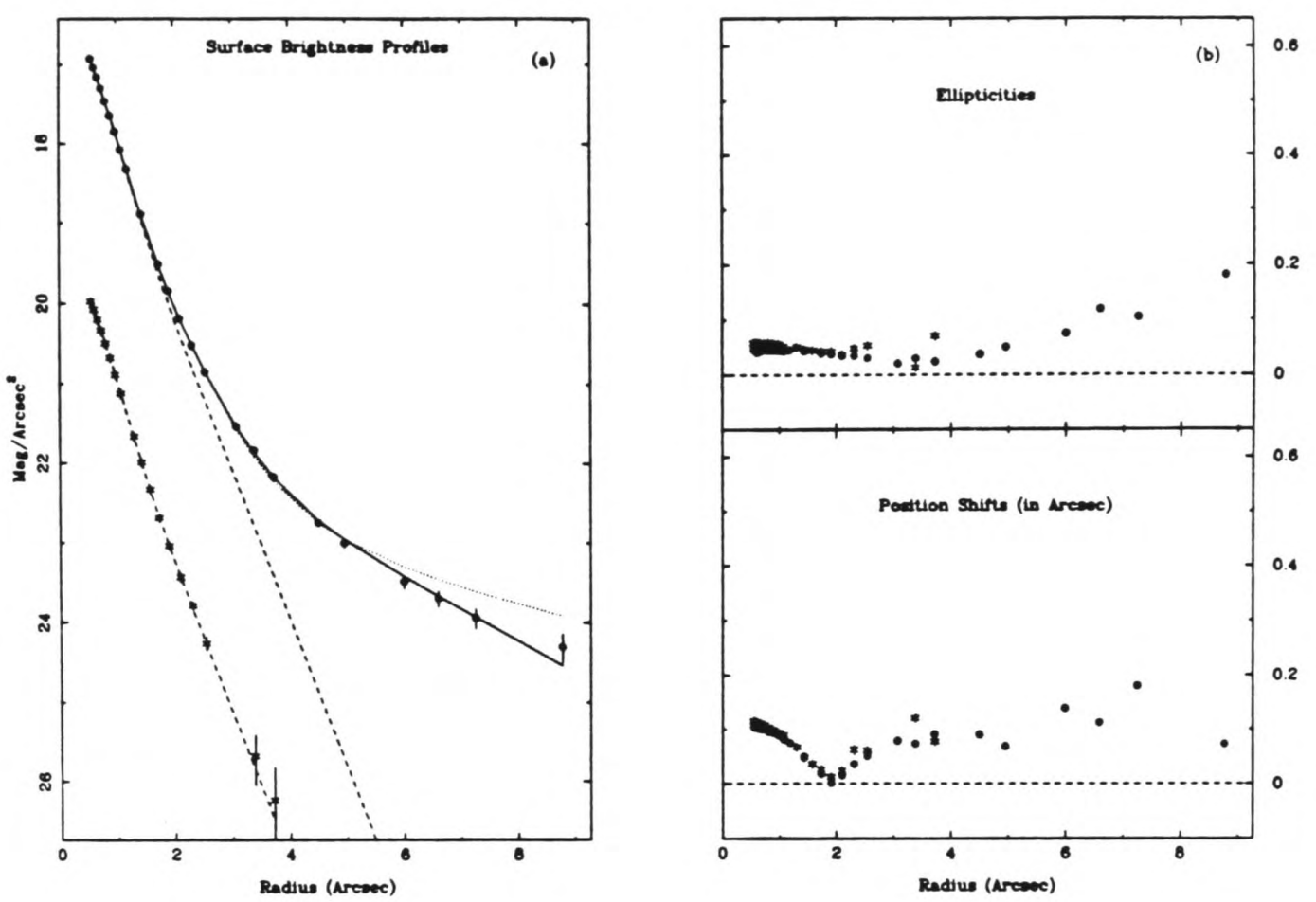

Figure 3.1 (continued)

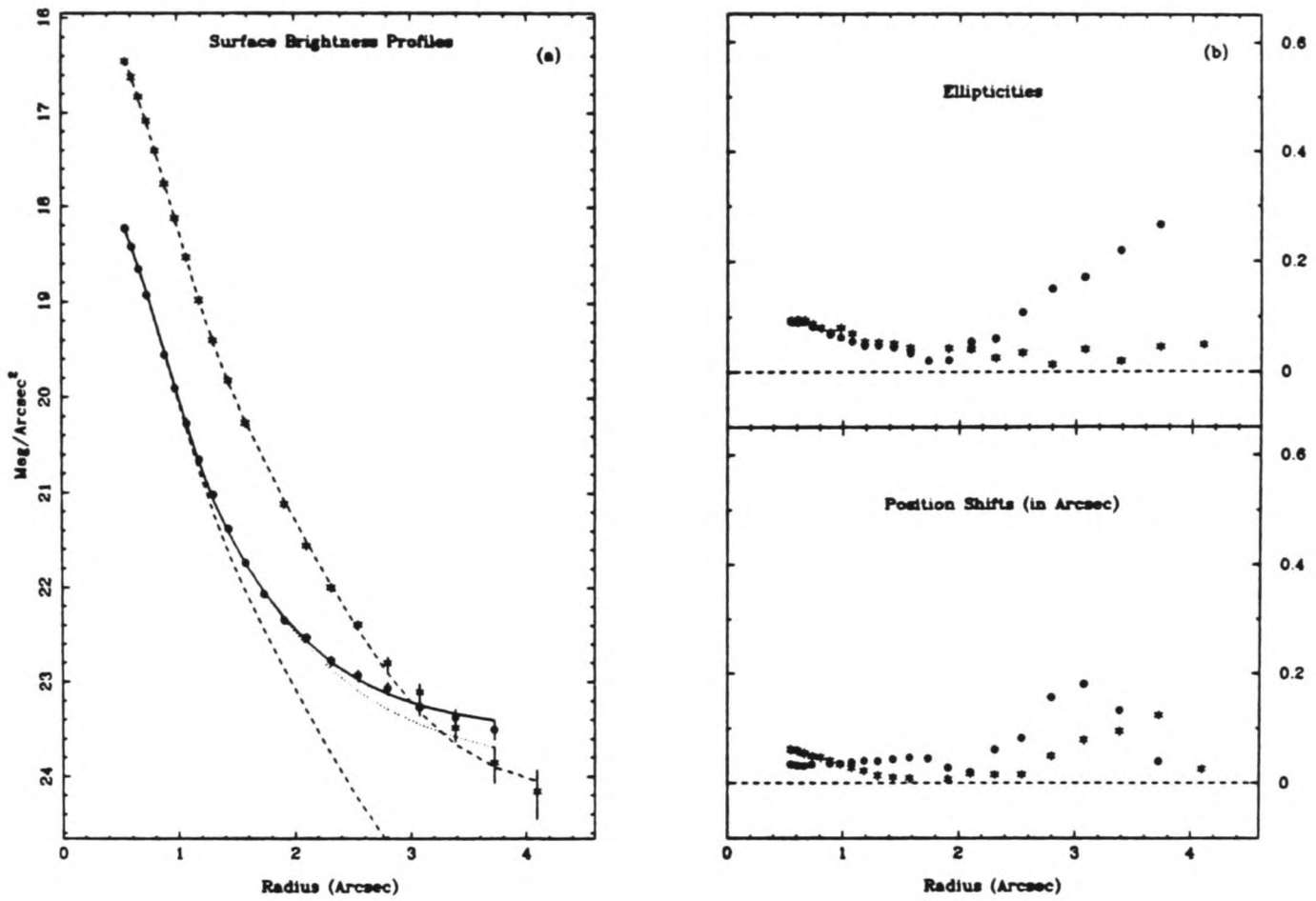

Figure 3.1 (continued)

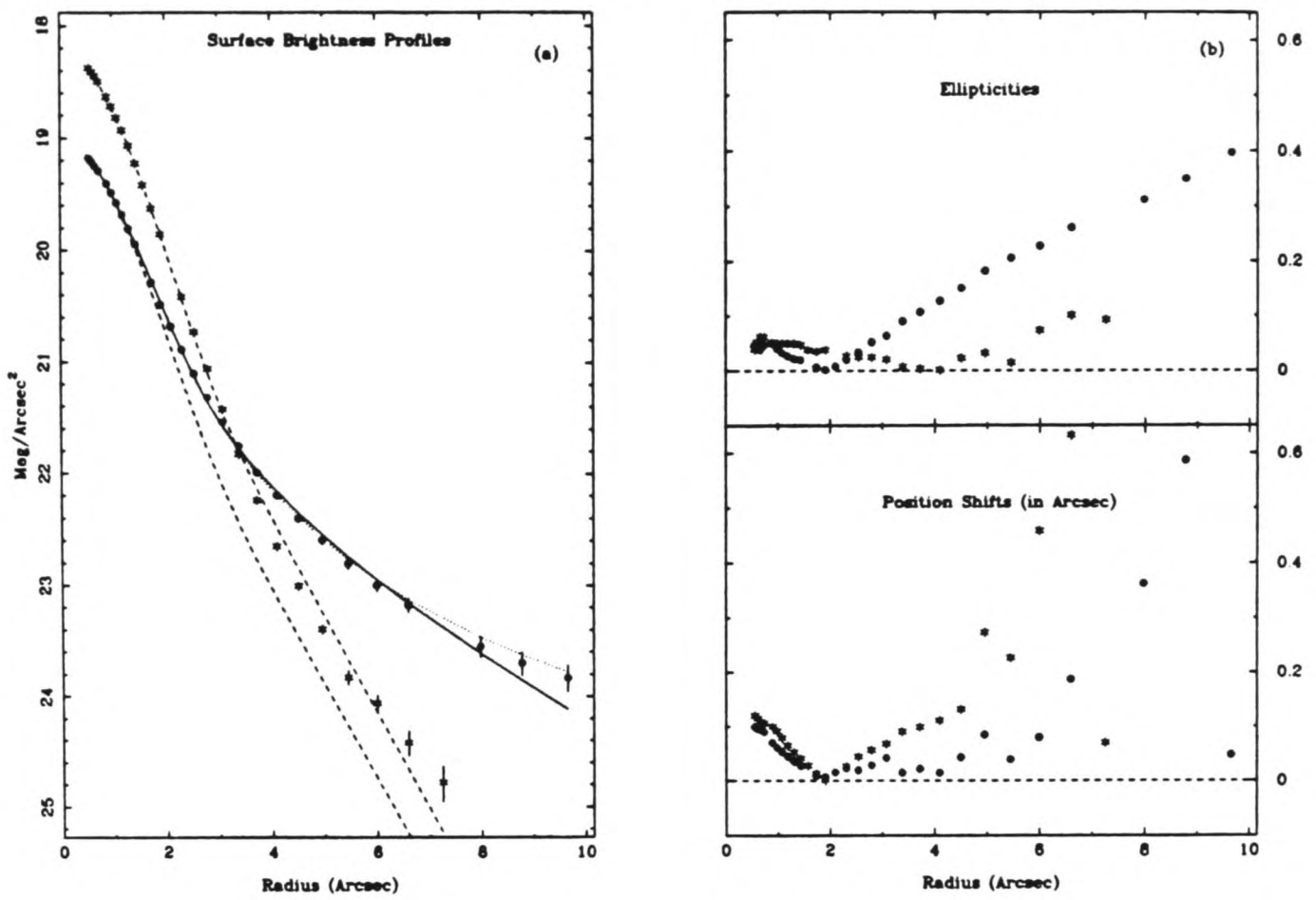

Figure 3.1 (continued)

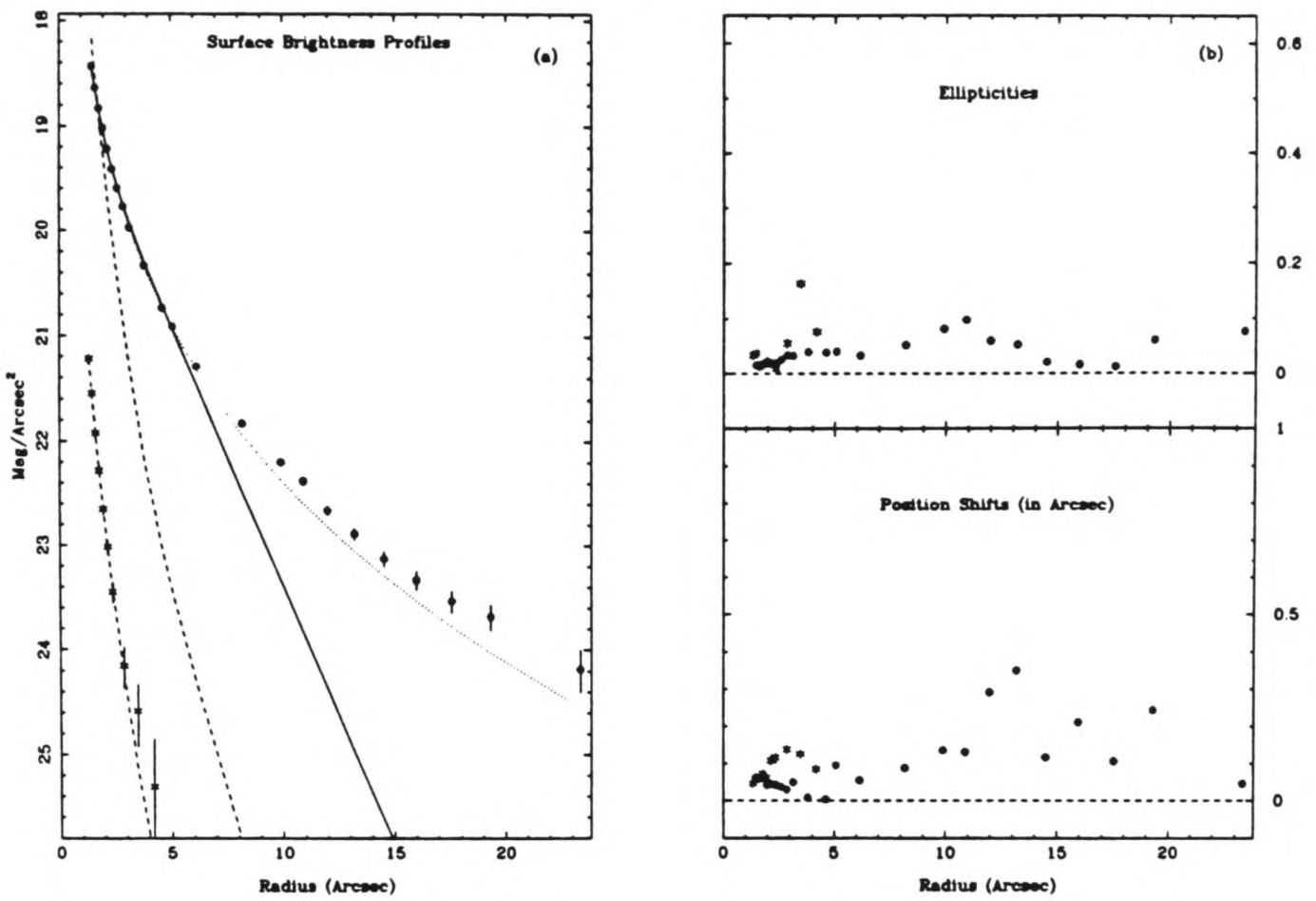

Figure 3.1 (continued)

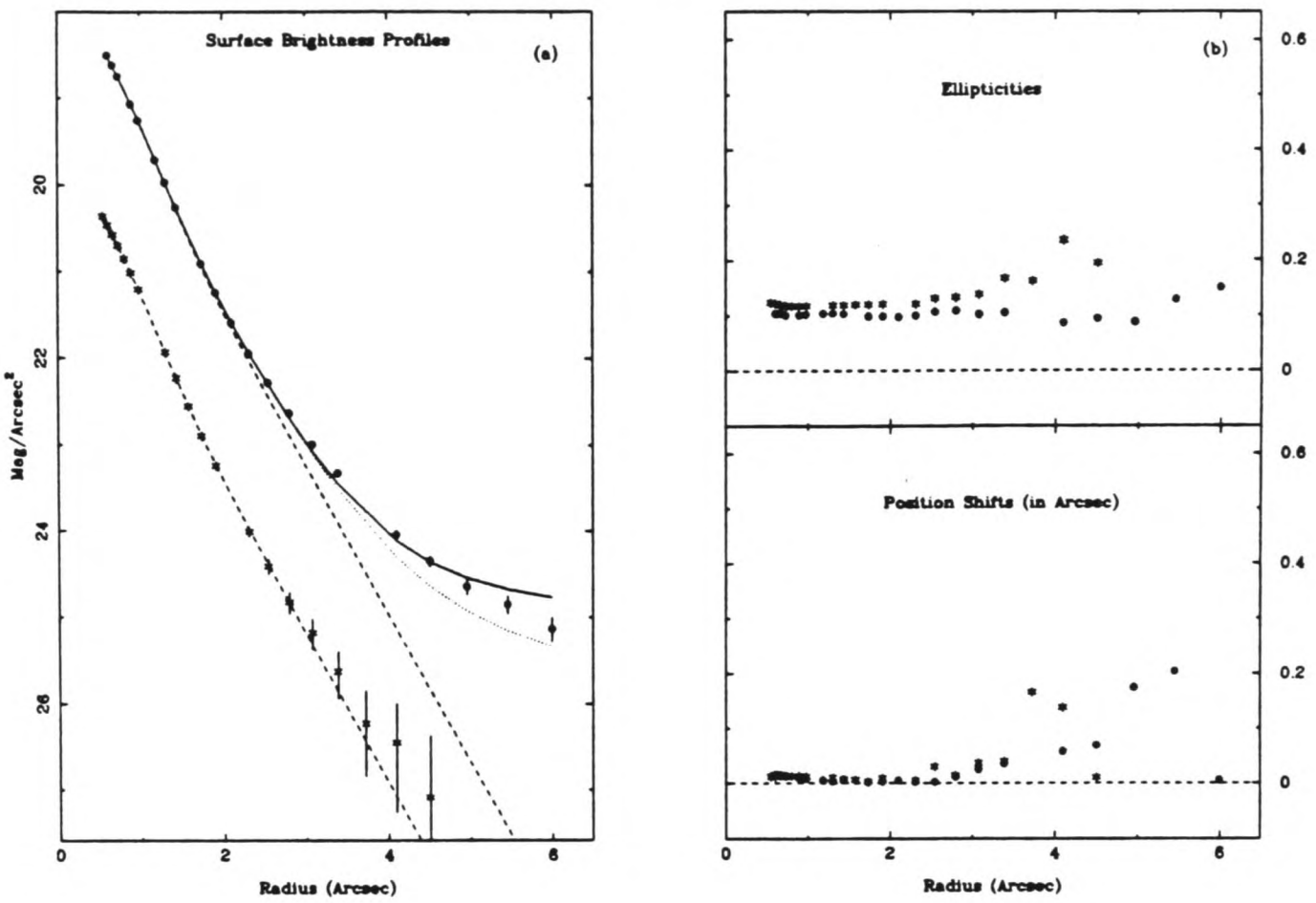

Figure 3.1 (continued)

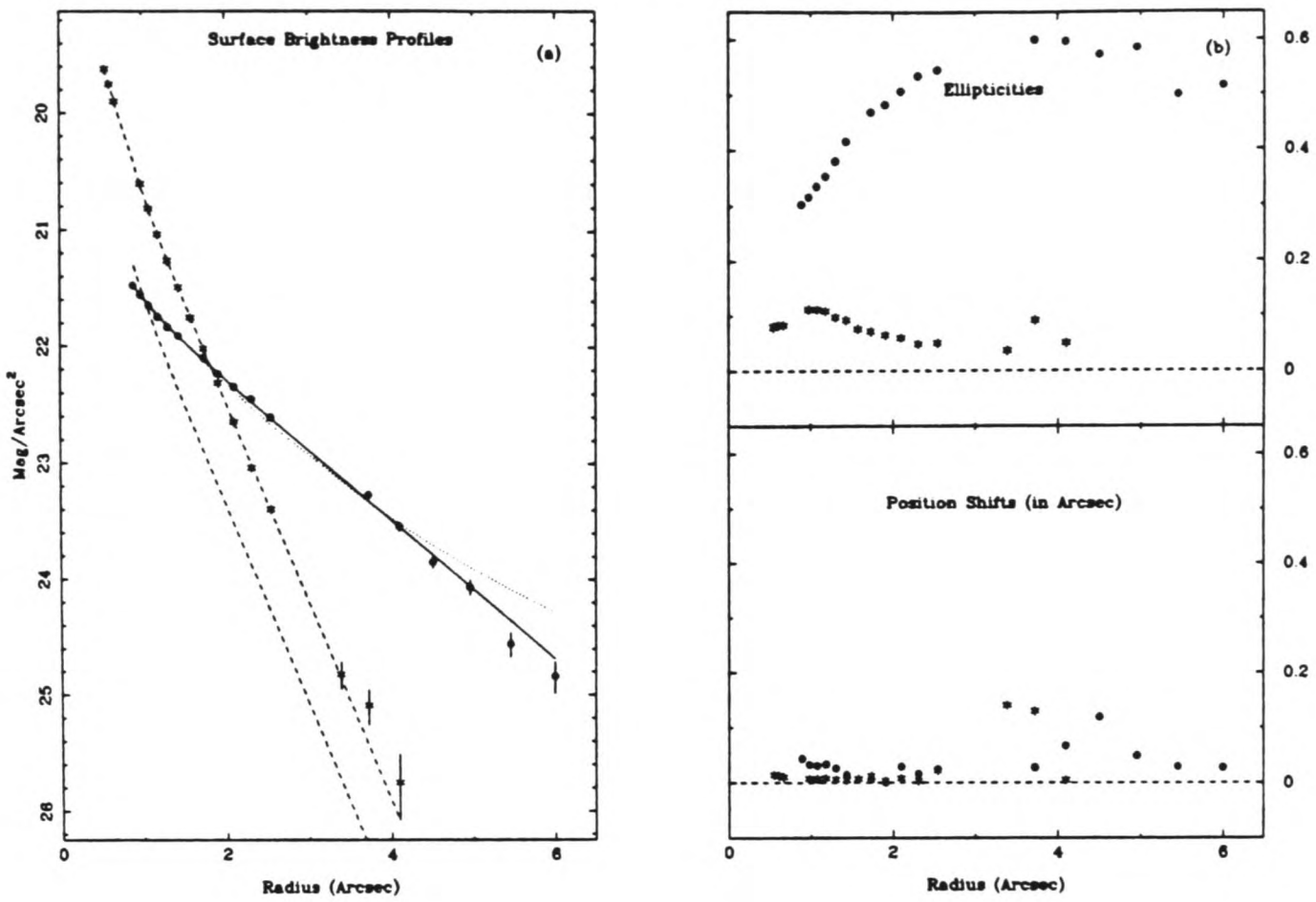

Figure 3.1 (continued)

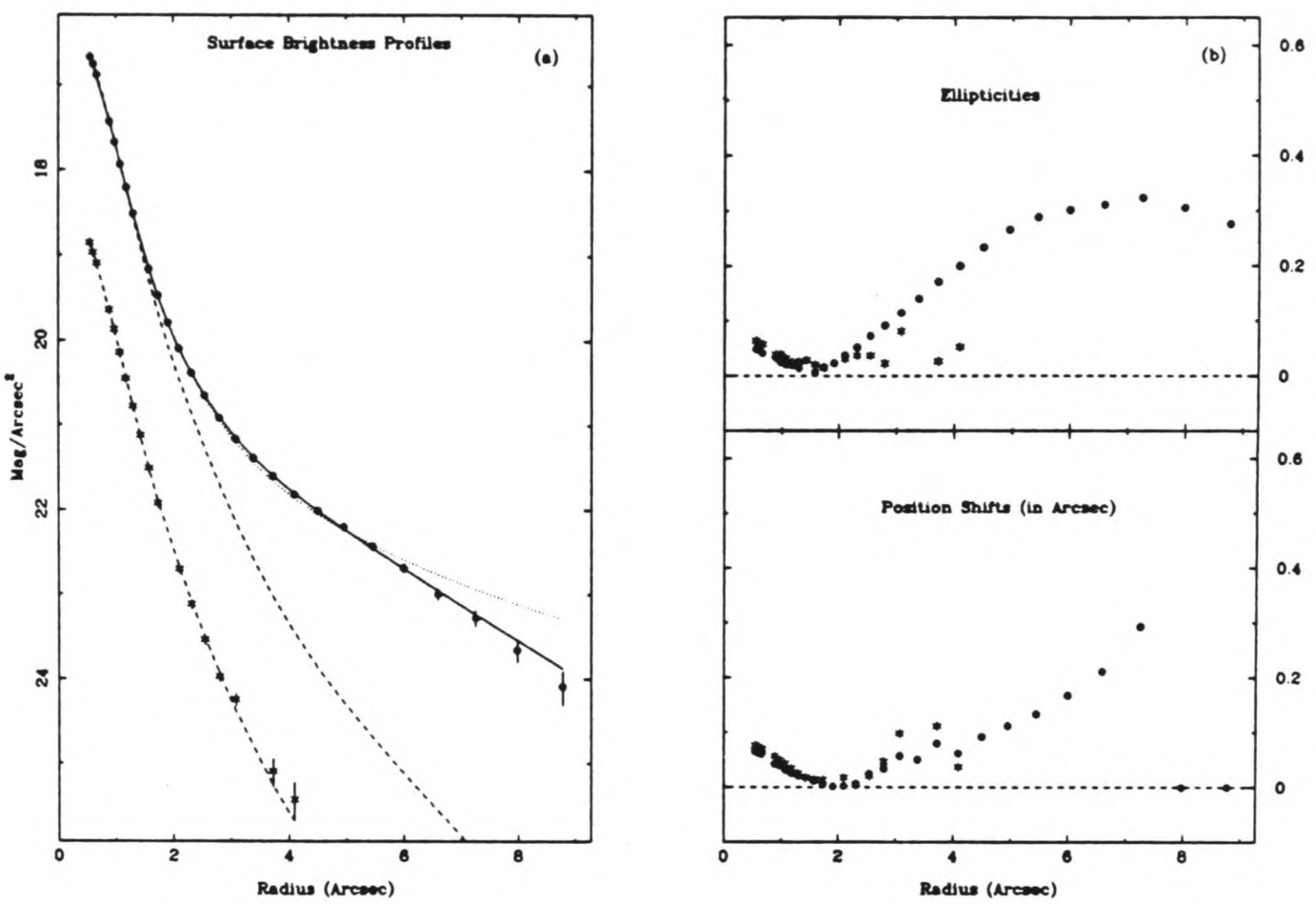

Figure 3.1 (continued)

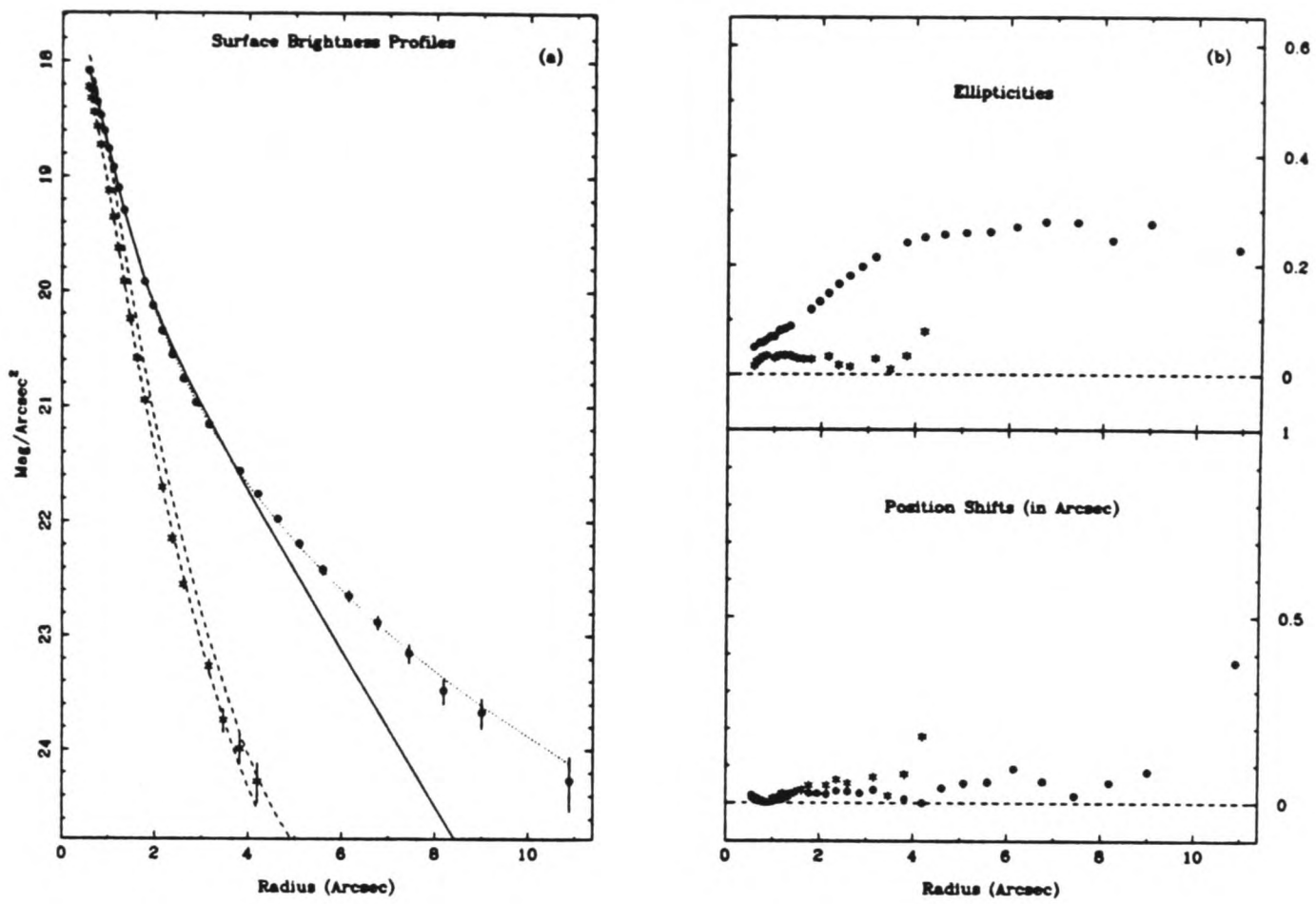

Figure 3.1 (continued)

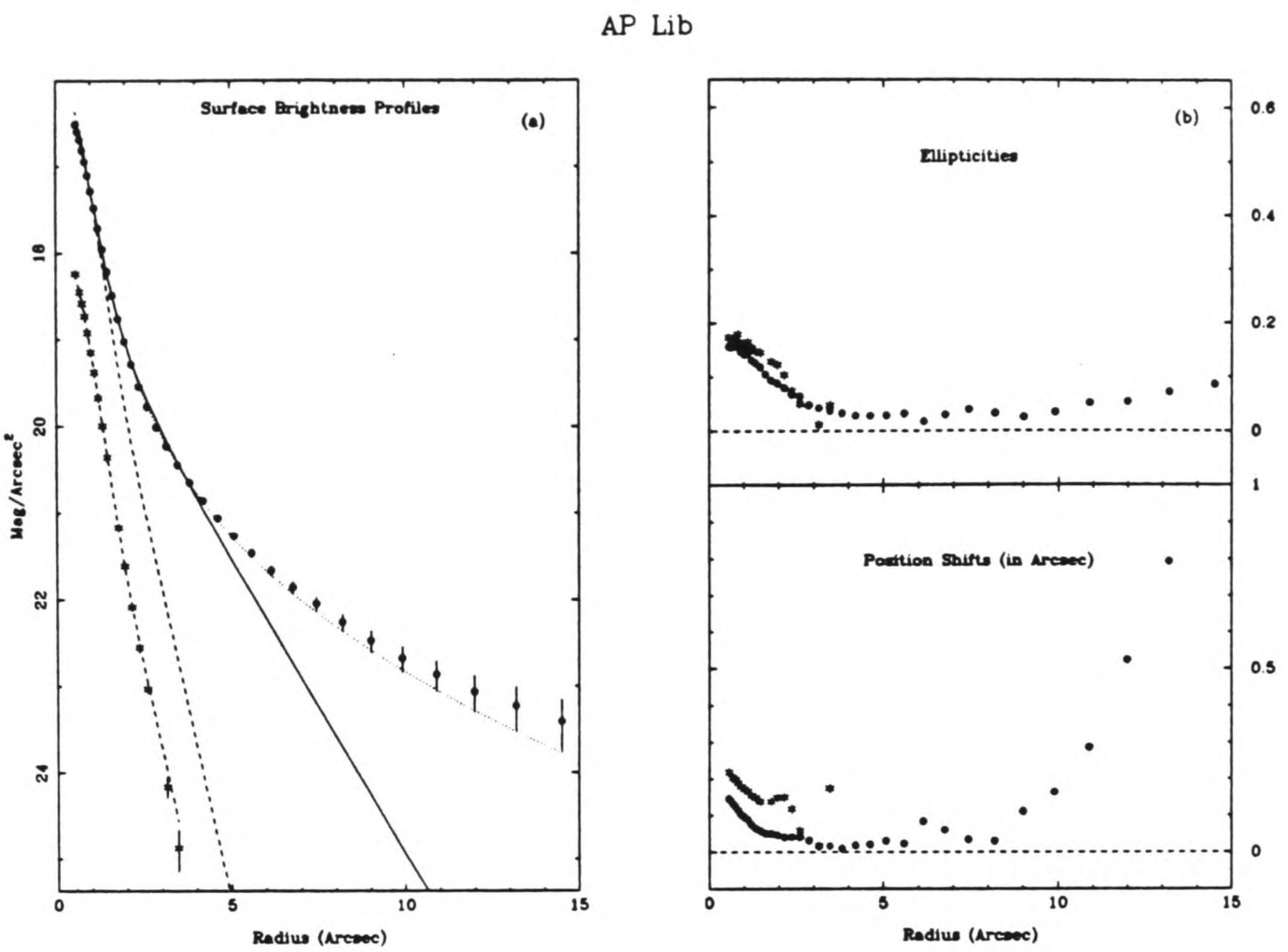

Figure 3.1 (continued)

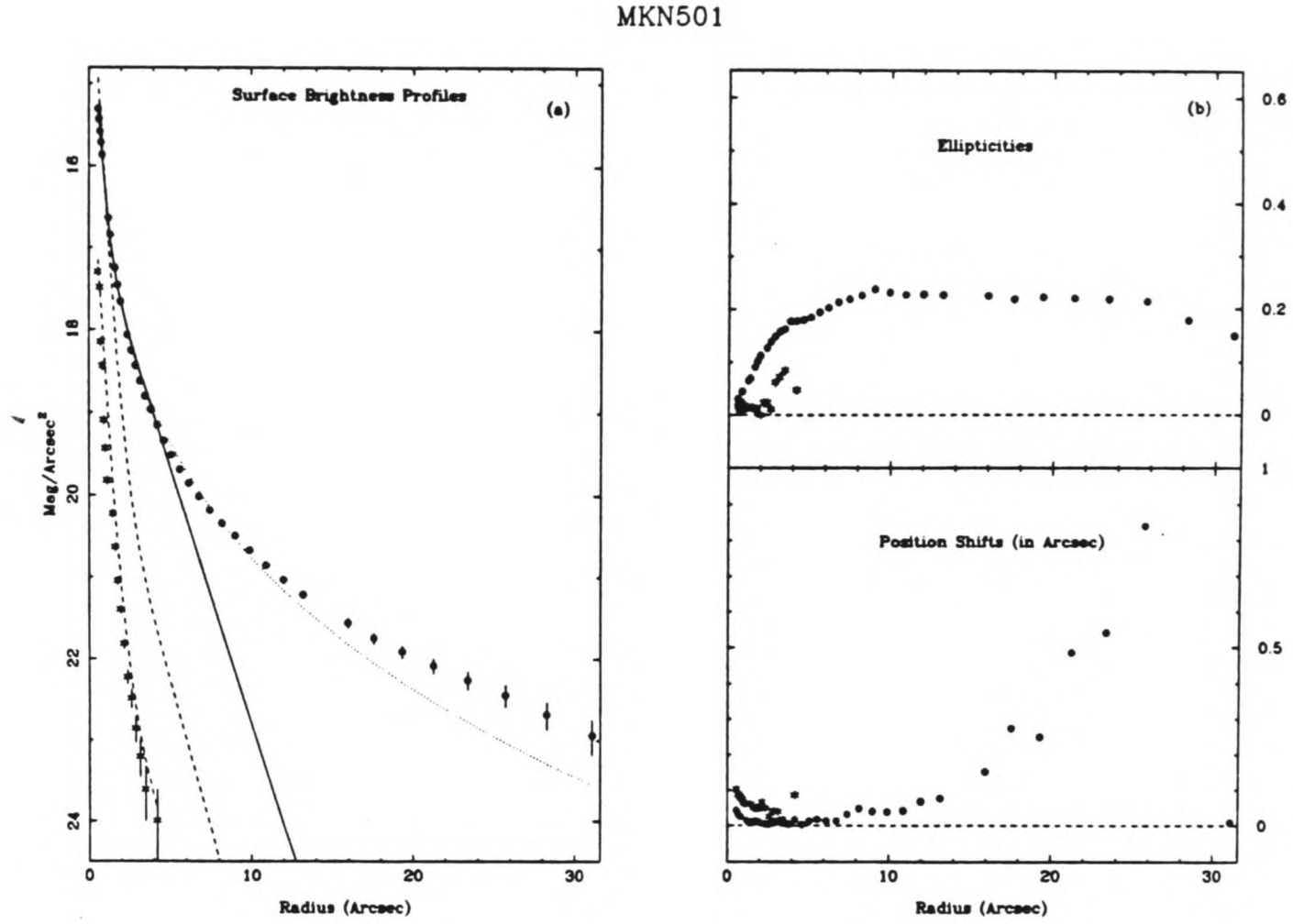

Figure 3.1 (continued)

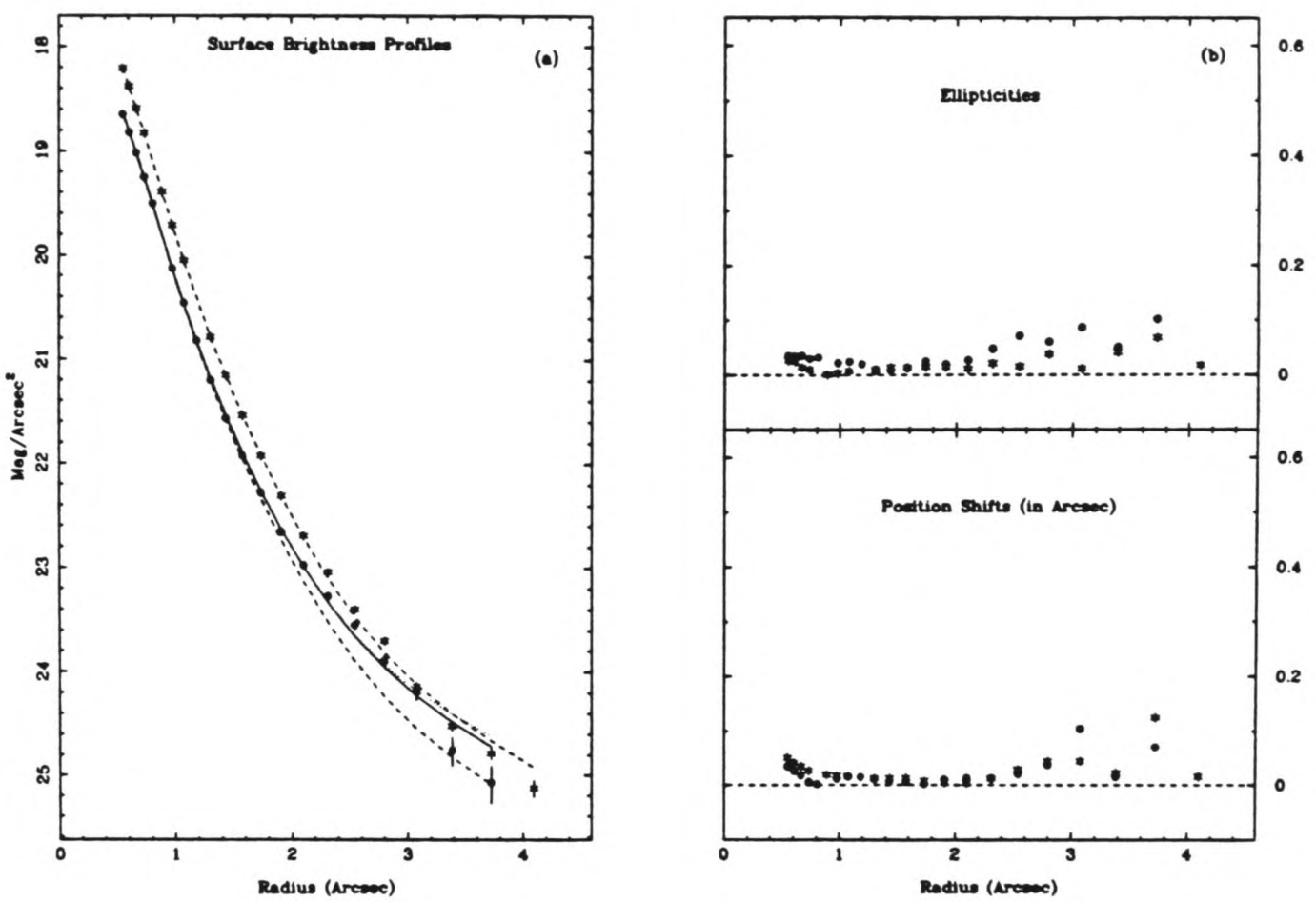

Figure 3.1 (continued)

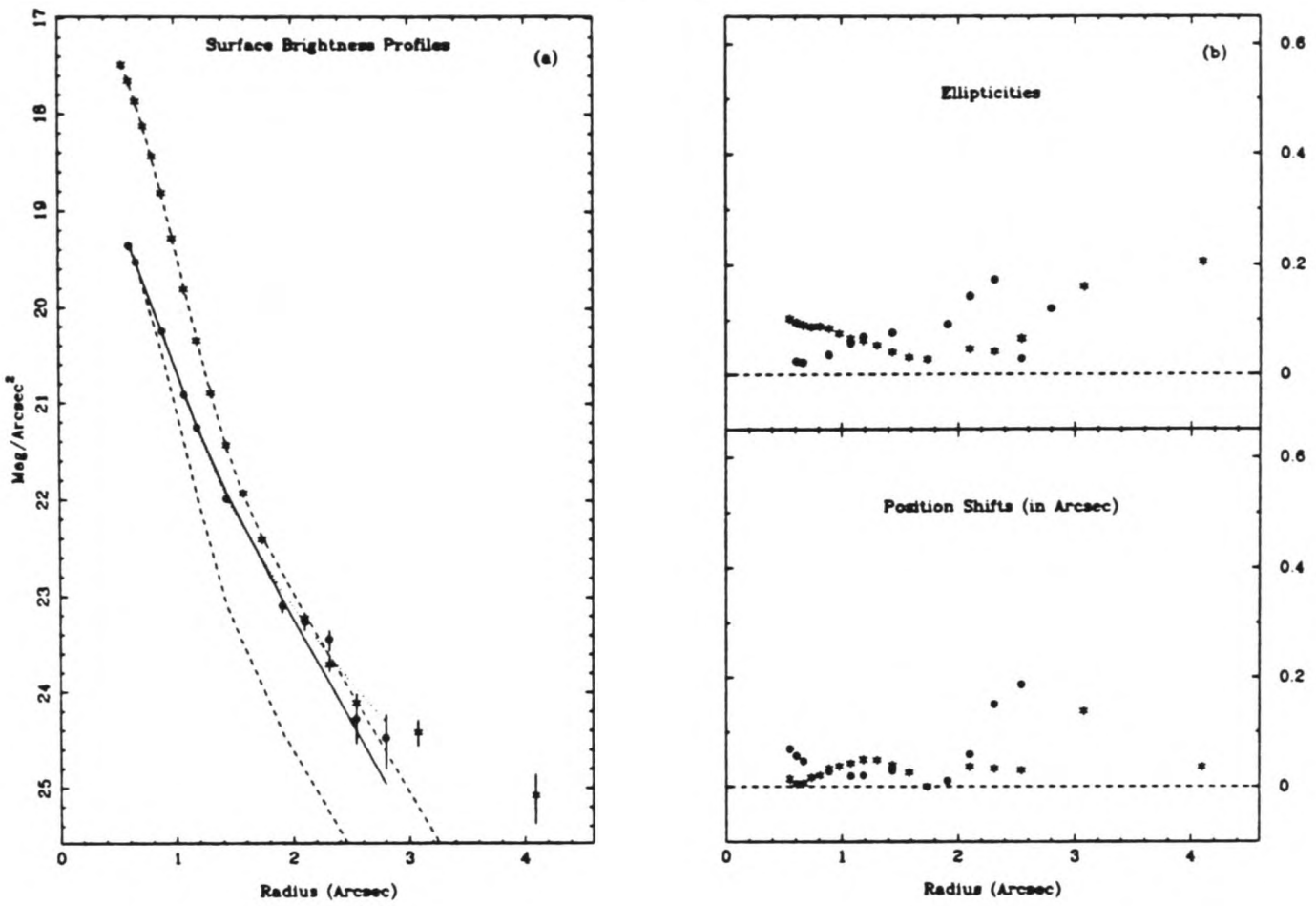

Figure 3.1 (continued)

Chapter Four

PKS1413+135 – MULTIWAVEBAND OBSERVATIONS

INTRODUCTION

Of the two objects classified as discs in the previous chapter, PKS1413+135 is the more compelling example of a disc host. The weak core in this object leads to a more statistically significant F-test disc classification, and the high ellipticity of the host is strong subsidiary evidence in support of this conclusion. The purpose of this chapter is to describe follow-up observations of PKS1413+135 that shed additional light on this enigmatic object.

Section 4.1 describes the basis upon which this object is classified as a BL Lac, and the steps we have taken to ensure that we have correctly identified PKS1413+135 on our CCD frames. Section 4.2 describes the results of additional optical and near infrared imaging observations of this object. Section 4.3 describes how these results fit in with the results of a multi-waveband observing program (being undertaken by McHardy, Robson, and others) to monitor flux variability in this object. Section 4.4 describes the previous precedents for disc host galaxies underlying powerful radio sources. Finally, Section 4.5 summarizes the important results in this chapter.

The host galaxy of PKS1413+135 was studied as part of our CCD imaging survey of BL Lacs, and was classified as a disc. Viewed in retrospect, this unexpected classification seems altogether apppropriate for an object that has exhibited several similarly strange properties: PKS1413+135 has an extremely steep infrared spectrum, is "one of the strongest known emitters of millimetre radiation" (Beichman *et al.* [1981]), and has been described as "among the most variable extragalactic objects known" by Bregman *et al.* [1981].

How does this strange object fit into the picture we have presented in previous chapters, of relativistic beams, elliptical galaxies, and orientation effects? In terms of this standard model, PKS1413+135 can be viewed in three ways. Firstly, this object can be seen as an example of a disc galaxy with relativistic jets (this is our favoured interpretation). After all, radio-loud AGN disc host galaxies are not wholly unprecedented (although they are rare, as discussed in section 4.4 below), and there is certainly no compelling theoretical reason for the formation of jets being restricted to elliptical galaxies (although the denser interstellar medium in late type spirals may inhibit the distance propagated by jets, as discussed in Miyaji, Wilson, and Peŕez-Fournon [1991]). If we accept this view, the standard model remains basically unchallenged, although it has to be broadened somewhat to accept some disc hosts.

An alternative viewpoint is that BL Lac disc hosts are incompatible with the standard model, and therefore there is something fundamentally wrong with this model. We feel because of the precendents for radio-loud disc AGN, and in view of the small number of known BL Lac disc hosts, this viewpoint is overly pessimistic. It is also worth remembering that present lensing model for BL Lacs are inconsistent with the data from our survey.

A final viewpoint is to challenge the interpretation of the observations presented in this thesis, or to challenge the original classification of this object as a BL Lac. We feel

that the disc classification of host galaxy underlying PKS1413+135 is unambiguous, and we have discussed this point at length in the previous chapter. The next section of this thesis describes the basis upon which PKS1413+135 is classified as a BL Lac.

4.1 CLASSIFICATION AND IDENTIFICATION

4.1.1 Discovery observations

The discovery of the radio source PKS1413+135 is reported in Hoskins *et al.* [1972]. The original finding chart for the proposed optical counterpart (also from Hoskins *et al.* [1972]) is reproduced in Figure 4.1 below. An asterism visible on our later CCD frames is superimposed on this finding chart, as an aid to identifying the field. A finding chart is also given in Condon *et al.* [1977], with a different optical counterpart indicated. Later work by Bregman *et al.* [1981] has confirmed the original Parkes finding chart and position, with the optical, infrared, and X-ray positions for this object all agreeing to within measurement error.

4.1.2 Classification as a BL Lac

Classification systems for AGN tend to be subjective and complicated. It is not yet certain that astronomers are today using a physically meaningful classification system for AGN. This is largely a manifestation of our lack of understanding about which of the myriad properties of AGN are truly important. A real-world analogy (too good to be original, but which eluded a reference search) would be a system for motor-vehicle classification based on size or number of wheels versus one based upon colour. The classification criteria can at least be set forward in a reasonably clear fashion, however,

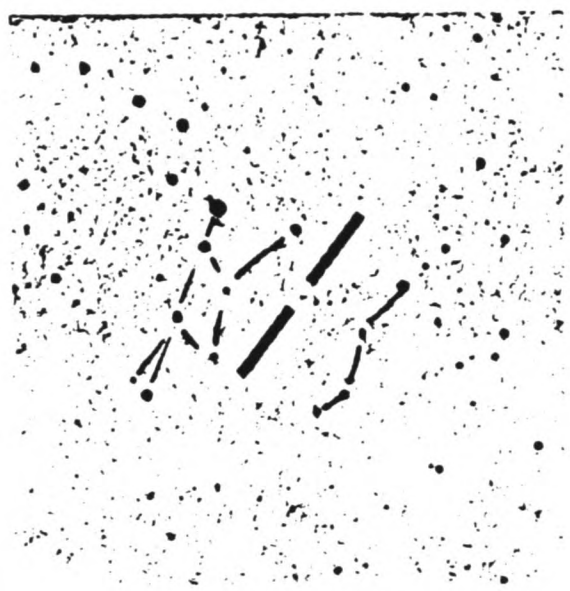

Figure 4.1 Original Parkes finding chart, taken from Hoskins *et al.* [1972].

and a concise illustration of the standard classification system for AGN is given in Impey [1989], and is reproduced in Figure 4.2 below. In addition to illustrating the standard classification system, Impey also intended this figure to illustrate the many biases and selection effects inherent in this classification system. For example, the final classification of many objects depends on the order in which observations are undertaken, and on the limiting sensitivity of the instruments used. That caveat aside, we will show that the "track" on this figure followed by PKS1413+135 does indeed lead to its classification

(first made in Beichman *et al.* [1981]) as a BL Lac.

4.1.2.1 On the track of a BL Lac

An examination of Figure 4.1 shows the optical counterpart to PKS1413+135 to be unresolved (indeed, it is at the limit of detection). A spectrum of PKS1413+135 taken with the MMT is shown if Figure 4.3. There are clearly no strong emission lines. The Calcium H&K break and several weak absorption features corresponding to a redshift of 0.26 are visible, however. Figure 4.4 illustrates the highly variable radio flux from this object, and Table 4.1 (from Bregman *et al.* [1981]) records the highly variable 2.2μ flux from this object. Polarization measurements in January 1980 obtained by Bregman *et al.* showed the infrared flux to be highly polarized (16 $\pm$ 3%), completing the requirements for classification as a BL Lac. Also evident in this figure is the extremely steep infrared-to-optical spectrum; indeed, as well as being classified as a BL Lac, PKS1413+135 is also classified as a "red QSO" by Riecke *et al.* [1979]. The overall track followed by PKS1413+135 on Impey's illustration is shown in Figure 4.5. It is interesting to speculate on what would have resulted if the optical counterpart to the radio source had been more clearly resolved on first inspection (if, for example, a CCD instead of a Palomar Sky Survey plate had been used to identify the optical counterpart to the radio source). It is entirely possible that PKS1413+135 would have been classified as a distant radio galaxy, and its enigmatic properties would still remain undiscovered.

4.1.3 Identification on our CCD frames

Figure 4.6 illustrates V, R, and I band CCD frames of PKS1413+135 and the surrounding field, with PKS1413+135 and reference stars corresponding to those on the finding chart in Figure 4.1 marked. The identification of PKS1413+135 is unambiguous. As a further check, the position of PKS1413+135 on these CCD frames was determined

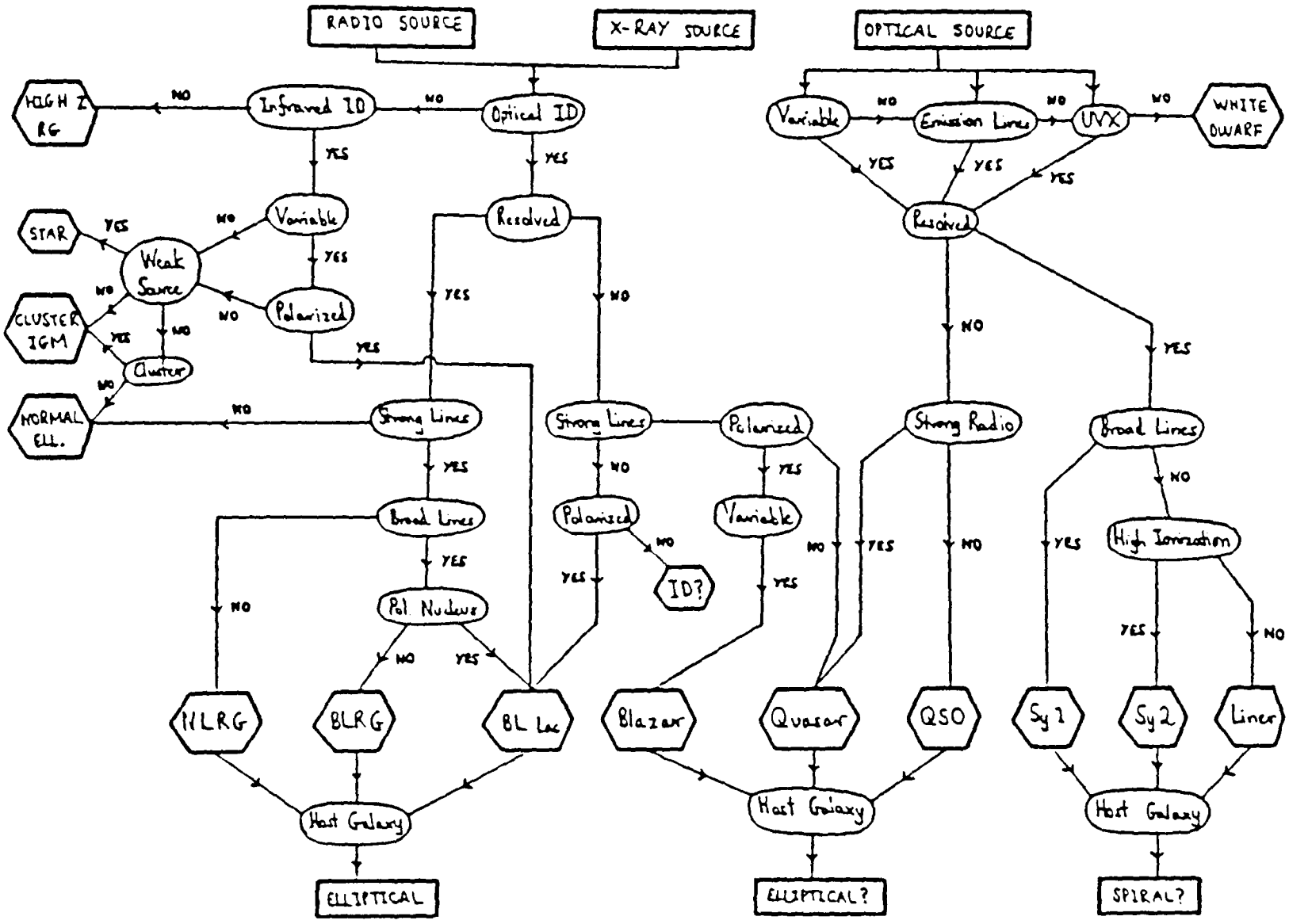

Figure 4.2 Flowchart illustrating the steps toward classifying an AGN. Taken from Impey [1989].

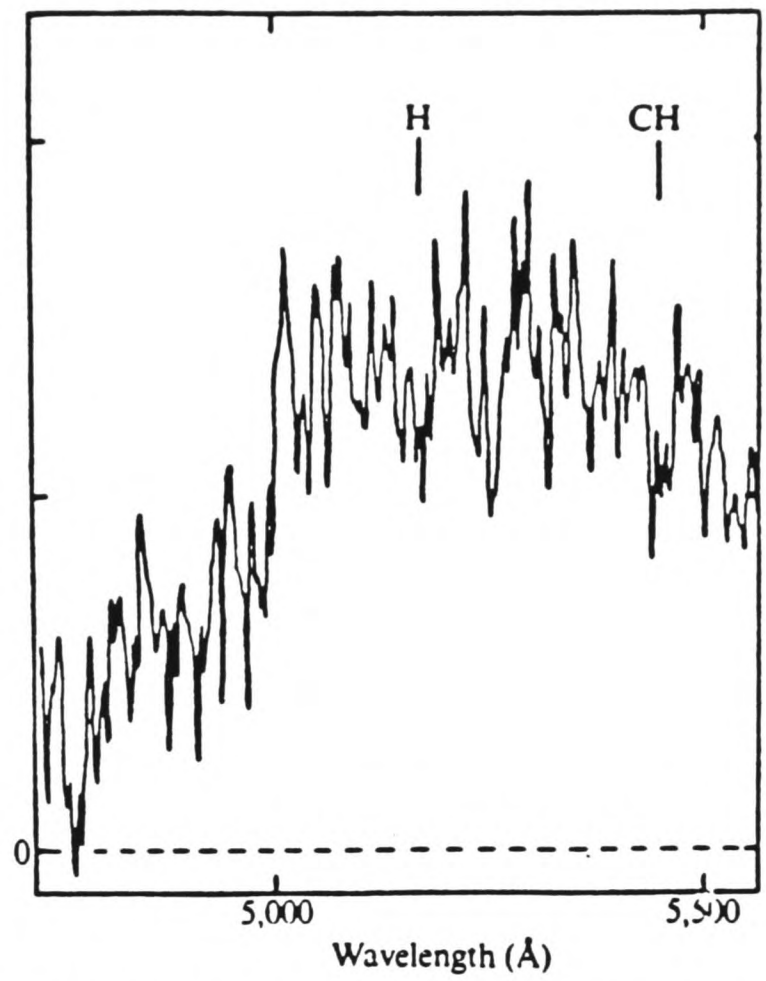

Fig. 3 The clear break at 5,000 Å in the galaxy around 1413+135 is interpreted as the H and K break redshifted by $z = 0.26$. The $H\delta$ and CH absorption features, denoted here by H and CH, appear weakly in this spectrum. The spectral resolution is ~10 Å, and the observations were made through a 2.5 arcs round aperture.

Figure 4.3 Spectrum of PKS1413+135, taken from Bregman *et al.* [1981].

using a laser-interferometric measuring engine (by Brin Cooke at the University of Leicester), and was found to be in excellent agreement with the radio, infrared, optical, and X-ray positions given for this object (Bregman *et al.* [1981]).

Table 1 Variability of 1413+135 at 2.2 μm

Date	Flux (mJy)	Ref.
10 February 1979	3.32±0.10	2
7 March 1979	1.72±0.12	2
8 March 1979	1.98±0.18	2
24 January 1980	5.5 ±0.3	This work
25 January 1980	4.6 ±0.2	This work
26 January 1980	3.7 ±0.2	This work
10 February 1980	2.55±0.2	7
27 February 1980	4.2 ±0.2	This work
26 April 1980	2.35±0.2	This work
21 May 1980	2.0 ±0.2	This work
22 May 1980	1.8 ±0.15	This work
23 May 1980	2.6 ±0.2	This work
21 July 1980	1.71±0.09	7
25 July 1980	2.15±0.20	7
4 August 1980	1.98±0.10	7
5 August 1980	1.76±0.14	7

Table 4.1 2.2μ flux from PKS1413+135. Taken from Bregman *et al.* [1981]

4.2 MULTICOLOUR IMAGING

Table 4.2 summarizes our imaging observations of PKS1413+135. The R band image has been discussed at length in the previous chapter. The 1300s I band image was obtained on our behalf by A. C. Fabian and R. M. Johnstone from the University of Cambridge, using the 2.5m Isaac Newton Telescope on La Palma in 1.3 arcsecond FWHM seeing. Problems with the telescope's auto-guider restricted the length of the exposure

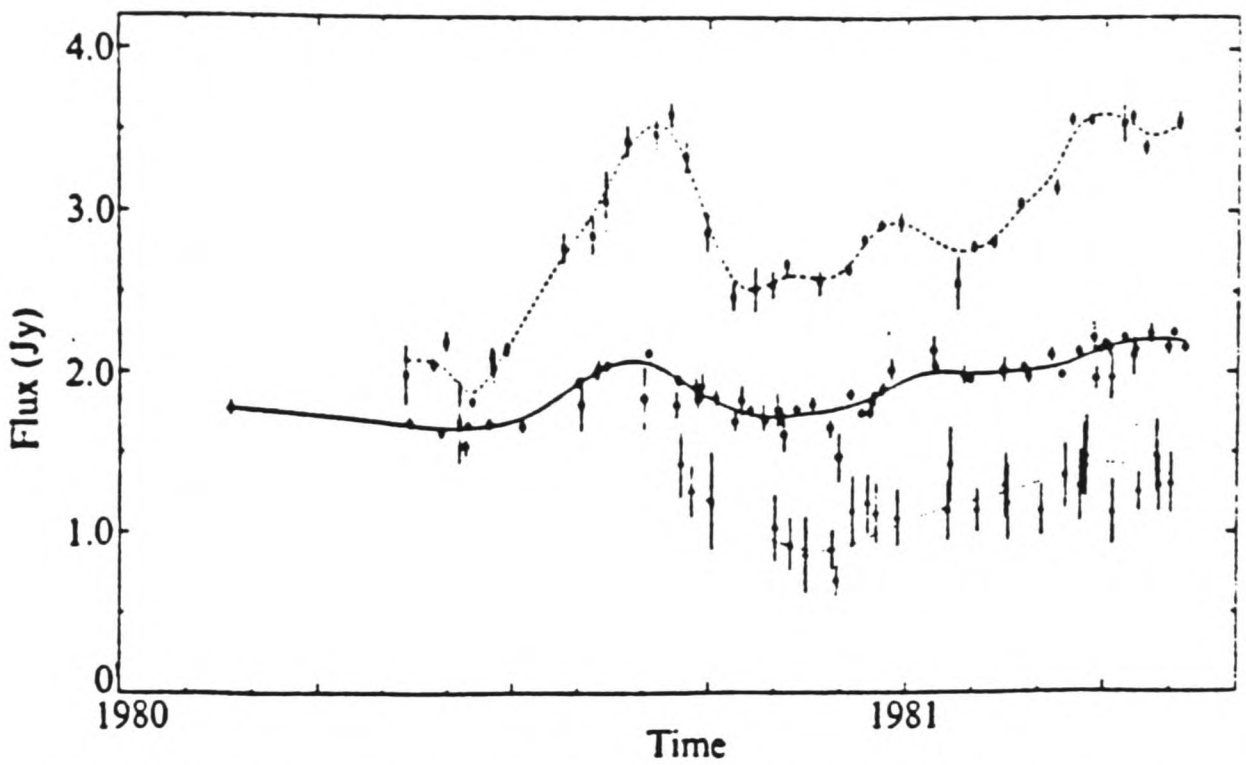

Fig. 2 The radio observations of 1413 + 135 show that this source is extremely active at 14.5 GHz (×) and less active at 8 GHz (○) and 4.8 GHz (△). The radio spectrum, which is always inverted, becomes most steeply inverted during outbursts ($\alpha = 0.9$). The rate of flux increase during the June–August 1980 and February–April 1981 outburst are nearly identical.

Figure 4.4 Radio variability of PKS1413+135, taken from Bregman *et al.* [1981]

times for individual frames, so thirteen 100s exposures were taken. These exposures were bias-subtracted, flat-fielded (with twilight flats), and co-aligned before being added to make a final image. The B and V band exposures were obtained on our behalf by our collaborators from the Massachussetts Institute of Technology, P. C. Mock and R. K. Vanderspeck, using the 2.4m Michigan-Dartmouth-MIT Telescope. The observations were made using the BRICC CCD Camera and a Lincoln Labs 840 x 840 pixel CCD. Subsequent reduction was undertaken by the MIT observers using the automated "Autoflat"

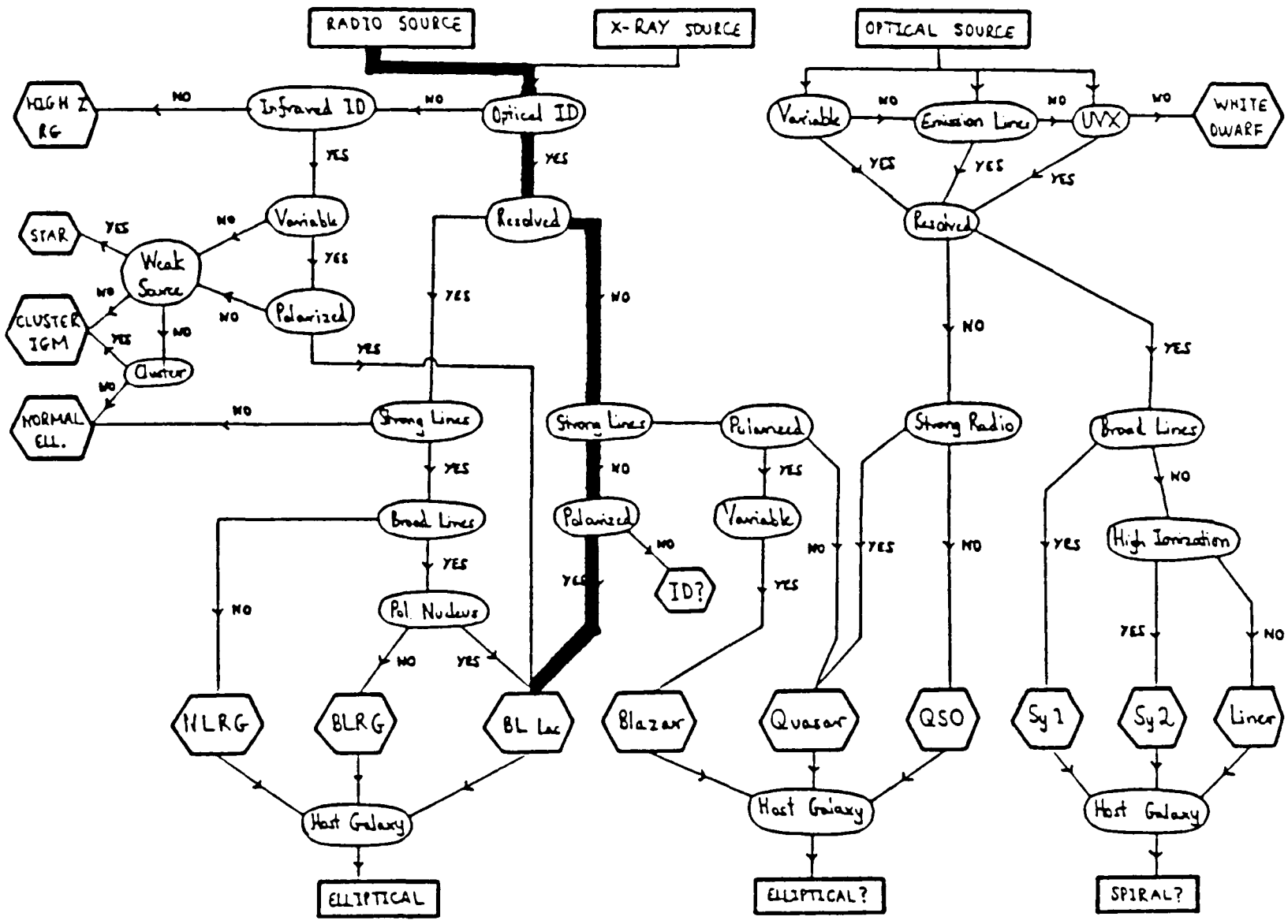

Figure 4.5 The path followed by PKS1413+135 on the Impey [1989] flowchart shown in Figure 4.1.

routine.

Finally, PKS1413+135 was also imaged for us in K-band during service observations with the 3.8m UKIRT infrared telescope (Figure 4.7). A total on-source integration time of 600s was obtained. The observations were carried out using the standard procedure of alternating short source exposures with nearby sky exposures several times during the total integration in order to generate a highly accurate flat field.

The total magnitudes for PKS1413+135 in the various bands were obtained by

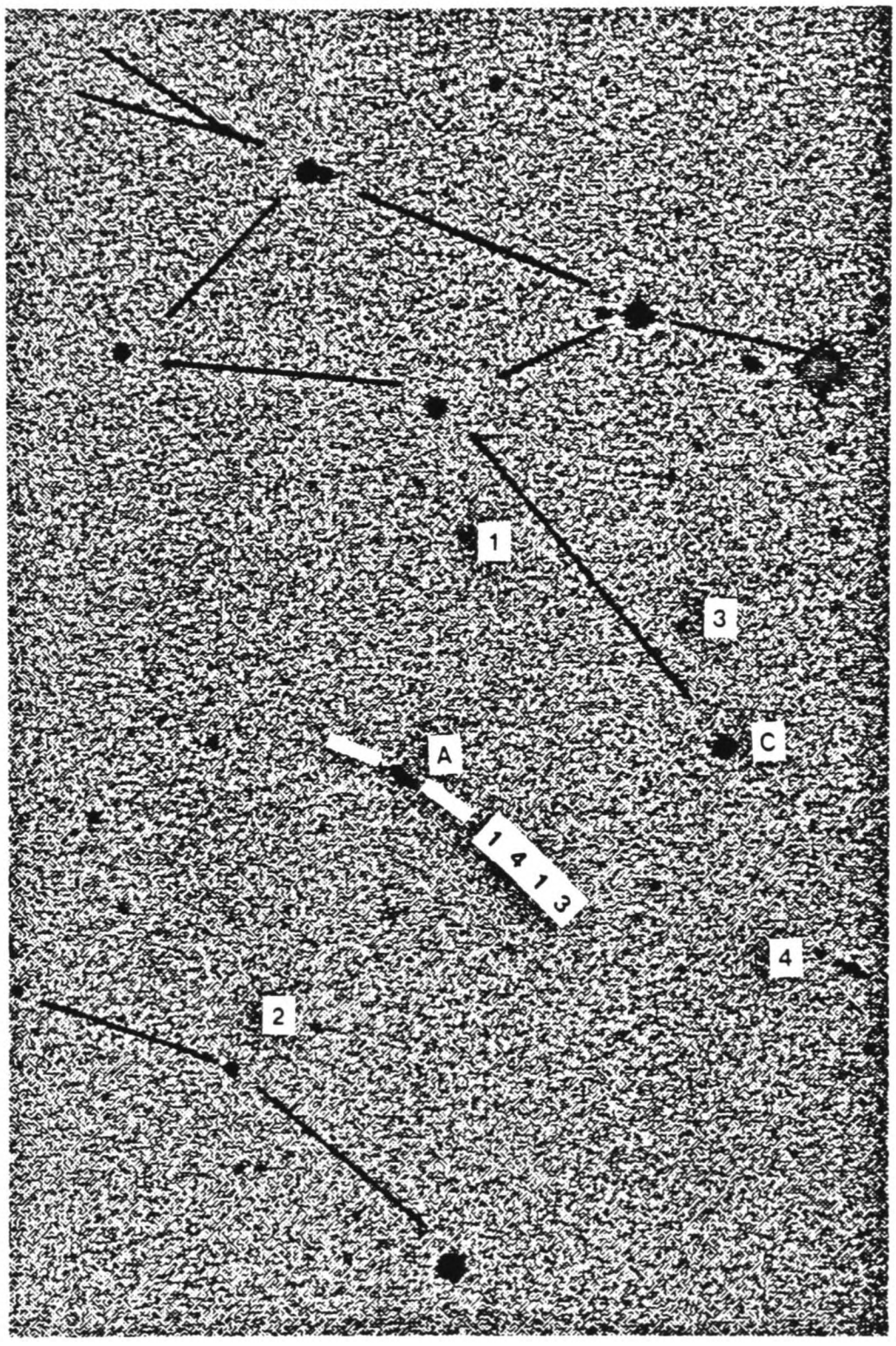

Figure 4.6(a) I band CCD frame of PKS1413+135. Reference stars corresponding to those on Figure 4.6(b) and Figure 4.6(c) are marked, and an asterism corresponding to that drawn on the finding chart in Figure 4.1 is also shown. In keeping with the ancient spirit of those who mapped out the constellations, we note in passing that this asterism bears a remarkable resemblance to the figure of a giant dinosaur devouring the city of Tokyo.

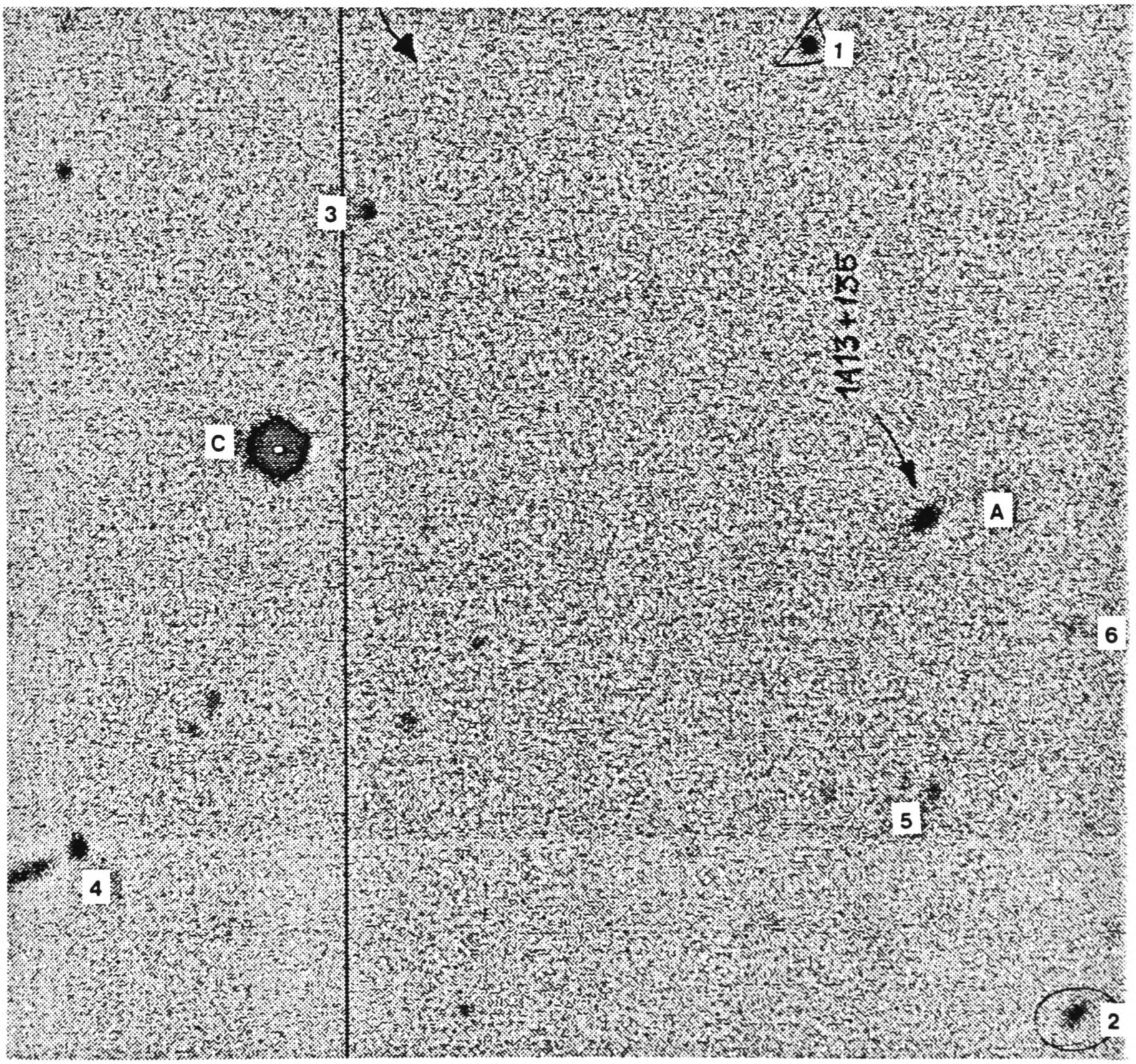

Figure 4.6(b) V band CCD frame of PKS1413+135.

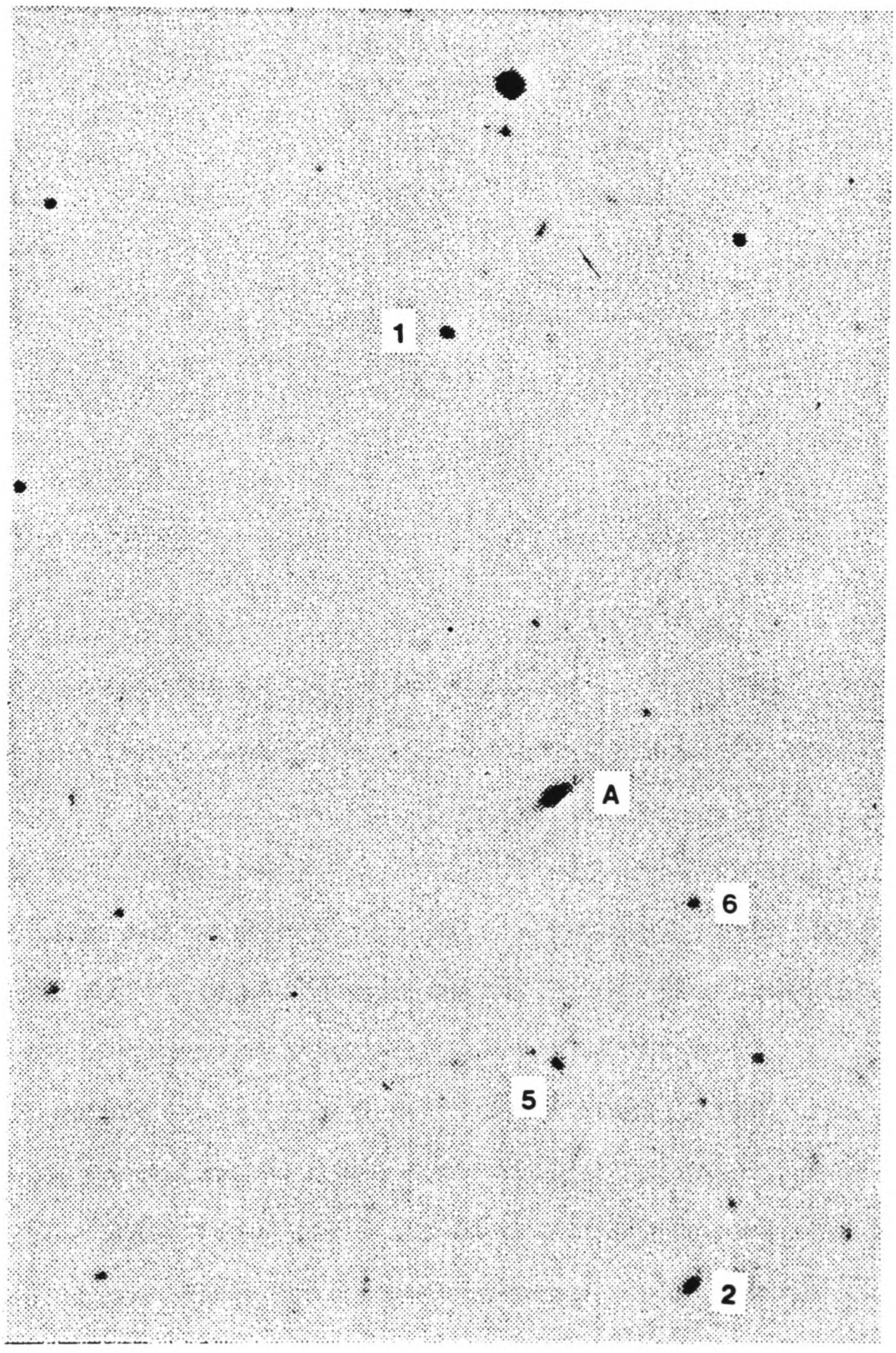

Figure 4.6(c) R band CCD frame of PKS1413+135.

Table 4.2 Summary of Observations

Date	Filter	Exposure (seconds)	Pixel Scale (arcsec/pixel)	Telescope
11 April 1989	R	1500	0.27	4.2m WHT
2 June 1989	B	7200	0.25	2.4m MDM
2 June 1989	V	3600	0.25	2.4m MDMI
2 July 1989	I	1300	0.54	2.5m INT
10 Feb 1990	K	600	0.60	3.6m UKIRT

synthetic aperture photometry on the images, and were found to be: $m_B = 20.6 \pm 0.2$, $m_V = 19.6 \pm 0.2$, $m_R = 18.6 \pm 0.1$, $m_I = 18.1 \pm 0.1$, and $m_K = 13.4 \pm 0.1$.

B, V, R, and I band surface brightness profiles from our imaging observation are shown in Figure 4.8. The R and I band images were obtained at a reasonably high signal to noise level, while the faintness of host in B and V band results in very noisy profiles. The K-band image exhibits slight evidence of an underlying host, but the lack of an adequate reference PSF does not allow us to rule out that this structure is ghosting from the IRCAM optics, so no surface brightness profile was extracted.

Elliptical and disc models were fit to the R and I band profiles, in the manner described in the previous chapter (the B and V band profiles were too noisy to allow this). In addition to disc + point source and elliptical + point source models described in the previous chapter, we also fitted a disc + deVaucouleurs law bulge + point source model to the profiles. The results are summarized in Table 4.3. It is immediately apparent that elliptical models give very poor fits to the data. All disc models gave acceptable fits (corresponding to absolute magnitudes around -23.0, as described in the previous

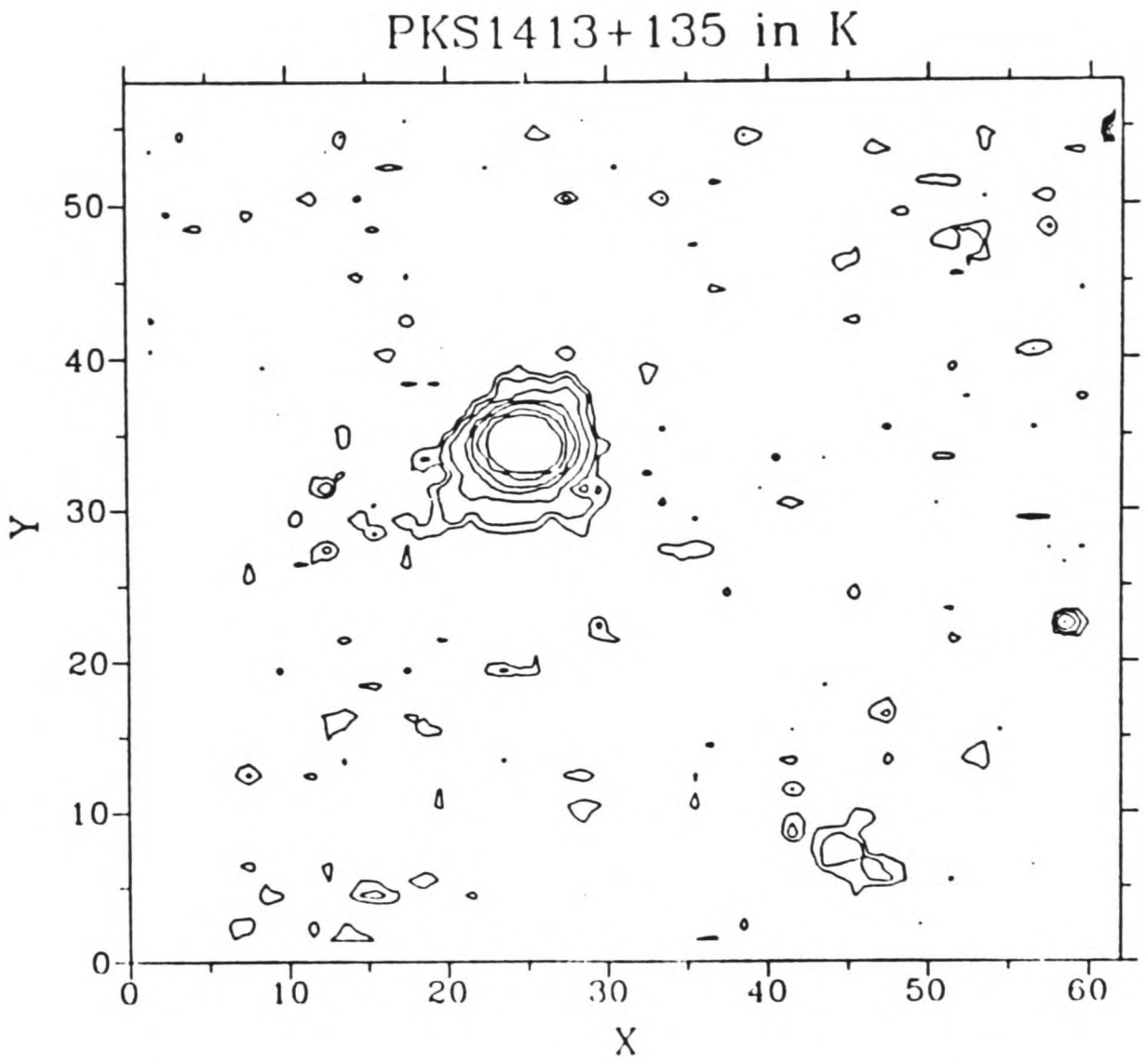

Figure 4.7 600s K band image of PKS1413+135 obtained with IRCAM 1 on UKIRT. Axes are in 0.6" pixels, and contours are at 3,5,9,17,25,43, and 75 counts/pixel above sky. North is up, and East to the left.

chapter), and we therefore cannot unambiguously determine the bulge contribution to the profile. We can, however, calculate a lower limit to the disc-to-bulge ratio on the basis of a pure disc + bulge fit to the profile (model [2] in Table 4.3). The disc-to-bulge ratio is defined (Mihalas and Binney [1981]) by:

$$\frac{D}{B} = 0.28\left(\frac{r_s}{r_e}\right)^2 \frac{\Sigma_s}{\Sigma_e} \qquad [4.1]$$

where Σ_e is the surface brightness at the effective radius for a deVaucouleurs law profile,

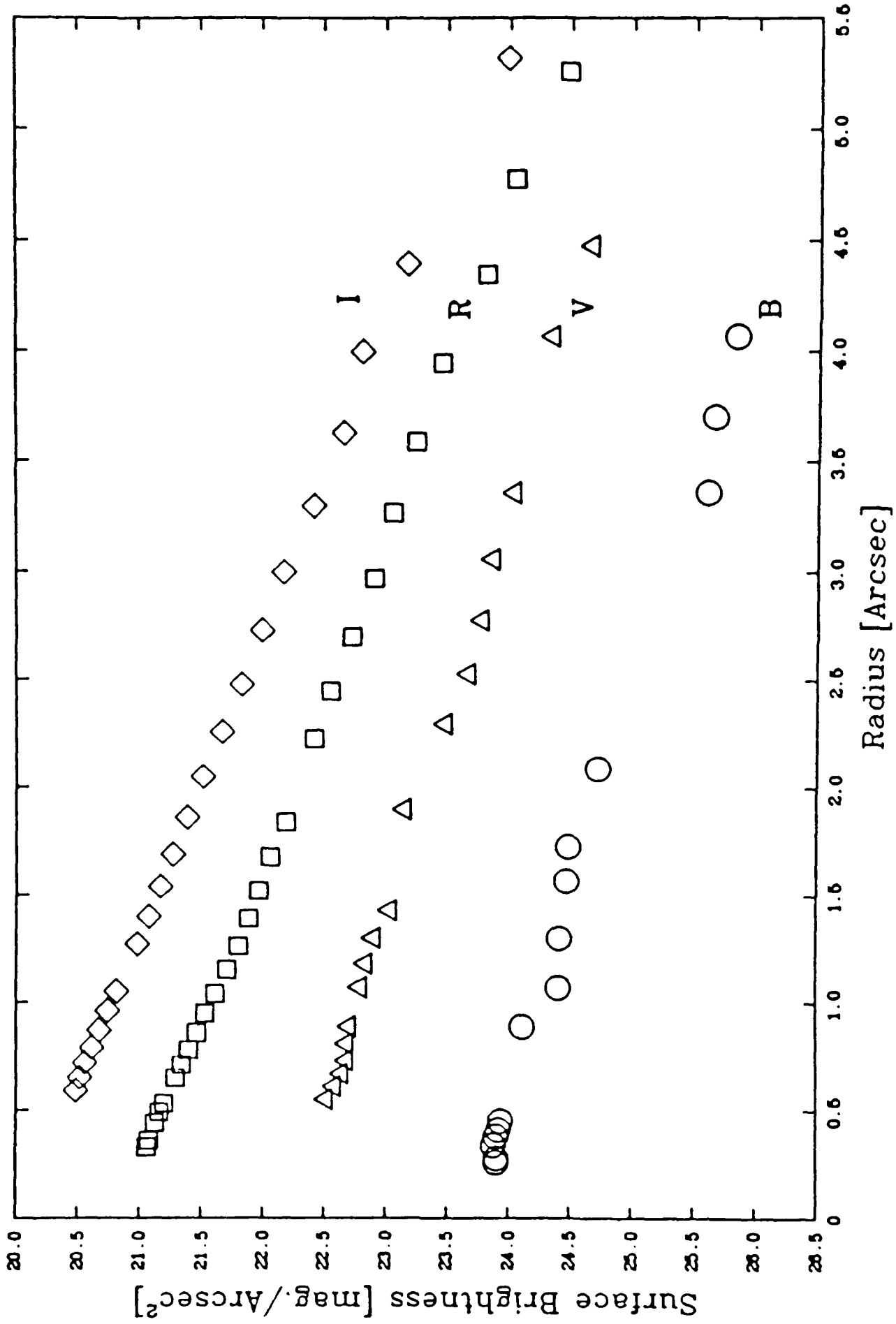

Figure 4.8 B, V, R, and I band surface brightness profiles of PKS1413+135.

Σ_s is the central surface brightness for an exponential law profile, r_e is the deVaucouleurs law effective radius, and r_s is the exponential radius. We obtain disc-to-bulge ratios around 5 for the R and I band images, suggestive of an Sb-c disc host.

Table 4.3: Summary of Radial Profile Model Fits

Model	Reduced χ^2 [a]	Σ_e (mag/arcsec^2)	Σ_s	r_e (arcsec)	r_s	Notes
R-Band:						
Disk+Point Source	9.1	-	20.62	-	1.41	
Disk+Bulge	1	24.17	21.06	1.90	1.67	$D/B = 3.8$
Disk+Point Source+Bulge	1.05	24.17	21.06	1.90	1.71	[b]
Bulge+Point Source	22.9	25.5	-	14.3	-	[b]
Bulge	22.0	25.5	-	14.3	-	
I-Band:						
Disk+Point Source	2.0	-	19.79	-	1.39	
Disk+Bulge	1	22.28	20.01	0.86	1.50	$D/B = 6.9$
Disk+Point Source+Bulge	0.9	22.62	19.97	0.94	1.47	$D/B = 7.9$
Bulge+Point Source	35	23.97	-	8.25	-	[b]
Bulge	33	23.97	-	8.25	-	

Notes:
[a] Reduced χ^2 values relative to Disk + Bulge model.
[b] Point source disappears in this model.

Given the best-fitting models in Table 4.3, we estimate that $m_R^{\rm disc} = 18.9 \pm 0.3$, and $m_I^{\rm disc} = 18.3 \pm 0.3$, and $m_R^{\rm bulge} = 20.6 \pm 0.3$, and $m_I^{\rm bulge} = 20.0 \pm 0.3$. At a redshift of 0.26, the K-correction effectively shifts the rest bandwidth by almost exactly a single colour band (i.e. observed R band corresponds to an emitted V band), so we can directly convert our observed colours to rest frame colours, and compare these with the colours

of standard galaxies of a given Hubble type. Table 4.4 shows rest frame colours for PKS1413+135 for various amounts of reddening, along with typical colours for spiral and elliptical galaxies. Unfortunately, the errors on our magnitude estimates for the host galaxy underlying PKS1413+135 preclude our being able to draw strong conclusions from our colour data, but the data are reasonably consistent with the (B-V) and (R-I) colours of an unreddened early type galaxy. The rest frame (U-B) colour does not agree well with any galaxy type, but this is unsurprising given the errors on our magnitude estimates. No amount of reddening improves the agreement between our colours and those of standard galaxies.

Table 4.4 Approximate Rest Frame Colours

A_V	U-B	B-V	V-R
0	1.0	0.9	0.6
1	0.70	0.57	0.27
2	0.40	0.24	-0.06
3	0.10	-0.09	-0.39
4	-0.20	-0.42	-0.72
5	-0.50	-0.75	-1.05
E0	0.45	0.90	0.89
Sc	-0.10	0.50	0.80

Bregman *et al.* [1981] have identified the weak features present present in the spectrum of PKS1413+135 with those of an early type galaxy. Given the marginally better

agreement of our host colours to an early type galaxy, we tentatively classify the host underlying PKS1413+135 as an S0b-c galaxy (using the DDO classification scheme of van den Bergh [1960, 1972, 1976]), rather than as an Sb-c system, although the latter classification is certainly possible. Higher resolution observations capable of determining host colours more accurately are needed in order to test this point. It is also worth noting that in the only systematic studies of the colours of the QSO hosts, Hutchings [1987] and Hutchings, Janson, and Neff [1989] found anomalous colours for many hosts, in the sense that early type hosts exhibited bluish colours, and late type hosts reddish colours.

Assuming that PKS1413+135 is a round disc galaxy, the observed ellipticity is consistent with an inclination near 66 degrees. This is not inconsistent with beaming models, however, because studies of radio jets in elliptical galaxies rarely show a correlation between the axis of the host galaxy and the jet axis (Jenkins [1981]). Total radio luminosity is usually correlated with optical absolute magnitude in elliptical galaxies, however. If we make the (speculative) assumption that the radio luminosity is correlated with the bulge luminosity in PKS1413+135, the high disc to bulge ratio in this source suggests weak total radio luminosity. We would then expect that the relativistic jet does not extend to large scales.

4.3 MULTIWAVEBAND PHOTOMETRY

Figure 4.9, taken from M^{c}Hardy *et al.* [1991], superimposes the optical and near IR flux densities (derived from the magnitudes given in the chapter) for PKS1413+135 on the multiwaveband data given in Bregman *et al.* [1981] and Beichman *et al.* [1991], along with submillimetre flux densities and a single Exosat X-ray flux density.

(Please note that my involvement in this particular aspect of our study was limited to reducing and analysing the optical and near infrared data for PKS1413+135. The sub-millimetre data reduction and analysis presented here was undertaken by Ian McHardy, and is part of an ongoing Blazar monitoring program being coordinated by Ian Robson. We are grateful to Ian Robson for allowing us to use these results in advance of publication.)

These flux densities are also given in Table 4.5. M^{c}Hardy has fitted a power law with an exponential cut-off to the high frequency radio and infrared points (assuming an optically thin source), i.e.:

$$S(\nu) \propto \nu^{-0.5} \exp\left(\frac{\nu}{\nu_s}\right) \qquad [4.2]$$

where $\nu_s = 4 \cdot 10^{13}$ Hz. It is clear that the contribution from the extremely steep core spectrum dominates the host galaxy contribution from the radio through to the infrared, but that this contribution begins to become small at optical wavelengths. The "hump" in Figure 4.9 near 10^{15} Hz is clearly due to the contribution from the host galaxy beginning to dominate the spectrum.

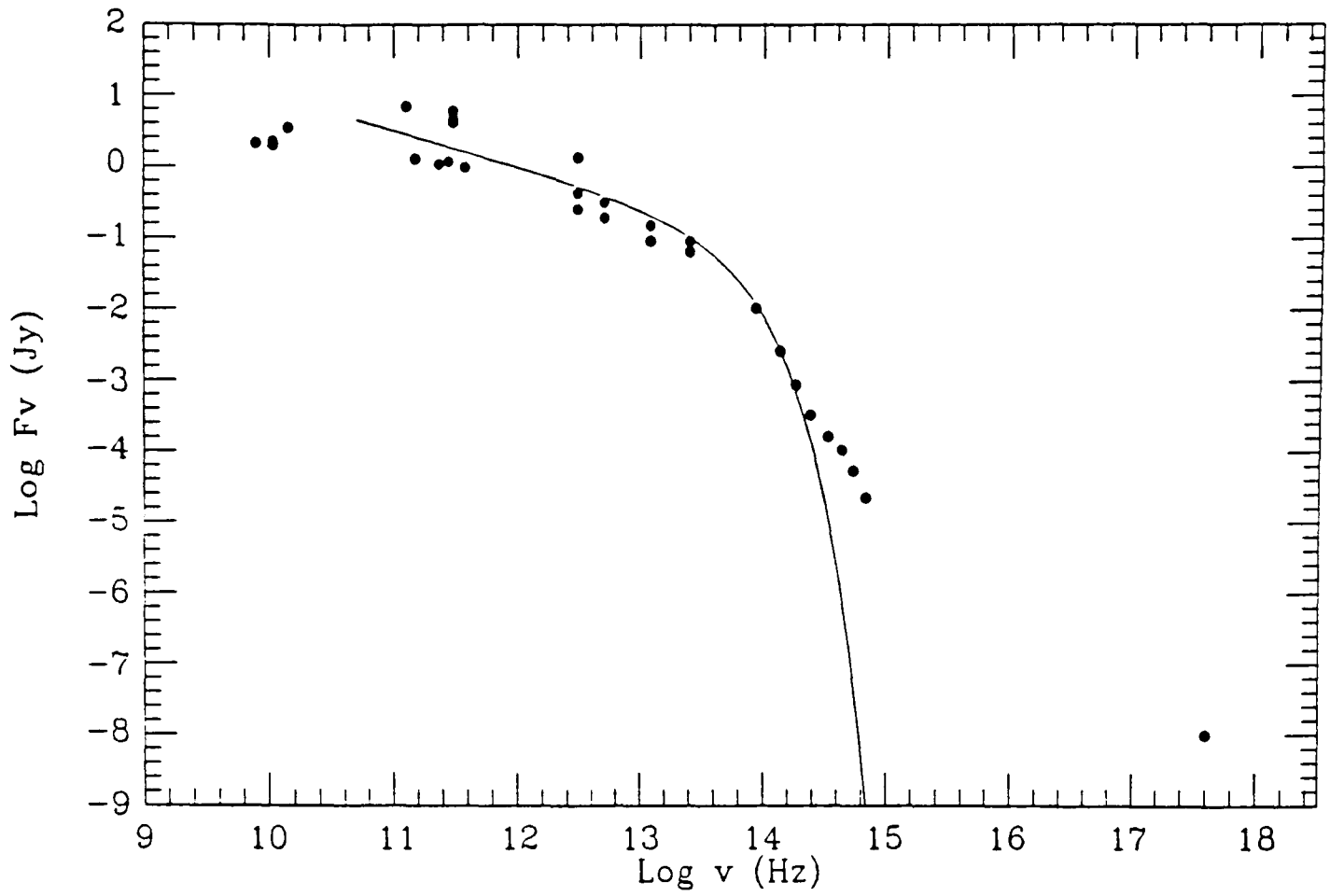

Figure 4.9 Multiwaveband photometry of PKS1413+135, as described in the text. Taken from McHardy *et al.* [1991].

4.4 DISC HOSTS AND STRONG RADIO SOURCES

It is important to recognize that, while comparatively rare, there *are* precedents for strong radio sources in disc galaxies. Several earlier surveys (for example Smith *et al.* [1986]) have classified a few radio loud QSO hosts as discs, although the majority of classified hosts from these surveys are ellipticals. Most of these surveys do not give statistical confidence levels on these host classifications, however, so it is difficult to judge the reliability of individual classifications from these surveys (although the trend for radio-loud objects to lie in ellipticals is clear).

A few well studied nearby radio galaxies almost certainly are discs, however. An

Table 4.5 Flux Densities for PKS1413+135

Date	Log ν (Hz)	Flux Density (mJy)	Reference
15 April 1981	9.90	2100 ± 200	
4 December 1980	10.03	2300 ± 300	
22 December 1980	10.03	2100 ± 100	
8 January 1981	10.03	2000 ± 100	
15 April 1981	10.15	3500 ± 200	
20 January 1981	11.10	7000 ± 2000	
30 June 1989	11.17	1300 ± 100	Robson *et al.* in preparation
30 June 1989	11.36	1100 ± 100	Robson *et al.* in preparation
30 June 1989	11.44	1200 ± 100	Robson *et al.* in preparation
25-27 November 1980	11.48	4800 ± 500	
21-24 December 1980	11.48	4300 ± 400	
23 March 1981	11.48	6100 ± 1500	
17-21 January 1981	11.48	4300 ± 300	
30 June 1989	11.57	1000 ± 100	Robson *et al.* in preparation
22 April 1981	12.48	1400 ± 1000	
21 July 1983	12.48	440	4.5 σ IRAS upper limit
14 August 1983	12.48	264	4.5 σ IRAS upper limit
21 July 1983	12.70	325 ± 46	IRAS
14 August 1983	12.70	203 ± 29	IRAS
21 July 1983	13.08	160	4.5 σ IRAS upper limit
14 August 1983	13.08	97	4.5 σ IRAS upper limit
21 July 1983	13.40	95	4.5 σ IRAS upper limit
14 August 1983	13.40	68	4.5 σ IRAS upper limit
15 March 1981	13.93	11 ± 1	
15 March 1981	14.13	2.8 ± 0.13	
11 February 1990	14.135	2.75 ± 0.25	UKIRT Service Observation
15 March 1981	14.26	0.91 ± 0.05	
15 March 1981	14.38	0.34 ± 0.03	
2 July 1989	14.52	0.168± 0.03	This work
11 April 1989	14.63	0.109± 0.02	This work
2 June 1989	14.73	0.055± 0.009	This work
2 June 1989	14.83	0.023± 0.004	This work
21 & 24 January 198	117.6	$1.0 \cdot 10^{-5} \pm 1.0 \cdot 10^{-6}$	

excellent example is 3C31 (NGC383). This nearby radio galaxy was first classified as an S0 by Arp [1968], and this classification has recently been confirmed by the shape

of the surface brightness profile given in Fraix-Burnet *et al.* [1991], and reproduced in Figure 4.10. Radio imaging of this object shows a characterictic double-lobed, edge darkened structure, with two prominent jets (Figure 4.11, taken from van Breugel [1982]). This object also exhibits spectral evidence for the existence of a disc, in the form of an extended rotating ring of emission-line regions centred on the nucleus of the galaxy (Owen *et al.* [1990]). Another well-known nearby radio galaxy that is usually classified as an S0 is 3C120 (Arp [1975], Moles *et al.* [1988]), although the obviously distorted optical morphology of this object (Fraix-Burnet *et al.* [1991]) makes this classification somewhat less convincing than for 3C31.

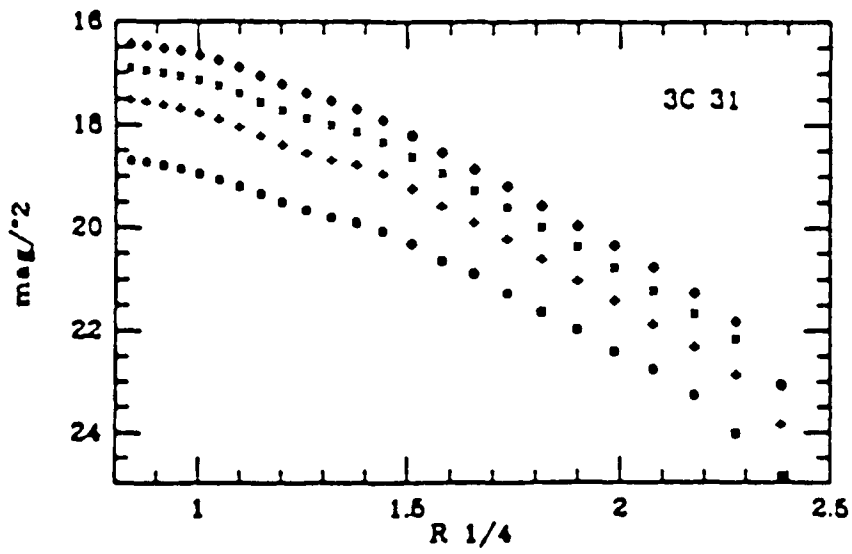

Figure 4.10 Surface brightness profile of 3C31, taken from Fraix-Burnet *et al.* [1991]. Note that the figure is plotted as a function of $r^{1/4}$, and that deVaucouleurs profiles are straight when plotted in this manner, while exponential profiles are convex in the manner exhibited by 3C31.

A convincing example of a disc host underlying a radio-loud quasar is 1223+252. (Hutchings and McClure [1990]). Unlike radio-loud quasar disc classifications based upon model fits, the classification of this moderately distant ($z = 0.27$) host is based upon clear evidence for spiral structure in the underlying host (Figure 4.12). Resolving this structure was only possible due to the superb seeing conditions (0.4" FWHM) available with CFHT when using the fast-guiding DAO/UM High Resolution Camera.

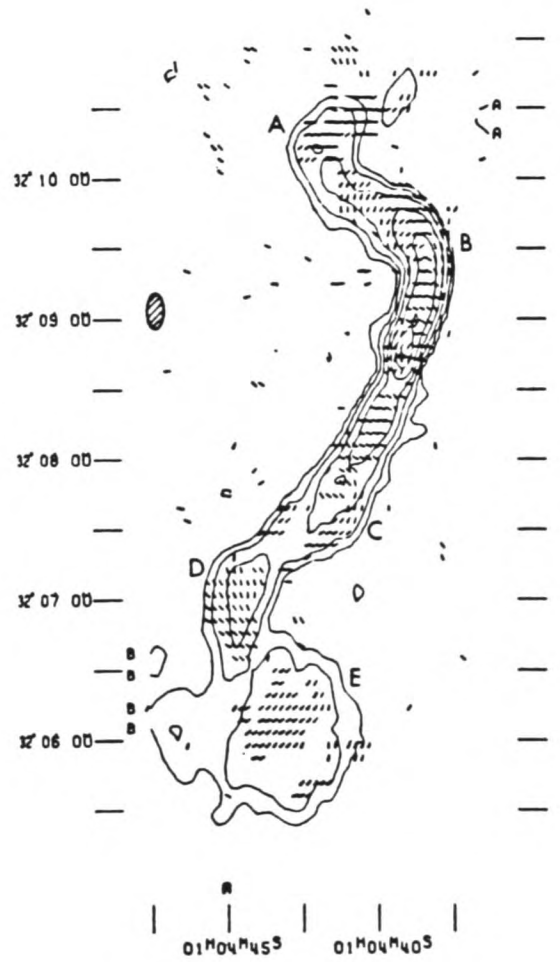

Figure 4.11 6cm radio map of 3C31, taken from van Breugel [1982]

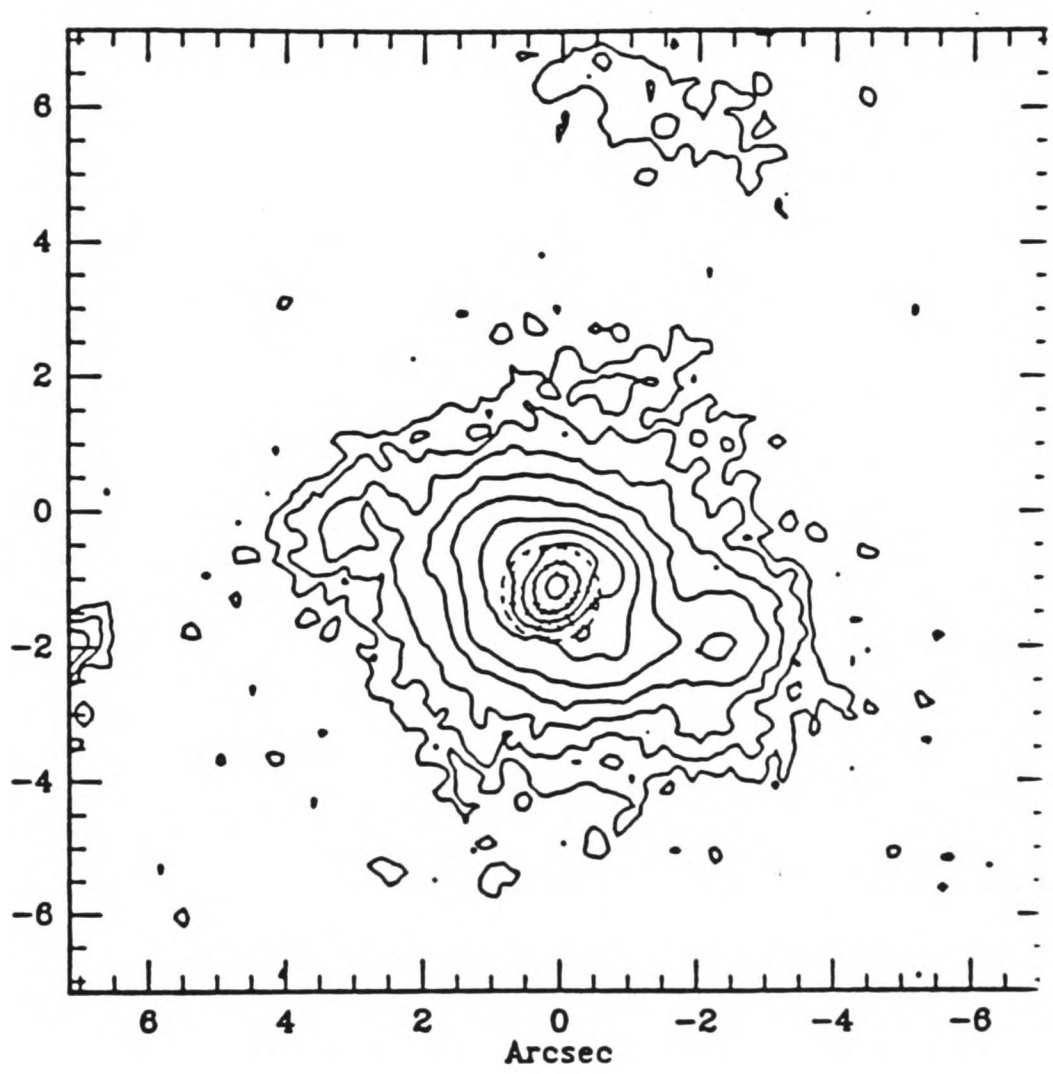

Figure 4.12 1200s CFHT/HR-Cam image of1223+252, taken from Hutchings and McClure [1990]

There are, therefore, quite convincing examples of radio loud disc galaxies. If we accept the popular beaming models for these objects, observing one of these radio-loud discs at a very small angle to the beaming axis could result in this object being seen as a BL Lac or an OVV quasar. Since radio-loud discs such as 3C31 and 1223+252 evidently do exist, it would be very surprising if a few of these were not occasionally seen along the jet axis. At present, the small (and uncertain) number of securely classified BL Lac hosts makes statistical tests of this hypothesis based on the number of classified BL Lac hosts vs. radio-loud disc AGN of other types impractical. The increased number of classified hosts brought on by the advent of 8m telescopes and adaptive optics may make eventually make this test possible.

4.5 SUMMARY

In this chapter, we have presented additional observations of PKS1413+135 obtained in several optical and infrared bands. These observations are consistent with our disc classification for the underlying host of this object. We have also put this classification into context, by demonstrating several examples of other radio-loud discs taken from the literature.

Chapter Five

MODELLING AND SIMULATIONS

INTRODUCTION

This central theme of this chapter attempts to answer the following two questions:
(1) At what redshift does it become difficult to distinguish elliptical BL Lac host galaxies from disc BL Lac host galaxies?
(2) What are the uncertainties on the host galaxy parameters returned from model fitting of the type described in this thesis?

We seek to answer these questions for various telescope apertures, seeing conditions, observing bands, and core magnitudes. As a preliminary step in achieving this goal, the predictions of simple models for BL Lacs, based upon their spectral energy distributions, are investigated. These predictions are then tested and quantified through detailed Monte Carlo simulations. We show how these simulations allow us to determine the errors on the parameters returned by model fits, and by extension the limiting redshift at which morphological classification becomes difficult.

Section 5.1 describes the wavelength dependence of the BL Lac core to host-galaxy contrast ratio, and illustrates some of the practical difficulties inherent in observing BL Lacs at infrared wavelengths. Section 5.2 describes the Monte Carlo simulations, the results of which are recorded in Section 5.3. Section 5.4 summarizes the important results of the chapter, and speculates on the prospects of future observations of BL Lac hosts.

Previous chapters of this thesis have demonstrated the feasibility of finding and classifying the host galaxies of BL Lac objects. The success of our BL Lac imaging survey can largely be attributed to the excellent seeing conditions experienced on La Palma, along with recent advances in CCD detector technology. In an absolute sense, however, the observations remain far from ideal: we were limited by CCD spectral response to observing between 4500 and 9000 angstroms, and atmospheric conditions limited the seeing FWHM to just under 1 arcsecond, which is of course good by conventional reckoning but at least an order of magnitude worse than the diffraction limit of a perfectly figured 4m telescope.

It may soon be possible to undertake observations that will greatly push back the limitations of high resolution ground-based imaging. In the next few years, proposed 8m class telescopes appear set to take over from the present generations of 4m telescopes as the premier instruments of astronomers observing in the optical and near-IR. Adaptive and active optics (ranging from the already successful HR-Cam on CFHT to the proposed primary mirror active adjustment system of the VLT) seem set to push back the lower limit on seeing to below 0.3 arcseconds (0.4 arcseconds can now be achieved on CFHT and the NTT). Finally, advances in infrared array technology hold forth the promise of extending the techniques described in this thesis to longer wavelengths.

This chapter determines, through simulations and detailed modelling, the promise held forth by 8m telescopes, adaptive and active optics, and infrared imaging in the investigation of distant AGN host galaxies. We demonstrate that these emerging technologies look to radically transform this field, primarily by improvements in resolution, but also by making possible the realization of "wavelength optimized" observations of BL Lac hosts, in the sense that it will be possible to image hosts at wavelengths that maximize the contrast between the core and host galaxy, thereby increasing the probability of host galaxy detection and classification.

5.1 CORE-TO-HOST CONTRAST

The previous chapters of this thesis have demonstrated that for very distant BL Lacs, resolving the underlying hosts is a difficult task. It is clear that the correct choice of observing wavelength can be a critical factor in the successful detection and classification of underlying hosts, but there are various competing effects which make it far from obvious what this optimal wavelength is. For example, is it better to observe in V band, where the sky and core flux are both low, or to observe at longer wavelengths in order to avoid the 4000 angstrom break in the host galaxy spectrum, which may be redshifted into the filter bandpass? One wishes to understand how this optimal wavelength depends on the steepness of the core spectrum, redshift, and host morphology. Because in the past these questions were largely academic (since the very high resolution required for these observations necessitated observing in the optical, and limited instrumental response was often the major factor in determining choice of observing bands) these have hitherto received scant attention.

5.1.1 The contrast factor

In order to determine the optimal wavelength for maximum host galaxy to core contrast, we define the Contrast Factor, C, given by the ratio of the ~~core~~ host flux density (SED) $S_\nu^{\text{~~core~~ host}}$ to the ~~host~~ core ~~galaxy~~ flux density $S_\nu^{\text{host core}}$ (~~the Spectral Energy Distribution, or SED~~):

$$C = \frac{S_\nu^{\text{~~core~~ host}}}{S_\nu^{\text{host core}}} \qquad [5.1]$$

In applying this equation, we assume that the core flux density is a known function (a reasonable assumption given the wealth of multiwaveband observations that exist BL Lacs, eg. Impey [1988]), and model it as a power law as a function of frequency:

$$S_\nu^{\rm core} \propto \nu^{-\alpha} \text{ erg cm}^{-2} \text{ s}^{-1} \text{ Hz}^{-1} \qquad [5.2]$$

or as the equivalent power law as a function of wavelength:

$$S_\lambda^{\rm core} \propto -c \cdot \lambda^{\alpha-2} \text{ erg cm}^{-2} \text{ s}^{-1} \text{ Å}^{-1}. \qquad [5.3]$$

The SEDs for underlying host galaxies, kindly supplied to us by Alfonso Aragon-Salamanca at Durham, are based upon data from Pence [1976] in the ultraviolet and optical regimes, and upon the broad-band photometry of Person, Frogel, and Aaronson [1979], and Gavazzi and Trincheri [1989] in the infrared. We consider two different SEDs, the first corresponding to that of an elliptical or S0 galaxy, and the second representing an Sbc system. Both SEDs are illustrated in Figure 5.1, along with the corresponding filter response functions for the B, V, R, I, J, and K bands. Throughout this work we have assumed no evolution in the shape of the SEDs with redshift; calculations by several authors (Bruzual and Kron [1980]; Bruzual [1983]; Koo [1985]) suggest that the effects of evolution on broadband colour are small at redshifts less than 0.6.

In order to determine the wavelength corresponding to maximum core-to-host contrast, we have determined the contrast functions C(λ,z,α) for different redshifts and core spectral indices. Graphs of these functions for the E/S0 and Sbc models are shown in Figure 5.2.

Several points are immediately apparent from an inspection of Figure 5.2. Firstly, the figure suggests that the maximum core-to-host contrast for most of the (ν,z) parameter space lies in the infrared. It is clear that for most combinations of redshift and spectral index, the avoidance of the sharp decrease in flux density near the 4000Å break obtained by imaging higher redshift objects in the infrared overcomes the disadvantage of having a brighter core. Only objects whose cores have quite steep ($\alpha > 2$) spectral indices

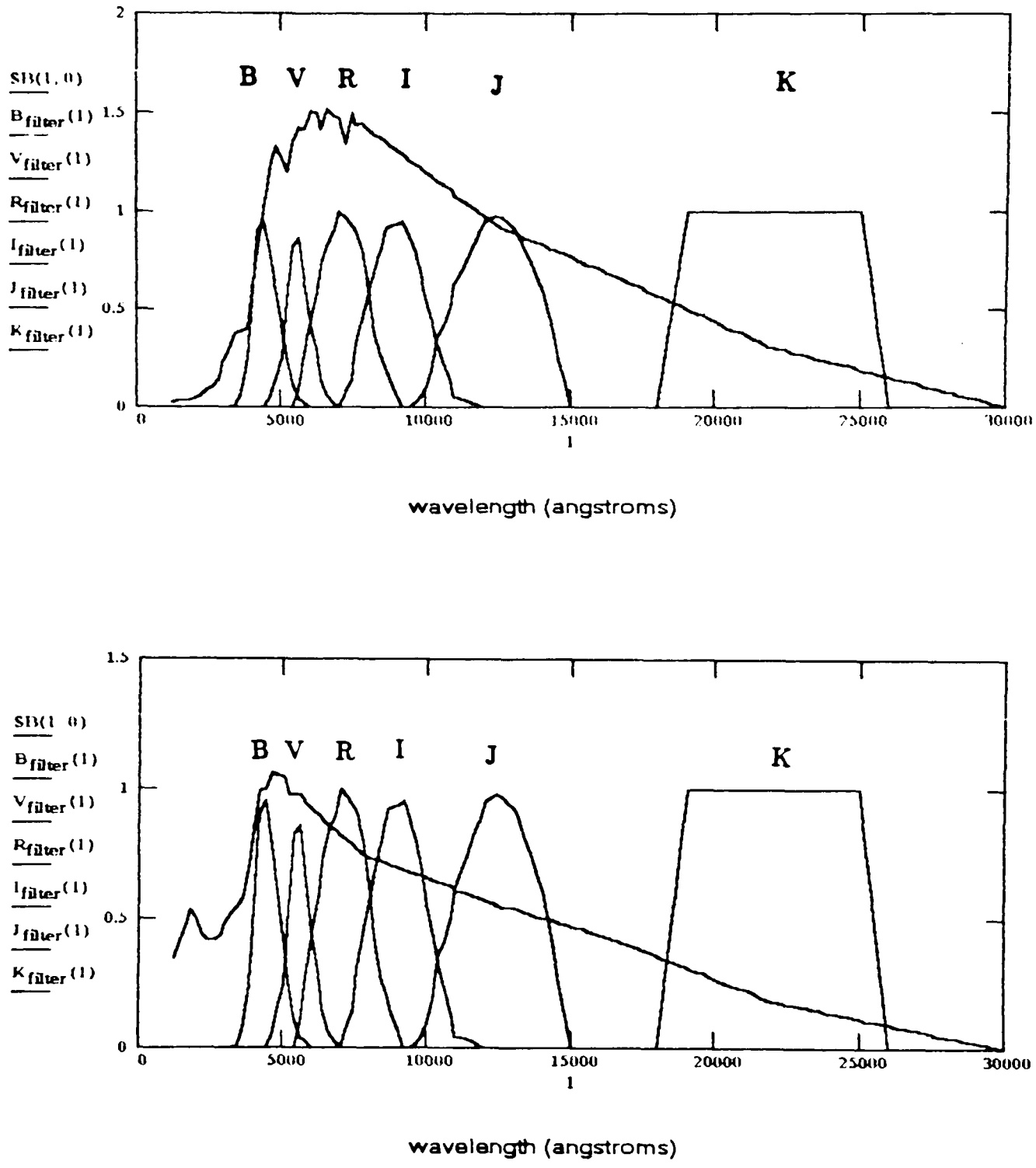

FIGURE 5.1 SED's and filter response functions for E/S0 (top) and Sbc (bottom) galaxies.

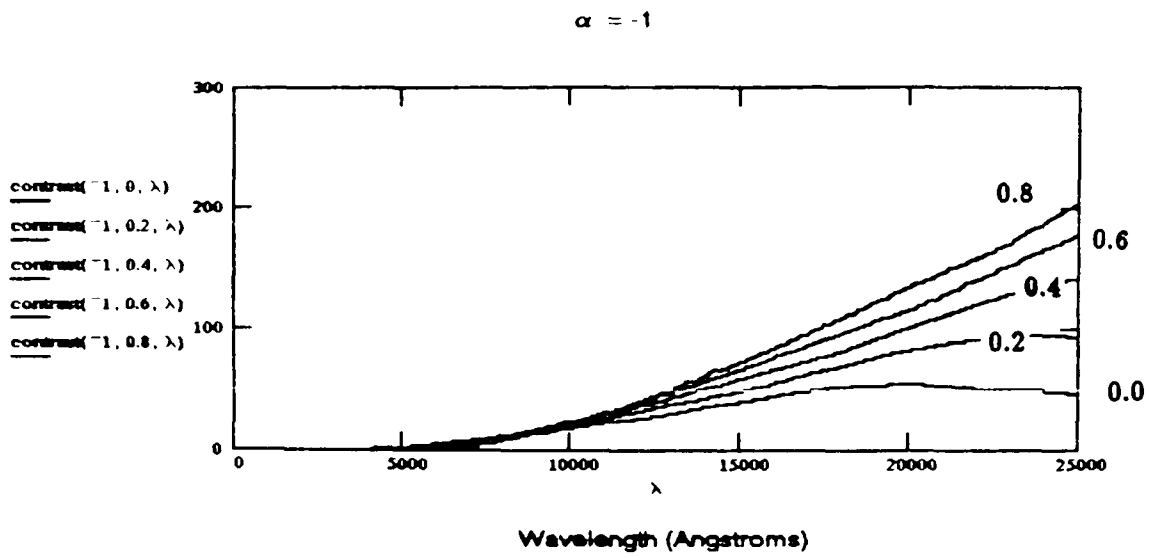

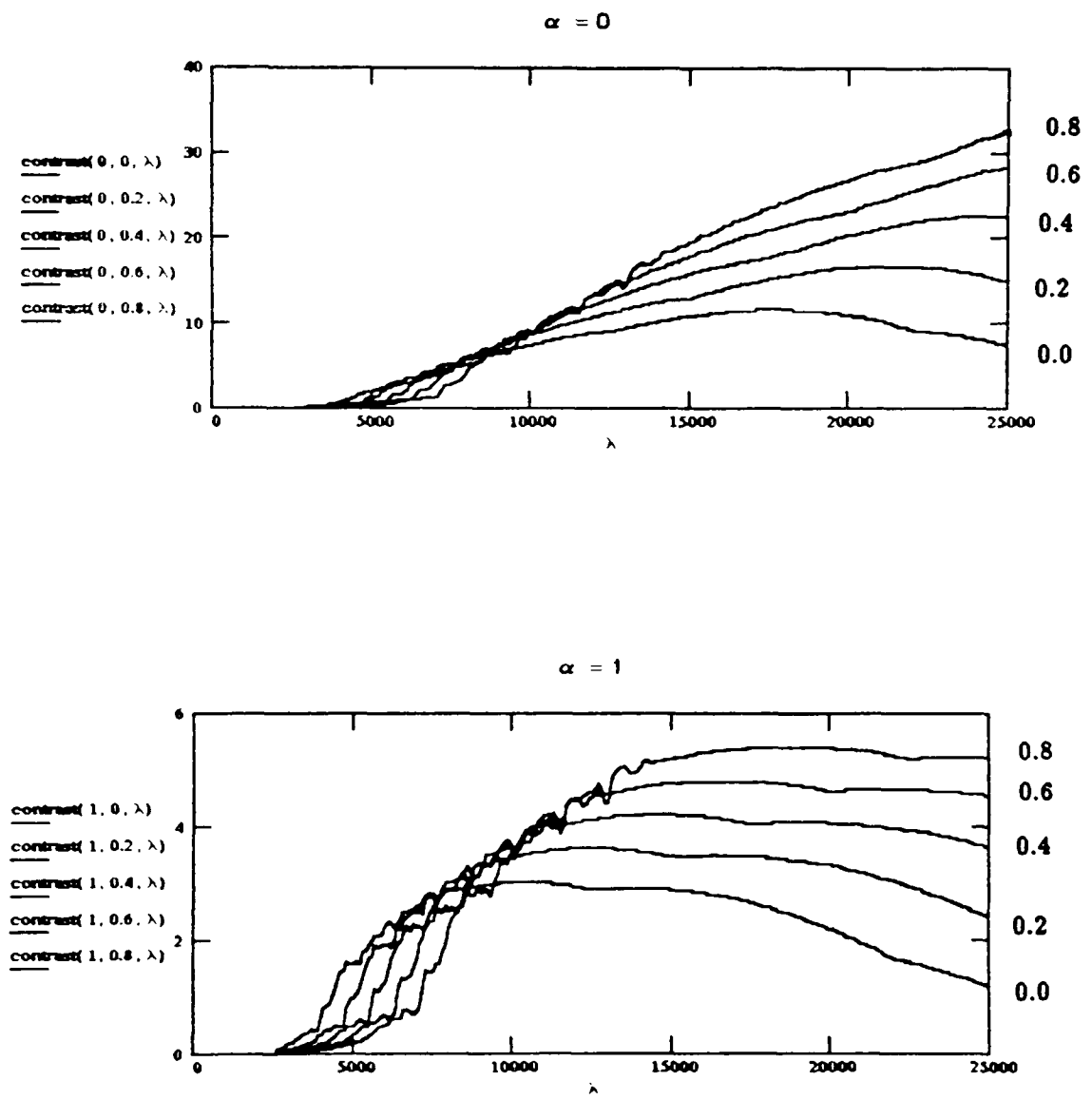

FIGURE 5.2a Contrast functions for E/S0 galaxies as a function of wavelength, for various spectral indices. Contrast functions corresponding to z=0.0, 0.2, 0.4, 0.6, and 0.8 are shown. Note that the normalization of the vertical axis for the contrast functions at each redshift is arbitrary.

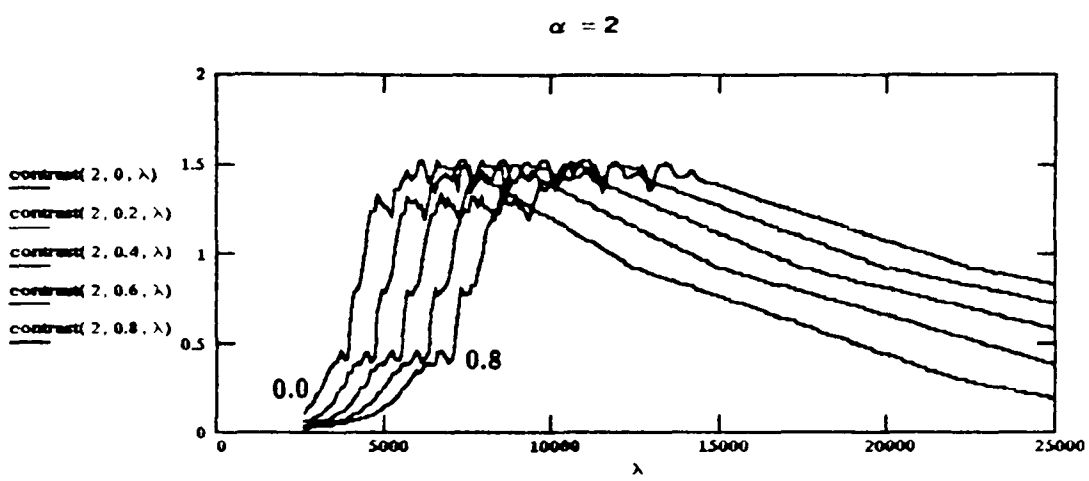

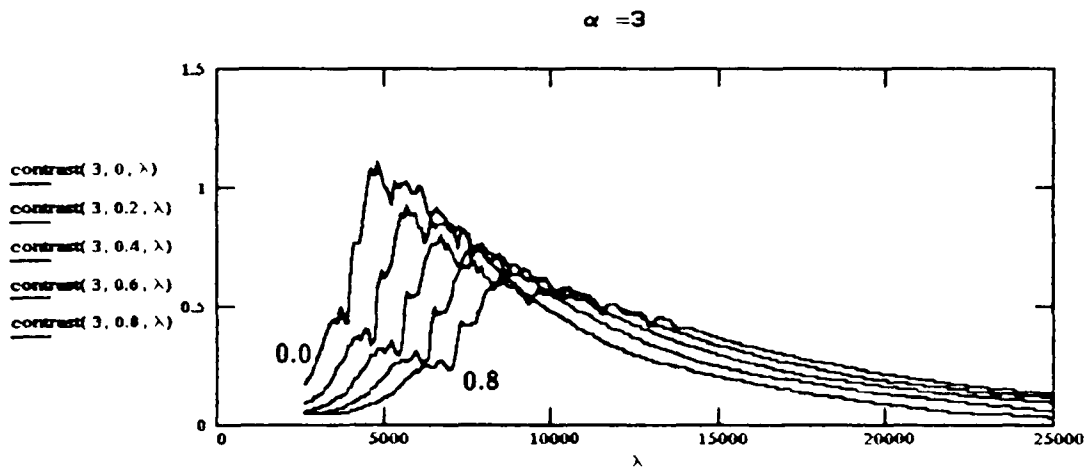

FIGURE 5.2a (continued)

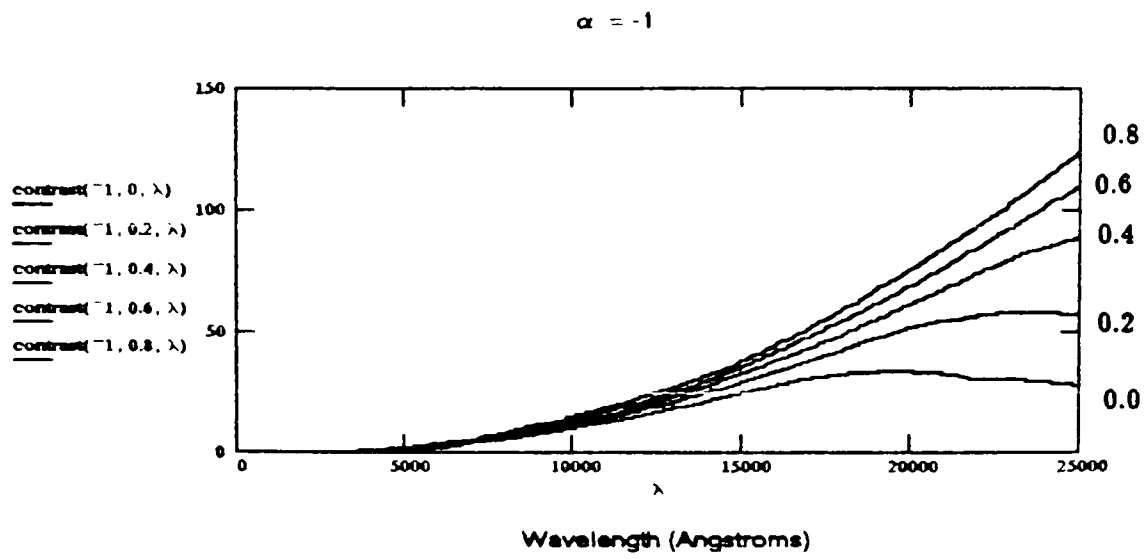

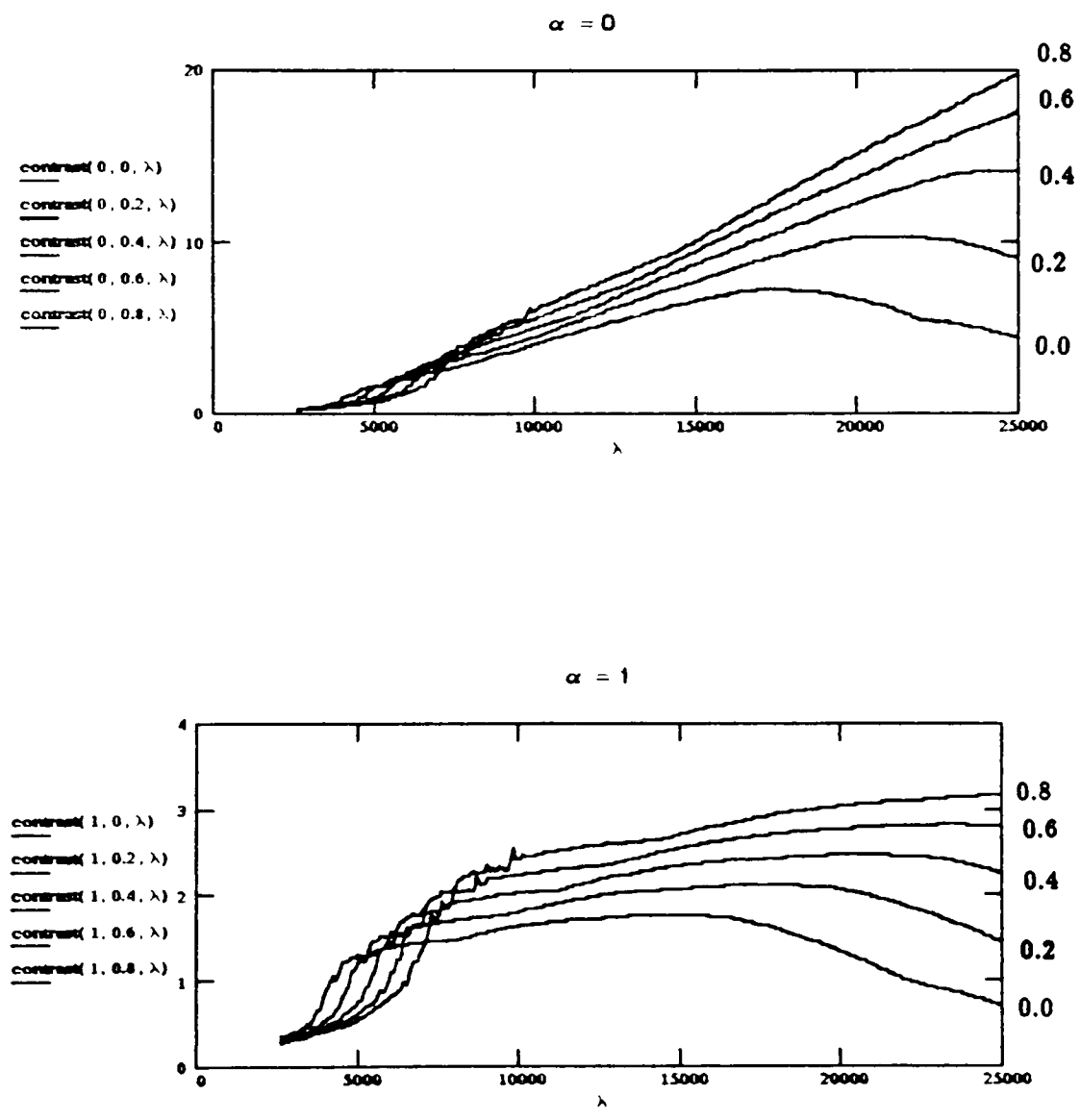

FIGURE 5.2b Contrast functions for Sbc galaxies as a function of wavelength, for various spectral indices.

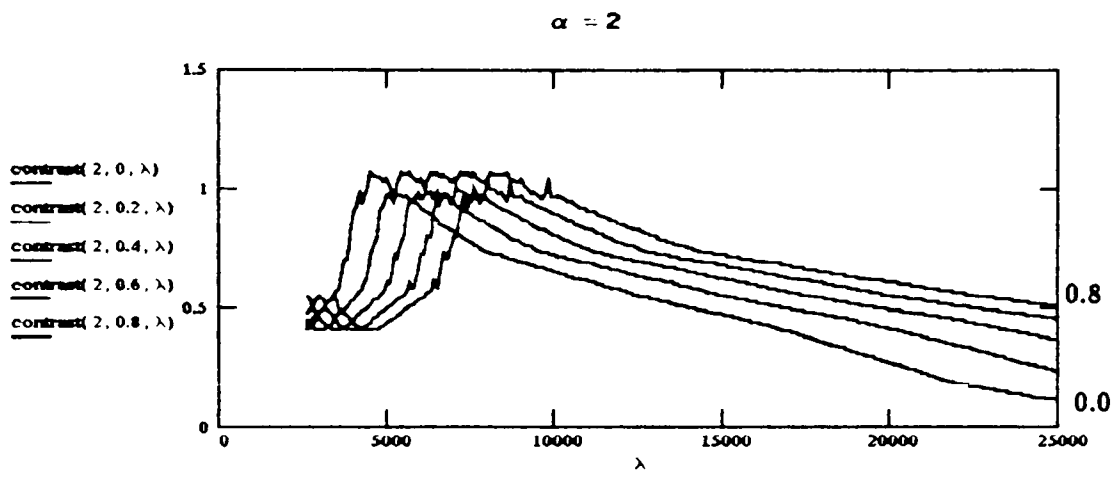

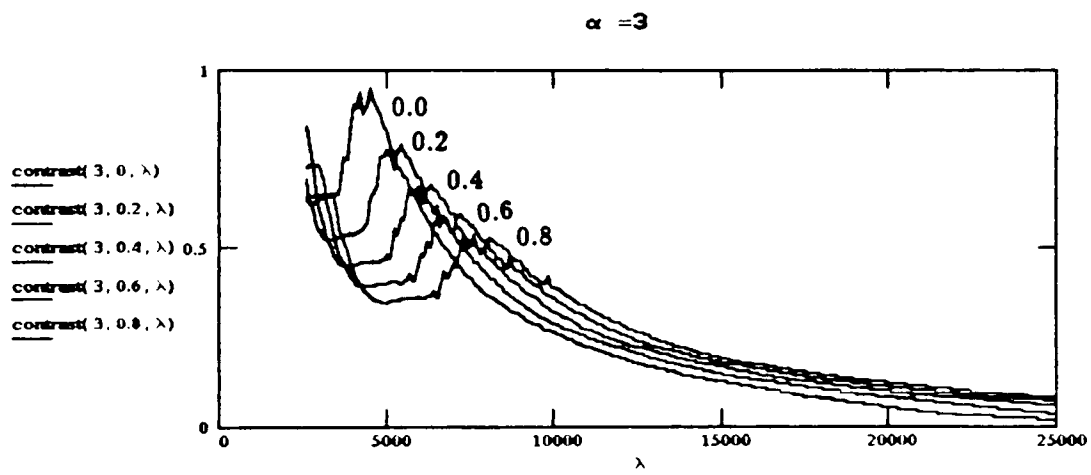

FIGURE 5.2b (continued)

and are at low ($z < 0.3$) redshifts have higher contrast in the optical regime. Another point worth making about the Figure 5.2 is that the optimal wavelengths for imaging are systematically longer for the Sb/c model (for all but the steepest values of α) relative to the E/S0 model, suggesting the *possibility* of a selection effect biasing against the discovery of underlying disc systems in optical surveys of host galaxies. I emphasize the word "possibility" in the preceding sentence because the contrast functions do not generally peak sharply; instead they tend to be plateau shaped. The "peak" of these functions is therefore quite wide, and it is somewhat artificial to designate a particular wavelength, as opposed to a range of wavelengths, as optimal for separating the core from the host. The distribution of BL Lac and OVV Quasar spectral indices given in Impey *et al.* [1988] makes it is clear that very steep ($\alpha > 2$) cores are quite rare. This suggests that for $z > 0.3$ *virtually all* underlying hosts are more prominent, relative to their cores, in the infrared than in the optical.

5.1.2 Practical difficulties

The results of the contrast function analysis suggest that infrared imaging of host galaxies would be more effective than optical imaging for resolving many distant host galaxies. There are, however, practical difficulties that largely mitigate the advantages obtained by infrared imaging. The difficulty in constructing large format, high quantum efficiency infrared arrays is one of these (current arrays are typically around 64×64, with several 256×256 arrays in the prototype stage), while another difficulty is the need for careful thermal isolation of the detector. Nevertheless, infrared detector technology is fast advancing to the point that in a few years these technical difficulties may no longer be a problem. A more fundamental difficulty is the *much* brighter night sky surface brightness: $J_{sky} \sim 17.0$ mag/arcsec^2 and $K_{sky} \sim 12.5$ mag/arcsec^2. This severely limits ground-based observations by greatly lowering the signal-to-noise level of a detection at a

given surface brightness (the predominant component of the night-sky surface brightness at wavelengths longer than 1.5μ originate from chemical reactions in the atmosphere, so space-based infrared observations should be comparatively unaffected).

5.1.2.1 An example: K-band Imaging of PKS1413+135

The extent of the problem can be illustrated with a simple calculation of K-band results for PKS1413+135, the disc BL Lac described in Chapters 3 and 4. We start by making the rough approximation that, using an infrared 4m telescope, the limiting surface brightness on radial profiles is six magnitudes fainter than the sky brightness (i.e. about 0.5% of the sky) for 1500 second exposures, in agreement with our R band WHT images. If we assume an K-band sky surface brightness of 12.5 mag/arcsec^2, we therefore expect a limiting isophote around 19 mag/arcsec^2. This is quite consistent with tabulated limiting magnitudes for stars imaged through IRCAM on UKIRT: the *IRCAM User's Guide*, (Table 4, 1990 edition) records that in 1000s (assuming an equal exposure time generating a flat field) UKIRT detects an 18th magnitude star with a 5 sigma confidence level, and a 19th magnitude star at 2 sigma.

The practical limitations imposed by these limits are best seen by comparison with the R band results for our survey. For example, our 1500s WHT exposure of PKS1413+135 (z=0.26), shown in Figure 3.1, can be traced out to R=25 mag/arcsec^2 at a radius of 6 arcsec. If we displace the PKS1413+135 profile up by 2.5 mag/arcsec^2 (roughly corresponding to the gain expected from the R-K colours and K-correction at z=0.3, as given in Tables 5.2 and 5.3, below), we could trace the profile out to around 2 arcsec at 2 sigma. This is 30% of the limiting radius of the observed R-band profile. These results are in good agreement with the K-band exposure of PKS1413+135 shown in Figure 4.7 (note that this object's extremely steep infrared spectrum would make it a poor choice for infrared imaging in any case). Clearly, for similar exposure times, and at

redshifts less than around 0.5, K-band infrared surface brightness profiles will extend to much shorter radii than the corresponding optical profiles, although the K-band profiles will be less contaminated by light from the core (unless the core spectrum is very steep, as discussed earlier).

This somewhat pessimistic view of the promise of infrared host galaxy imaging applies only to observations done in K-band, where the sky is extremely bright. The UKIRT IRCAM 1 detection limit for J-band images is two magnitudes fainter than for K-band (for identical exposures; cf *IRCAM User's Guide*, Table 3, 1990). Applying a J-band analysis to PKS1413+135 identical to that used earlier for K-band, we expect the J-band profile to extend almost as far as the optical profile. Furthermore, for the majority of BL Lacs, the J band infrared profiles are still much less contaminated than the optical profiles with light from the central core. Finally, it is worth emphasizing that our analysis has been limited to examining the potential of infrared imaging with regard to easier host galaxy detection, and that this is a *very* narrow viewpoint on the field of IR imaging of AGN. A wealth of other studies are made possible by moving into the infrared (eg. mapping and studying star-forming regions in hosts), and these will doubtless have as great an impact on our understanding of AGN as will improved host galaxy imaging.

5.2 SIMULATIONS OF DISTANT BL LAC OBJECTS

The considerations of the preceding section strongly suggest that near-infrared imaging may hold significant advantages over optical imaging for resolving the underlying hosts of BL Lac objects. The ability to detect and classify underlying hosts depends on much more than the observing wavelength, however. Seeing, core-brightness and spectral

index, exposure time, and telescope aperture are also critical factors in determining the success of observations. The large parameter space spanned by these factors is probably responsible for the large range in astronomers' estimates for the limiting redshifts for classification of the morphology of QSO host galaxies; values from $z = 0.2$ to $z = 0.5$ (Woltjer [1991]) are found in the literature. Given the large amounts of telescope time required to observe these objects, it is clear that it would be hugely advantageous to have a realistic idea of the efficacy of present (and future) telescope/instrumentation combinations for observing distant underlying host galaxies. By simulating a number of BL Lac surface brightness profiles, and subjecting these profiles to the same procedures used to analyse our survey, we can not only determine the limiting redshift for host classification as function of the parameters described above, but also put realistic error estimates on the host galaxy parameters obtained during our survey.

Before describing the simulations, it is worth emphasizing why they are necessary. Confidence estimates on parameters returned by model fits can be obtained analytically from the covariance matrix of χ^2 minimization routines. These uncertainty estimates will be correct if the errors on the fitted points are Normally distributed; this is a fairly general assumption, since the Central Limit Theorem of statistics implies that the sum of a large number of independent error distributions has an approximately Normal distribution. The errors on the surface brightness profiles fitted in this thesis are however, unlikely to be independent. The actual counts on the CCD frame are Normally distributed (assuming 1 electron/adu; at the counts levels considered, Poisson and Normal distributions are virtually identical), but the points on the final profile are the result of fitting ellipses to isophotes, and are therefore non-independent. Another source of non-independence is the interpolation that has been used at two stages in the reduction process. Finally, systematic errors are likely to be introduced into the fits during background subtraction.

Deriving confidence limits on fitted parameters by numerical Monte Carlo simu-

lations does not require that the errors on the fitted points are Normally distributed. Instead, it requires something of us, namely that *we understand the sources of error, and are able to model them.* The method proceeds as follows: we synthesize a number of simulated profiles, use random number generators to add the appropriate random and systematic errors to the profiles, and then fit these "observations" in the same way as the real ones were fitted. By determining the spread in the parameters returned by this procedure, we gain insight into the uncertainty inherent in fitting the real profile. We can then use the same F-test criteria used on the real profiles to "classify" the morphology of the simulated hosts, and determine at what redshift such classifications become ambiguous.

The advantages of this procedure over traditional analytical uncertainty estimates are eloquently summed up by Press et. al. (*Numerical Recipes, The Art of Scientific Computing*, Cambridge University Press, 1986):

"...the ability to do Monte Carlo Simulations *in this fashion has revolutionized many fields of modern experimental science. Not only is one able to characterize the errors of parameter estimation in a very precise way. One can also try out on the computer different methods of parameter estimation, or different data reduction techniques, and seek to minimize the uncertainty of the result according to any desired criteria. Offered the choice between mastery of a five-foot shelf of analytical statistics books and middling ability at performing statistical Monte Carlo simulations, we would surely choose to have the latter skill."*

5.2.1 Simulated surface brightness profiles of distant BL Lac hosts

Simulated surface-brightness profiles were generated using a FORTRAN program (SIMPROF) that we have written. The simulated surface brightness profiles were taken along the major axis of the synthesised BL Lac core + host model. All host galaxy

models were two-dimensionally convolved with a circularly symmetric PSF in order to simulate the effects of seeing.

SIMPROF generates the profiles as a function of the following parameters:

(a) *Filter Band.* B, V, R, I, J and K can be selected. For convenience, the important parameters defining this standard photometric system (taken from Zombeck's *Handbook of Astronomy and Space Physics* (Cambridge University Press, 1990, p.100) are shown in Table 5.1. Night sky surface brightnesses in B,V,R, and I are well known, but the infrared night sky surface brightness can be strongly affected by thermal photons from the local environment (detector housing, telescope, etc.). We adopted sky brightnesses based upon the results obtained by McCaughrean and McLean [1987] in simulating the performance of IRCAM on UKIRT, as shown in Figure 5.3.

(b)*Host morphology.* Elliptical or Disc morphologies can be simulated. Morphological parameters for these are chosen to be similar to the hosts found in our survey; host colours are calculated from the SEDs and filter response curves shown in Figure 5.1 (taken to be typical of E/S0 and Sbc galaxies), using the following methodology:

$$\text{Colour (A} - \text{B)} = -2.5 \log \frac{\int_0^\infty S(\lambda) R_A(\lambda) C_A d\lambda}{\int_0^\infty S(\lambda) R_B(\lambda) C_B d\lambda} \qquad [5.4]$$

where $S(\lambda)$ is the spectral energy density of host, R_i is the response of filter i, and C_i is absolute spectral irradiance for a zeroth magnitude star in that band of the filter system. Galaxy colours obtained by this formalism are shown in Table 5.2, and are in excellent agreement with typical galaxy colours (Mihalas and Binney [1981]).

(c) *Redshift.* K-corrections for the underlying hosts are calculated using formula [2.5], by assuming the spectral energy distributions and filter response functions shown in

Filter Band	λ_o^*	$\Delta\lambda_o$	Absolute Spectral Irradiance for mag = 0.0 $f_\lambda(0)$	$f_\nu(0)$
U	0.365 μm	0.068 μm	4.27×10^{-9} erg cm^{-2}s^{-1}Å^{-1}	1.90×10^{-23} Wm^{-2}Hz^{-1}
B	0.44	0.098	6.61×10^{-9}	$4.27(4.64)^+ \times 10^{-23}$
V	0.55	0.089	3.64×10^{-9}	3.67×10^{-23}
R	0.70	0.22	1.74×10^{-9}	2.84×10^{-23}
I	0.90	0.24	8.32×10^{-10}	2.25×10^{-23}
J	1.25	0.3	3.18×10^{-10}	1.65×10^{-23}
H	1.65	0.4	1.18×10^{-10}	1.07×10^{-23}
K	2.2	0.6	4.17×10^{-11}	6.73×10^{-24}
L	3.6	1.2	6.23×10^{-12}	2.69×10^{-24}
M	4.8	0.8	2.07×10^{-12}	1.58×10^{-24}
N	10.2		1.23×10^{-13}	4.26×10^{-25}

* $\lambda_o = \int \lambda S(\lambda) d\lambda \Big/ \int S(\lambda) d\lambda$, where $S(\lambda)$ is the photometer response function.
U,B,R,I,N values from Allen, C.W., Astrophysical Quantities, Athlone Press (1973).
V,J,H,K,L,M values from Wamsteker, W., Astron. Astrophys., 97, 329 (1981).

+ from S. Kleinmann.

Table 5.1 The standard photometric system (taken from Zombeck [1990].

Figure 5.1. K-corrections for various redshifts and observing bands are shown in Table 5.3.

(d) *Seeing.* The PSF is assumed to be well-represented by the sum of a gaussian and two exponentials. In order to mimic the errors inherent in deriving the real PSF from CCD frames, the simulated PSF is derived by fitting a star model to a simulated star profile. This PSF is then used to model the core and is convolved with the chosen host morphology to model seeing degradation.

(e) *Quantum efficiency of the detector.* This is determined by specifying the photometric constant, k_{PM} (defined to be the magnitude corresponding to a single count over the

Figure 1. This shows the anticipated background arriving outside the window of a camera on the UKIRT at the summit of Mauna Kea. The background is due to thermal emission from the sky, telescope, and warm optics, along with short wavelength non-thermal OH emission. The cold optics will reduce this flux prior to reaching the detector. Also shown is the zenithal transmission for the sky above Mauna Kea, along with the transmission curves for the standard near-IR filter set.

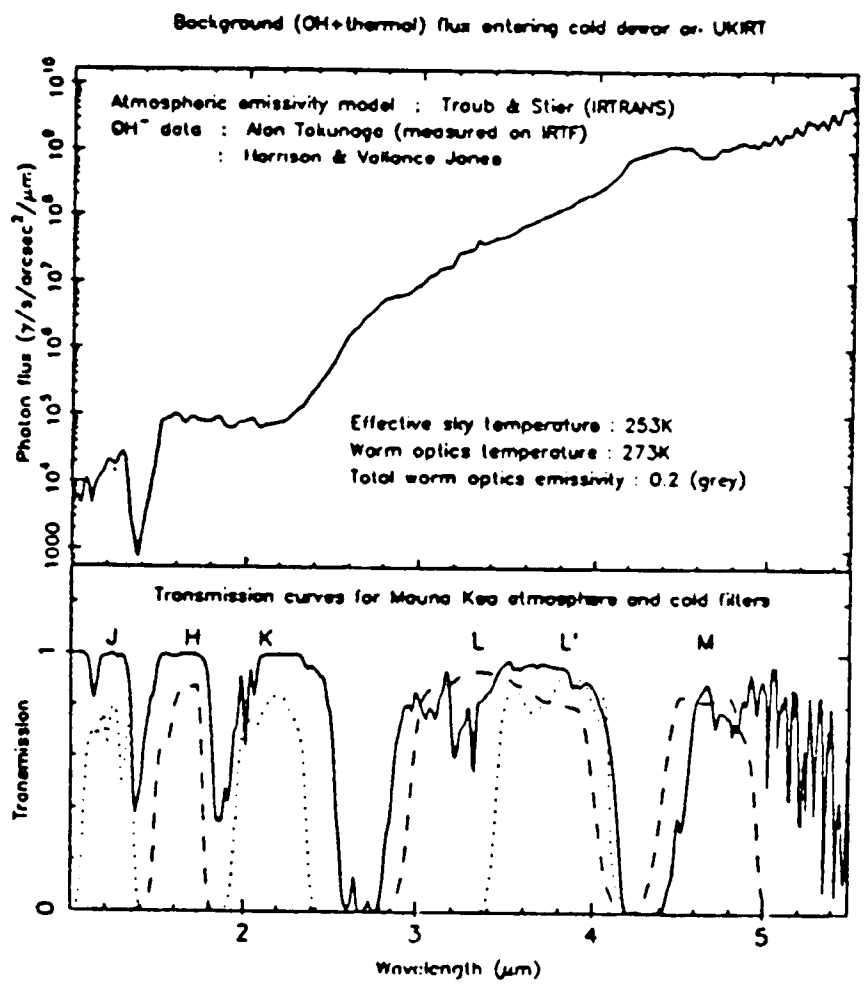

FIGURE 5.3 Infrared background (in photons sec^{-1} $Å^{-1}$ for IRCAM on UKIRT)

length of the exposure) of a 100s observation using a 4m telescope in the desired band. This parameter can either be determined directly from CCD frames, or calculated for typical telescope/instrument combinations, as follows: the total energy E from a zeroth magnitude star, collected by a telescope of aperture A, and transmitted through a filter i in an exposure time t, can be approximated by:

$$E = C_i \cdot \Delta\lambda_i \cdot \pi \cdot \left(\frac{A}{2}\right)^2 \cdot t \qquad [5.5]$$

Table 5.2 Rest Frame Colours (using Fig.5.1 SEDs)

	E/S0	Sbc
V-R	0.80	0.56
R-I	0.68	0.62
I-J	0.87	0.97
J-K	1.15	1.19

where $\Delta\lambda_i$ is the FWHM of filter. Assuming one electron/adu, the total number of counts equals the total number of photons, and is then given by

$$N = \frac{E \cdot Q}{h\nu_i} \qquad [5.6]$$

where ν_i is the central frequency of the filter, and Q is the quantum efficiency. Since the photometric constant is the magnitude corresponding to a single count over the length of the exposure, it is then given by:

$$k_{PM} = 2.5 \cdot \log(N) \qquad [5.7].$$

(f) *R-band Core magnitude and Spectral Index.* Core magnitudes for other colours are calculated by approximating the filter bandpasses as step functions with widths corresponding to the FWHM of the appropriate filters. We can then calculate power-law core colours analytically. If filter A has a bandpass between wavelengths a_1 and a_2, and filter B between b_1 and b_2, then a core exhibiting a uniform power law spectral irradiance with

Table 5.3 K-corrections

z	K_B	K_V	K_R	K_I	K_J	K_K
			E/S0 Model			
0.0	0.0	0.0	0.0	0.0	0.0	0.0
0.1	0.471	0.189	0.102	0.037	-0.016	-0.214
0.2	0.946	0.409	0.220	0.092	-0.032	-0.357
0.3	1.353	0.758	0.350	0.161	-0.034	-0.439
0.4	1.724	1.198	0.507	0.243	-0.024	-0.484
0.5	2.096	1.598	0.698	0.336	-0.007	-0.506
0.6	2.471	1.905	0.922	0.437	0.015	-0.518
0.7	2.832	2.175	1.187	0.549	0.053	-0.528
0.8	3.161	2.469	1.484	0.676	0.095	-0.535
			Sbc Model			
0.0	0.0	0.0	0.0	0.0	0.0	0.0
0.1	0.245	0.054	0.026	0.041	0.018	-0.227
0.2	0.543	0.137	0.056	0.071	0.040	-0.379
0.3	0.817	0.292	0.092	0.092	0.068	-0.461
0.4	1.041	0.513	0.143	0.112	0.100	-0.500
0.5	1.217	0.776	0.218	0.135	0.135	-0.513
0.6	1.357	1.016	0.323	0.161	0.166	-0.511
0.7	1.464	1.204	0.462	0.193	0.187	-0.503
0.8	1.536	1.352	0.627	0.236	0.202	-0.493

spectral index α defined by $\nu^{-\alpha}$ has a colour:

$$A - B = -2.5 \log \left[\frac{\int_{a_1}^{a_2} \lambda^{(\alpha-2)} C_A d\lambda}{\int_{b_1}^{b_2} \lambda^{(\alpha-2)} C_B d\lambda} \right]$$
$$= -2.5 \log \left[\frac{(\exp[(\alpha-1)\cdot\ln(a_2)] - \exp[(\alpha-1)\cdot\ln(a_1)]) \cdot C_A}{(\exp[(\alpha-1)\cdot\ln(b_2)] - \exp[(\alpha-1)\cdot\ln(b_1)]) \cdot C_B} \right] \quad [5.8]$$

(g) *Pixel scale.* A pixel scale sufficiently fine to allow the effects of binning to be neglected is assumed.

(h) *Limiting isophote.* The simulated profiles were taken down to 2 sigma above the sky background level. This roughly corresponds to the best results obtained for real profiles in our survey.

5.2.2 Errors on the simulated profiles

5.2.2.1 Random errors

The most important source of random error in determining the surface brightness profiles of distant hosts is the $\sqrt{N}$ poisson counting error inherent in detecting the signal (if a CCD has 1 electron/ADU, N is simply the number of ADU in a given pixel). In the SIMPROF program, a random number generator is used to add an appropriate poisson noise to individual points on the profile. The standard deviation of the mean error around a given isophote (multiplied by a small factor to account for the existence of non elliptical and incomplete isophotes) is then added in quadrature to other sources of error described below, in order to replicate the procedure adopted in obtaining the profiles in our survey.

5.2.2.2 Systematic errors

Systematic errors that affect the simulated profiles can be divided into three types: (a) those that affect both real and simulated profiles, (b) those that only affect the simulations, and (c) those that only affect real profiles. Types (a) and (b) are largely tractable, in the sense that we can simulate them and by looking at the final results of the fits determine their relative importance, but type (c) errors plunge us into the great unknown beyond the parameter space of our models. We therefore emphasize the following caveat:

Monte-Carlo simulations intended to assess the accuracy and efficacy of model fits are only as accurate as the models themselves. We assume that deVaucouleurs law profiles are reasonable approximations to the shapes of real distant elliptical galaxies, and similarly that exponential profiles are reasonable approximations to the actual shapes of distant disc galaxies.

As noted in previous chapters, the assumptions put forward in this caveat are generally valid at low redshifts, although even at these redshifts real galaxies show deviations from the canonical empirical profiles. For example, a rigorous χ^2 test would usually reject a deVaucouleurs law fit to a nearby elliptical galaxy that passes the less rigorous "chi-by-eye" test by which galaxies are classified. We hope that distant galaxies remain well described by deVaucouleurs and exponential laws, but only time (and much higher resolution observations) will tell if the assumed models are accurate representations of the morphology of distant host galaxies, and the extent to which this source of error does or does not affect our simulations.

A more tractable source of systematic error in both our simulations and in the reduction of actual data is the estimate of the sky background on the CCD frame. This quantity must be subtracted from all the points prior to fitting the profile, and even small errors in sky background can radically alter the shape of the profile at low light levels.

This systematic error can be modelled in the simulations by mimicking the procedure used to estimate sky background values in the real data. SIMPROF determines the background sky level, adds poisson noise, adds a similar noise component corresponding to the noise introduced during the flat-fielding procedure, and then samples this sky level 400 times (roughly the number of pixels sampled near BL Lacs in our survey when determining the sky level). The mean sky level is then used in the simulations, with one-sigma standard deviation of the mean errors added in quadrature to the poisson errors from the profile. We note that this procedure does not account for systematic low frequency structures that often dominate the background uncertainty in CCD frames reduced using twilight-sky flats. This structure is usually due to slight differences in the pixel to pixel colour response of CCDs, and can be greatly reduced by using flat-fields generated by median-comparing object frames that are later co-added to make a final exposure. We assume in our simulations that low frequency background structure in the image frames has been reduced to a negligible level by adopting this, or a similar, procedure to generate the flat-fields.

A final source of systematic error is the weak dependence of the host galaxy fit parameters on the assumed ellipticity of the host. This effect is quite small, and is entirely due to seeing effects. As the host ellipticity can usually be estimated fairly accurately, and since the size of this error is small in comparison to other systematic effects, this error is not modelled in the simulations (which assume a host ellipticity of 0.2).

5.2.2.3 Comparison with actual profiles

Figure 5.4 compares two typical profiles generated using SIMPROF to real profiles from our survey. The agreement is excellent, the main difference being that the simulated profiles extend slightly deeper than the real profiles. This is consistent with the fact that

the real profiles exclude low surface brightness isophotes that are poorly fitted by ellipses, and therefore do not always extend to 2σ above the sky background.

5.3 RESULTS OF MONTE CARLO SIMULATIONS

In order to investigate the feasibility of accurately determining host morphologies at high redshift, and to better determine the uncertainty in the results from our survey, we use SIMPROF in the following manner. We pick a particular value for the host redshift, core magnitude, filter, exposure time, seeing sigma, pixel scale, and telescope aperture, and simulate ~20 BL Lacs and PSF stars with these values, addding to each of these random and systematic uncertainties distributed according the discussion in the previous section. We then apply our analysis technique to these simulated hosts, fitting elliptical and disc models to the profiles in order to see how well we can recover the true host galaxy parameters (i.e. the characteristic surface brightness and characteristic radius of the host; these are Σ_e and r_e for ellipticals, and Σ_s and r_s for discs). By fitting enough simulated hosts (the individual "realizations" of our statistical Monte Carlo experiment), we can build up an accurate distribution of the parameter values that are returned by our analysis techniques, given the errors inherent in the observations and data reduction. The spread in the parameter values returned by this procedure indicates the typical uncertainty in our parameter estimates. In addition, for each realization we apply an F-test to the models, in order to determine how often the sources of error discussed earlier lead to mistaken or uncertain host identifications.

Sets of simulations were made for a number of host redshifts between 0.3 and 0.7. Simulated exposure times of 1500s, 3600s, and 7200s were undertaken, under seeing

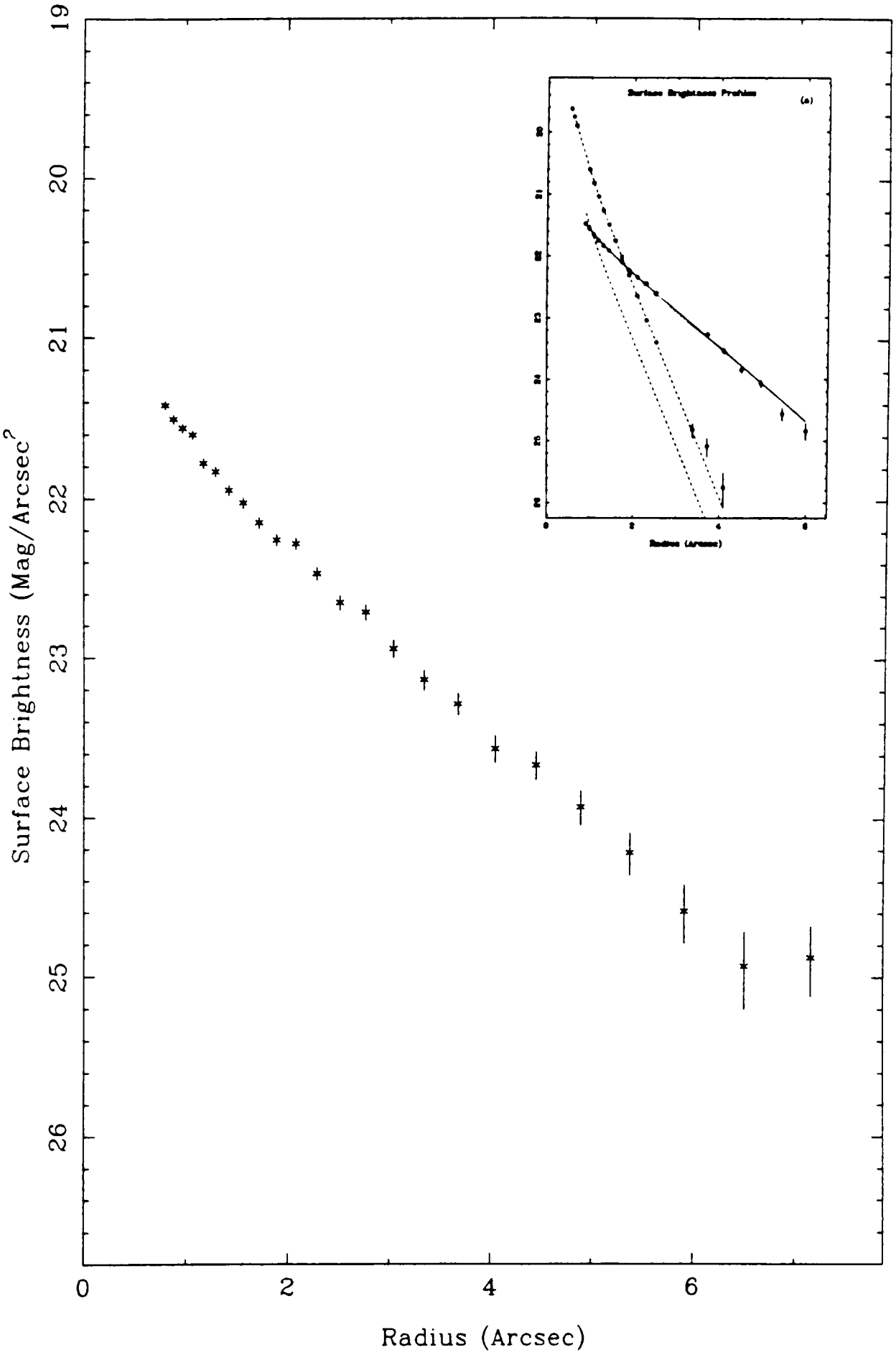

FIGURE 5.4a Simulated (top) and actual (bottom) 1500s R band WHT profiles of PKS1413 (disc host, z=0.26).

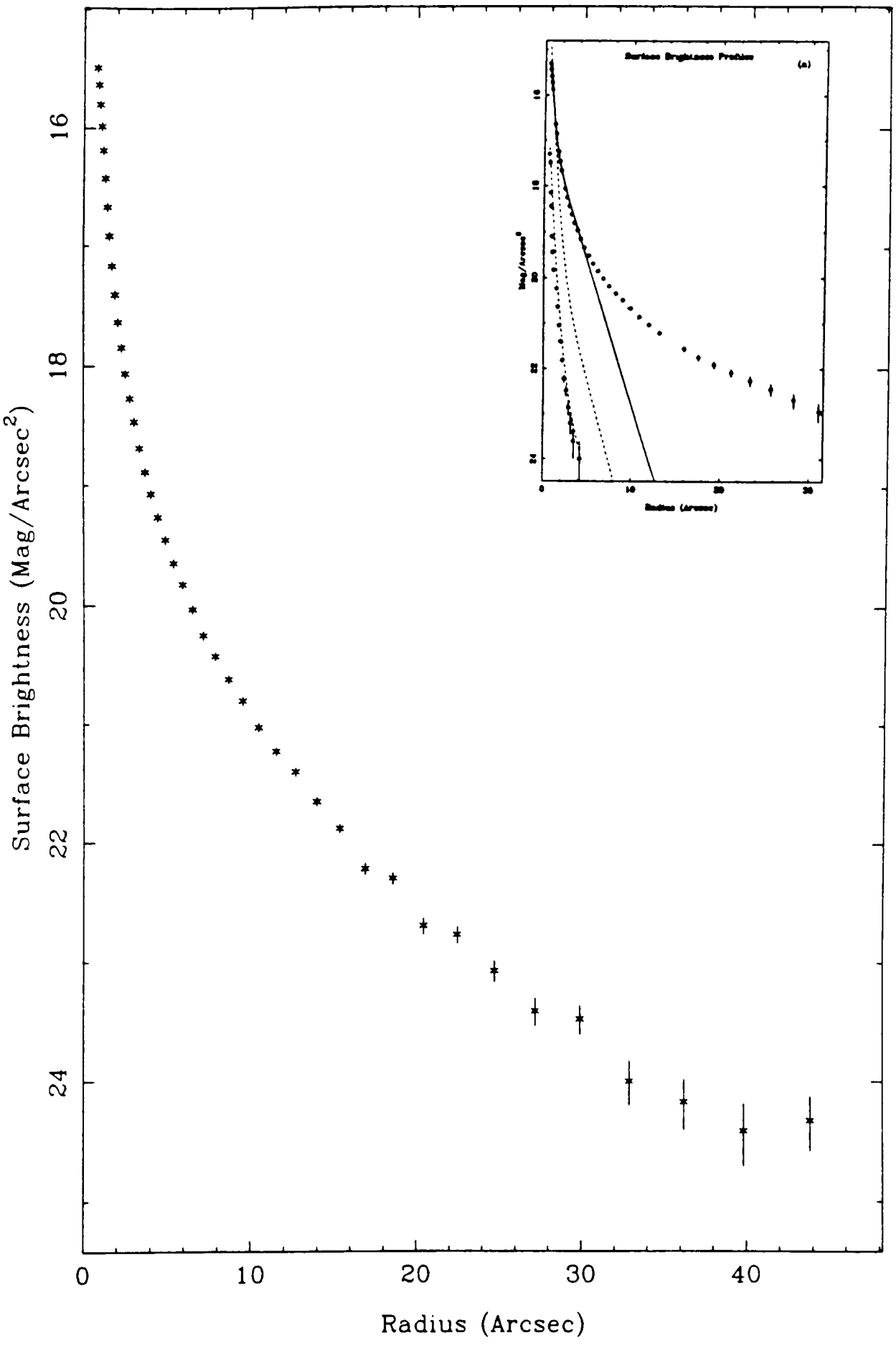

FIGURE 5.4b Simulated (top) and actual (bottom) 100s R band WHT profiles of MKN501 (elliptical host, z=0.034).

conditions varying between 0.5" FWHM (similar to the very best seeing presently attainable with CFHT and the NTT) and 1.2" FWHM (typical at many reasonably good sites throughout the world). We note parenthetically that although the best optical telescopes presently experience better seeing than the best infrared telescopes, this has more to do with telescope siting and optical quality than with observing wavelength, since at infrared wavelengths the size of the atmospheric isoplantic patch increases, leading to a slight improvement in overall seeing. We performed simulations using telescope apertures of 4m and 8m, in both R and J bands. Most simulations were of elliptical hosts in order to determine if these could be misidentified as discs (since the most surprising aspect of our survey was our discovery of disc hosts, and it is therefore important to test for misidentifications of this kind).

The results of the simulations are shown in Figure 5.6, and are summarized in Table 5.4. As outlined in the figure captions, the upper figures record the spread in host galaxy parameters returned by the realizations (Σ_e vs r_e in the upper-left hand part of the figures for the elliptical models, and Σ_s vs r_s for disc models in the upper-right hand section). The lower histograms record the corresponding apparent magnitudes of the hosts as determined by the fitting routines. Note that these apparent magnitudes are obtained by integrating the host galaxy parameters out to infinity, typically resulting in host galaxy magnitudes for ellipticals that are about half a magnitude brighter than obtained by integrating to the 26 mag/arcsecond^2 isophote (the other convention often adopted when citing magnitudes obtained from model fits; quoted disc host magnitudes are similar with either convention, due to the steeper exponential profile assumed).

The immediately striking result from Figure 5.6 is the obvious correlation between the surface brightnesses and radii returned by the model fits. The random and systematic errors we add to each simulated BL Lac prior to fitting it does not result in a "shotgun" distribution in the parameters recovered from the model fits. Instead, the distribution of

realizations in (r, Σ) space are scattered along a narrow strip. This actually turns out to be a fairly well-known result (Kormendy 1982) in the context of fitting models to normal galaxies, and is a consequence of the magnitude of the underlying host acting as a fixed constraint on the model fits. For example, the total signal, S, from a deVaucouleurs law galaxy with parameters r_e and Σ_e (integrated to infinite radius) is:

$$S = 7.22\pi {r_e}^2 \Sigma_e \qquad [5.9]$$

If we require this signal to be constant, and work in magnitude units, this implies that Σ_e and r_e are related according to:

$$\Sigma(r_e, m_{total}) = m_{total} + 2.5\log(7.22\pi) + 5\log(r) \qquad [5.10].$$

(This function is shown in Figure 5.5, for a 17th magnitude elliptical, along with the corresponding simulation for an elliptical at a redshift of 0.3). In other words, if we increase the effective radius of the model, we must also increase the surface brightness (decreasing the flux) at the effective radius if we wish to preserve the magnitude of the galaxy.

Figure 5.6 also records the number of correct, incorrect, and indeterminate host galaxy morphology classifications. All classifications were based upon 2σ F-test confidence levels.

The simulations suggest that a "typical" 4m observation of a BL Lac at redshift $z = 0.3$ (1.2" seeing, elliptical host, 1500s R-band exposure, 16th magnitude core, 16th magnitude star used to determine the PSF) correctly classifies the host morphology 60% of the time and is unable to differentiate an elliptical from a disc 40% of the time. This is in good agreement with the results from our survey. No misclassification of elliptical hosts as discs occurred for this set of simulation parameters (further strengthening our

Table 5.4 Summary of Simulations

z [1]	Core [2]	Seeing [3]	Band [4]	A [5]	t [6]	N [7]	HOST [8]	√ [9]	X [10]	? [11]
0.3	16.0	1.2"	R	4m	1500	20	Ell.	60%	0%	40%
0.3	16.0	1.2"	R	4m	1500	20	Disc	56%	0%	44%
0.3	16.0	0.6"	R	4m	1500	17	Ell.	82%	0%	18%
0.3	20	1.0"	R	4m	1500	31	Ell.	90%	0%	10%
0.3	20	1.0"	R	4m	1500	31	Disc	87%	0%	13%
0.5	17.0	0.5"	R	4m	7200	16	Ell.	56%	0%	44%
0.5	16.0	0.5"	J	4m	7200	14	Ell.	57%	0%	43%
0.7	17.0	0.5"	R	8m	7200	29	Ell.	0%	0%	100%
0.7	16	0.5"	J	8m	7200	14	Ell.	50%	7%	43%

Note: Column [1] is the redshift, Column [2] is the core magnitude, Column [3] is the seeing FWHM in arcseconds, Column [4] is the observing band, Column [5] is the telescope aperture, Column [6] is the exposure time in seconds, Column [7] is the number of realizations in the simulation, Column [8] is the host morphology simulated, and Columns [9], [10], and [11] are the percentage of correct, incorrect, and indeterminate identifications, respectively.

classification of PKS1413+135 as a disc). Decreasing the seeing FWHM to 1.0" and increasing the magnitude of the central core to $m_R = 20$ increased the percentage of successful classification to over 90%, while excellent 0.6" seeing resulted in successful classification of over 80% of hosts even with a bright central core. At this redshift, which

Table 5.5 Parameter Uncertainties From Simulations

z [1]	Core [2]	Seeing [3]	Band [4]	A [5]	t [6]	Host [7]	Δr_e [8]	$\Delta\Sigma_e$ [9]	Δr_s [10]	$\Delta\Sigma_s$ [11]
0.3	16.0	1.2"	R	4m	1500	ELL.	0.4	0.5	0.15	0.3
0.3	16.0	1.2"	R	4m	1500	DISC	1.5	0.7	0.2	0.3
0.3	16.0	0.6"	R	4m	1500	ELL.	0.3	0.5	0.6	0.8
0.3	20	1.0"	R	4m	1500	ELL.	0.4	0.6	0.1	0.2
0.3	20	1.0"	R	4m	1500	DISC	2.0	0.5	0.15	0.15
0.3	16.0	1.2"	R	4m	1500	ELL.	0.4	0.5	0.15	0.3
0.5	17.0	0.5"	R	4m	7200	ELL.	0.3	0.5	0.2	0.3
0.5	16.0	0.5"	J	4m	7200	ELL.	0.3	0.5	0.2	0.3
0.7	17.0	0.5"	R	8m	7200	ELL.	0.2	0.3	0.3	0.6
0.7	16.0	0.5"	J	8m	7200	ELL.	0.3	0.5	0.2	0.3

Note: Column [1] is the redshift, Column [2] is the core magnitude, Column [3] is the seeing FWHM in arcseconds, Column [4] is the observing band, Column [5] is the telescope aperture, Column [6] is the exposure time in seconds. Column [7] is the morphology of the simulated host. The remaining columns are the approximate full widths of the 90% confidence intervals for the fit parameters (note that these values are poorly defined for the simulation runs with comparatively few realizations). Uncertainties in the radii ([8] and [10]) are in arcseconds, and uncertainties in surface brightnesses ([9] and [11]) are in mag/arcsec^2.

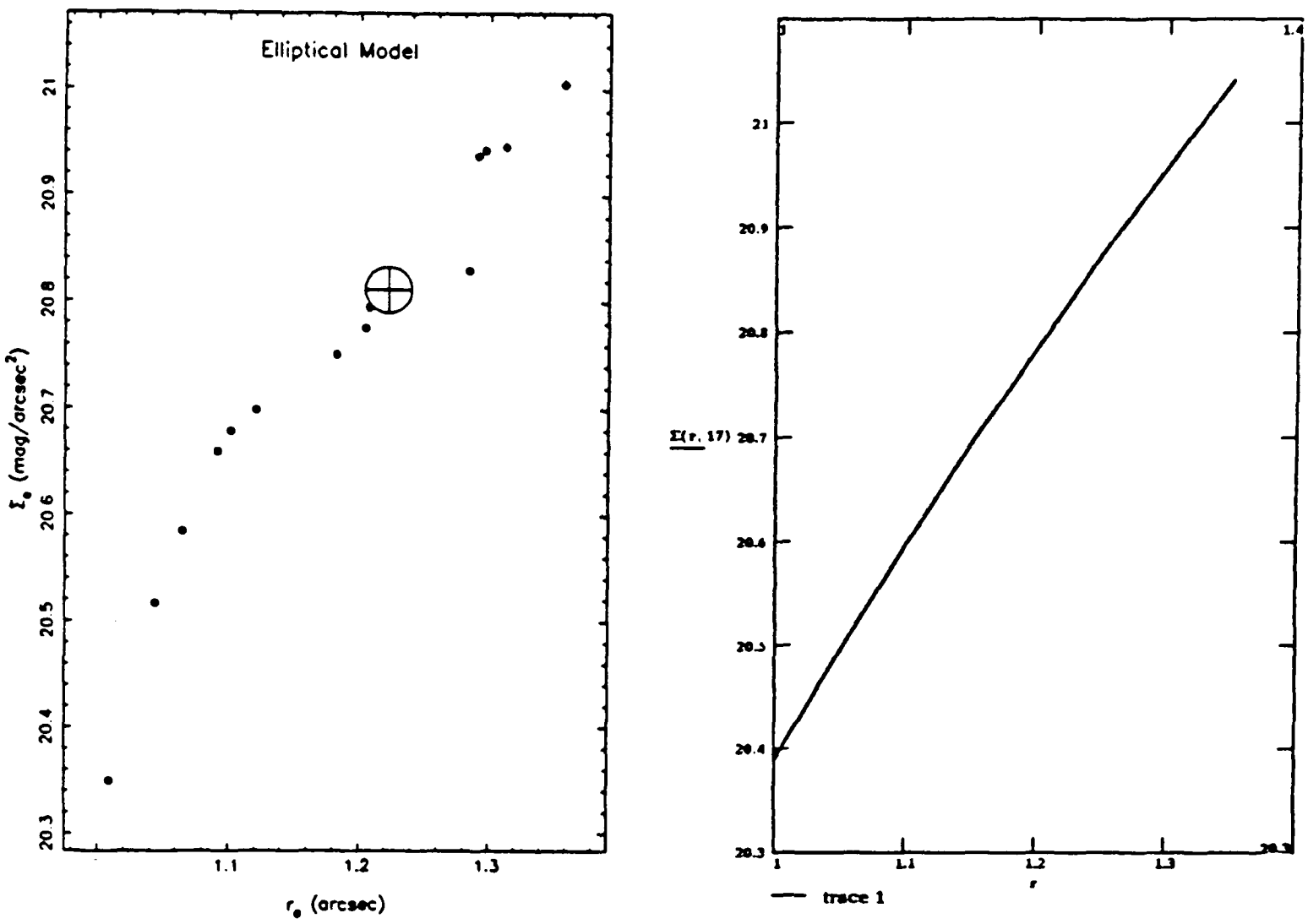

FIGURE 5.5 Graph of the parameters resulting from 14 simulations of an elliptical galaxy at z=0.3 (left), and the iso-magnitude curve for a 17th magnitude elliptical (right).

is approximately the redshift limit of our survey, the simulations suggest that there is at least a ±15% uncertainty in the effective radii returned by model fits, along with ± 0.3 magnitude/arcsec^2 uncertainty in surface brightness at these radii. We therefore expect that the uncertainties in the parameters for the more distant hosts in our survey ($z > 0.2$) are of this order. Detailed parameter uncertainties for all the simulations are given in Table 5.5.

The simulations also suggest that the highest redshifts at which present ground based 4m telescopes can hope to classify hosts at is near z=0.5, with long (7200s) exposures and superb (0.5") seeing. At z=0.5, R band and J band imaging give similar results, successfully classifying around 50% of hosts with fairly bright (R=16; J=15.4, corresponding to $\alpha = 0$) cores. The uncertainty in the measured effective radius at this redshift is around 20%, and uncertainty in the characteristic surface brightness is around 0.5 mag.

Morphological classification at redshifts higher than 0.5 would seem to be the exclusive domain the next generation of 8m telescopes, and it is here that infrared capability comes into its own. At $z = 0.7$, a 7200s R-band exposure with an 8m telescope and 0.5" FWHM seeing fails to classify a single simulated host, while the corresponding J-band exposure correctly classifies around 60% of the hosts, with the remainder still being classed as "unknown" rather than misclassified. The next generation of large telescopes therefore seem set to classify large numbers of previously inaccessible BL Lacs. For example, for $\Omega_o = 1$, the volume of space out to a redshift z is given by:

$$V(z) = \frac{8}{3}\left(\frac{c}{H_o}\right)^3\left[1 - \frac{1}{\sqrt{1+z}}\right] \qquad [5.11]$$

so the accessible volume of space is increased by a factor of 7 when we increase our redshift limit from $z = 0.3$ out to $z = 0.7$.

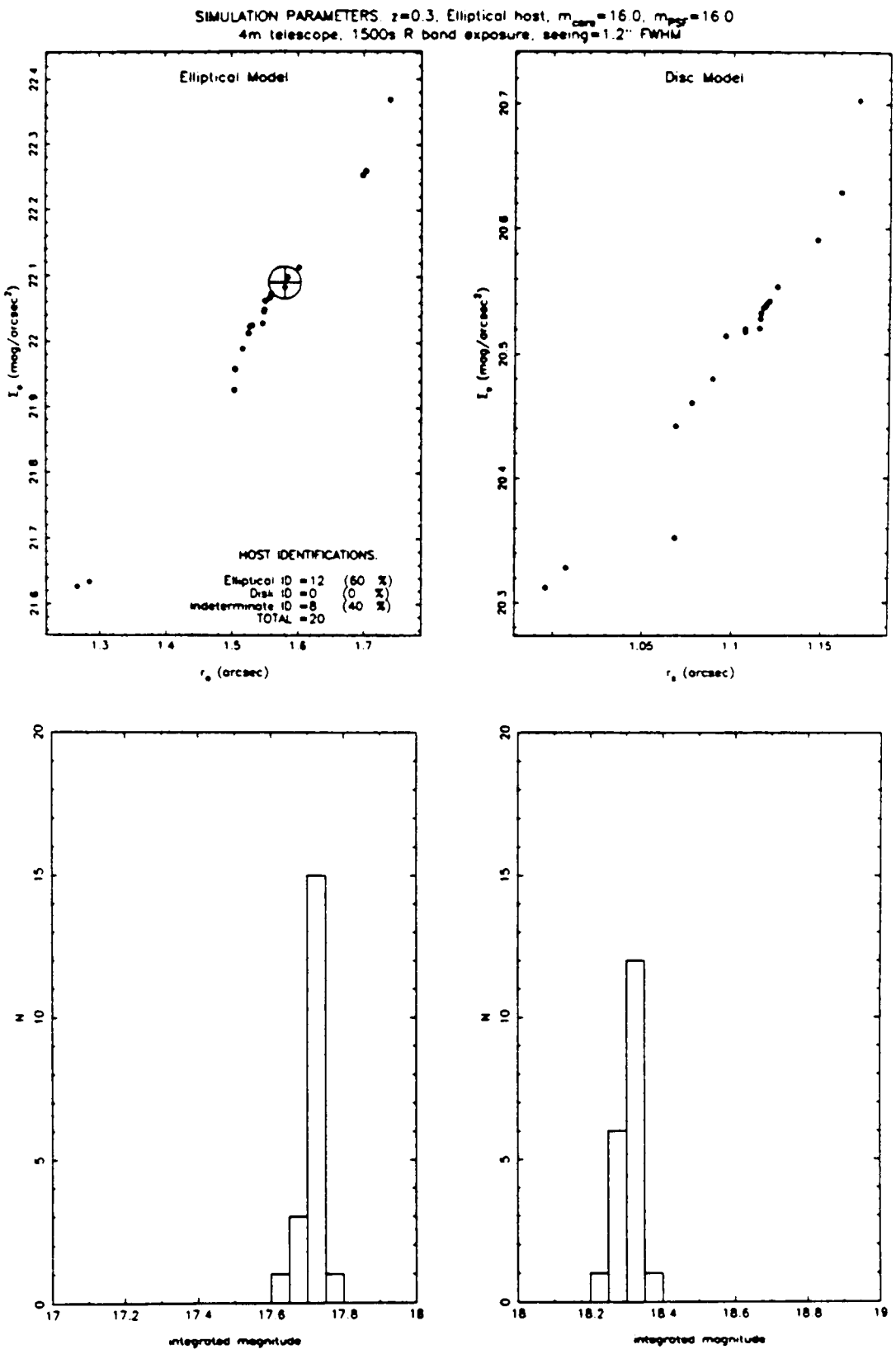

Figure 5.6 Simulations of BL Lac objects. The upper left hand box records results for individual simulations of elliptical hosts; the upper right hand box is the corresponding graph for disc hosts. The large circle with the crosshair corresponds to the parameters of the model being simulated (usually an elliptical). Results of F-test identifications are inset into the upper-left hand box. The lower boxes record the apparent magnitudes of the hosts corresponding to the fitted parameters, integrated out to infinity.

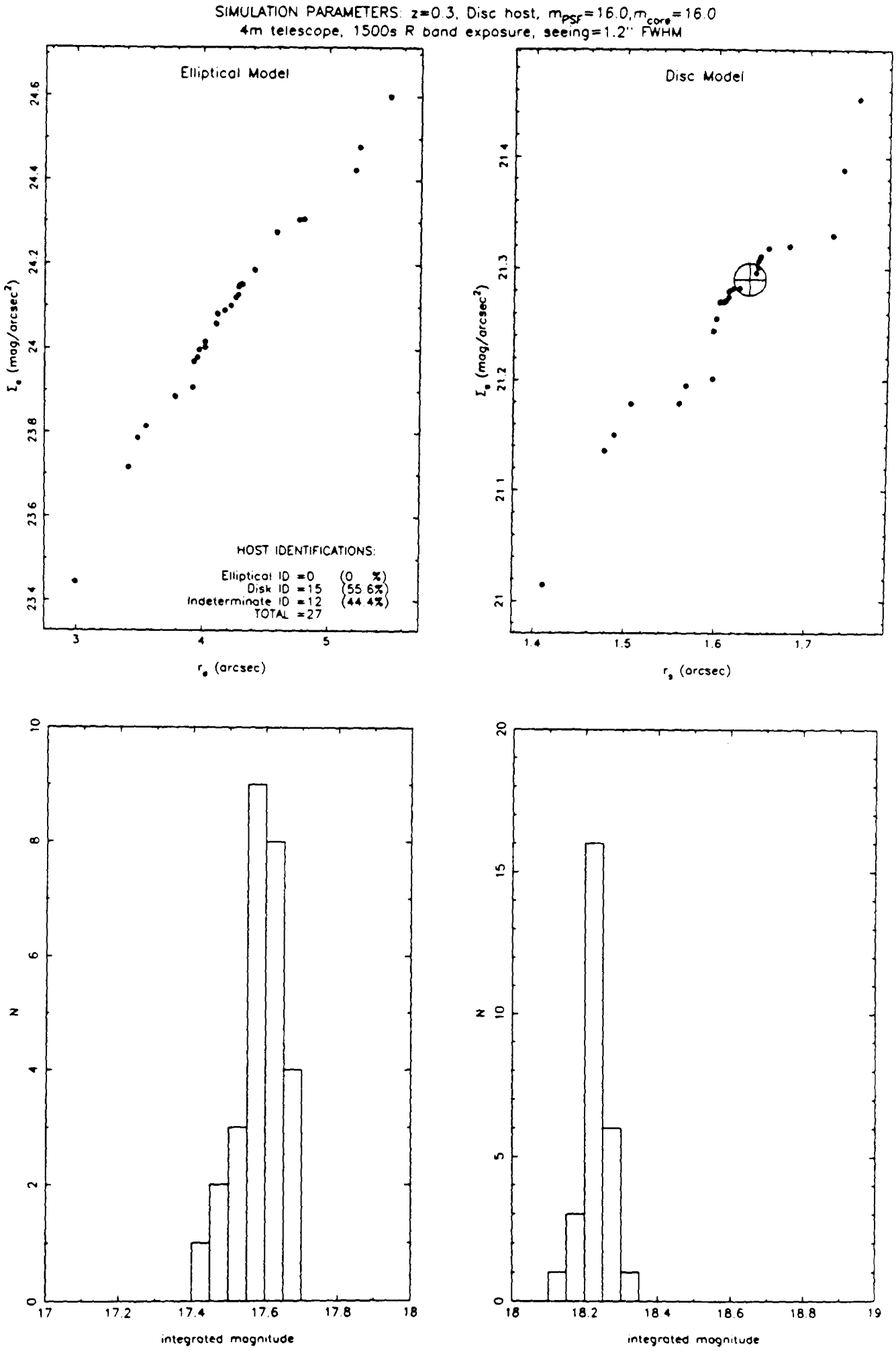

Figure 5.6 (continued)

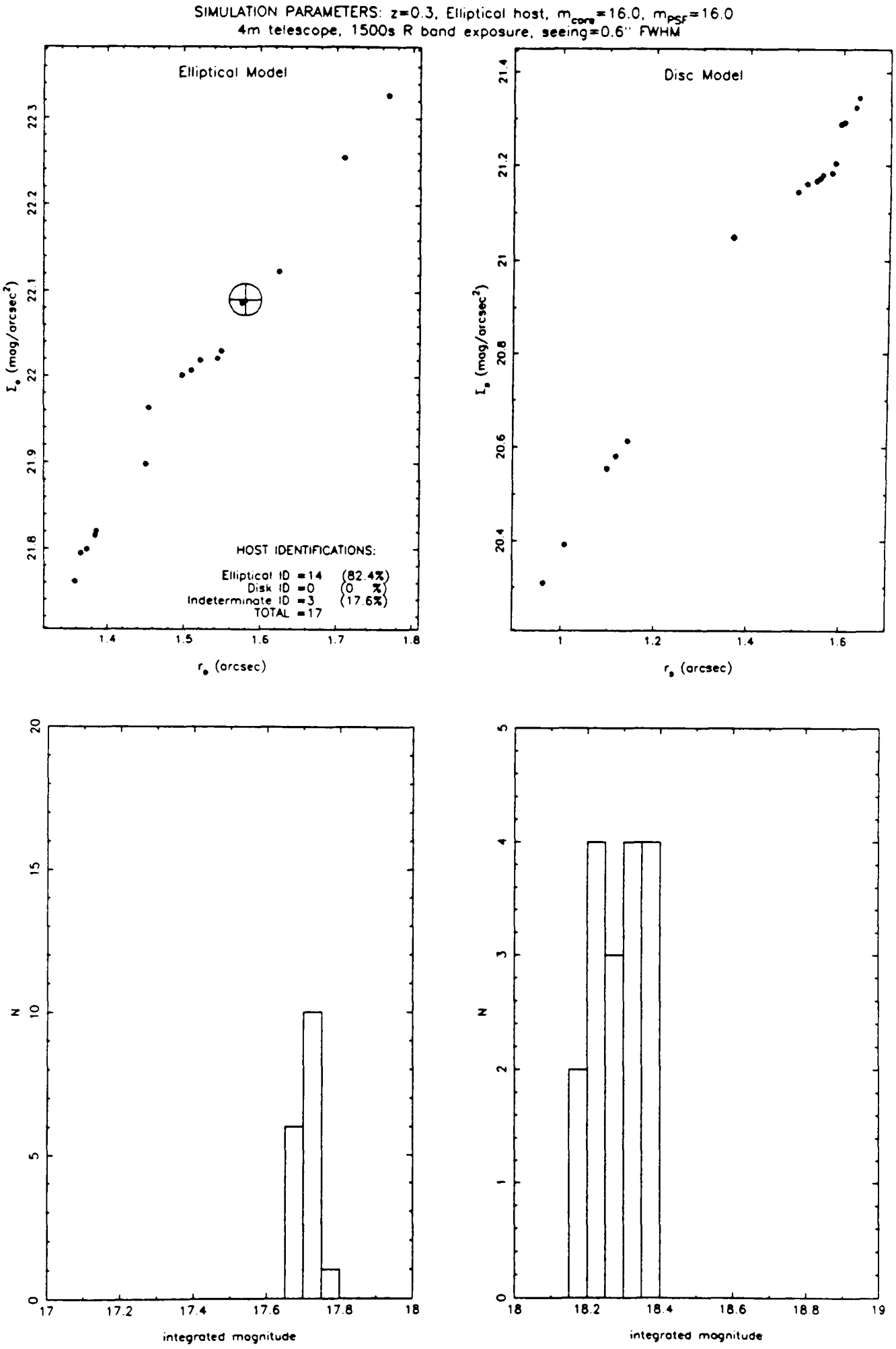

Figure 5.6 (continued)

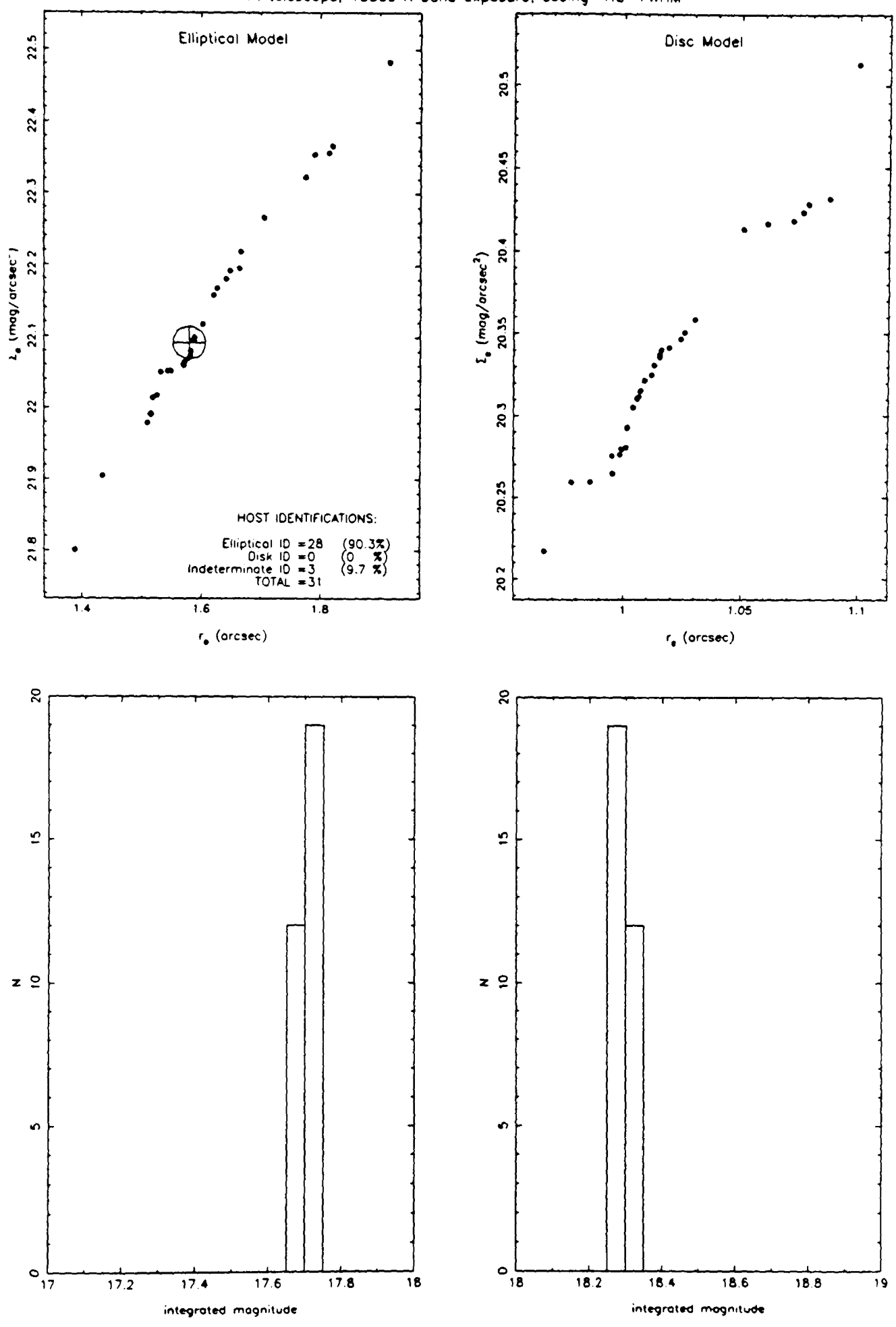

Figure 5.6 (continued)

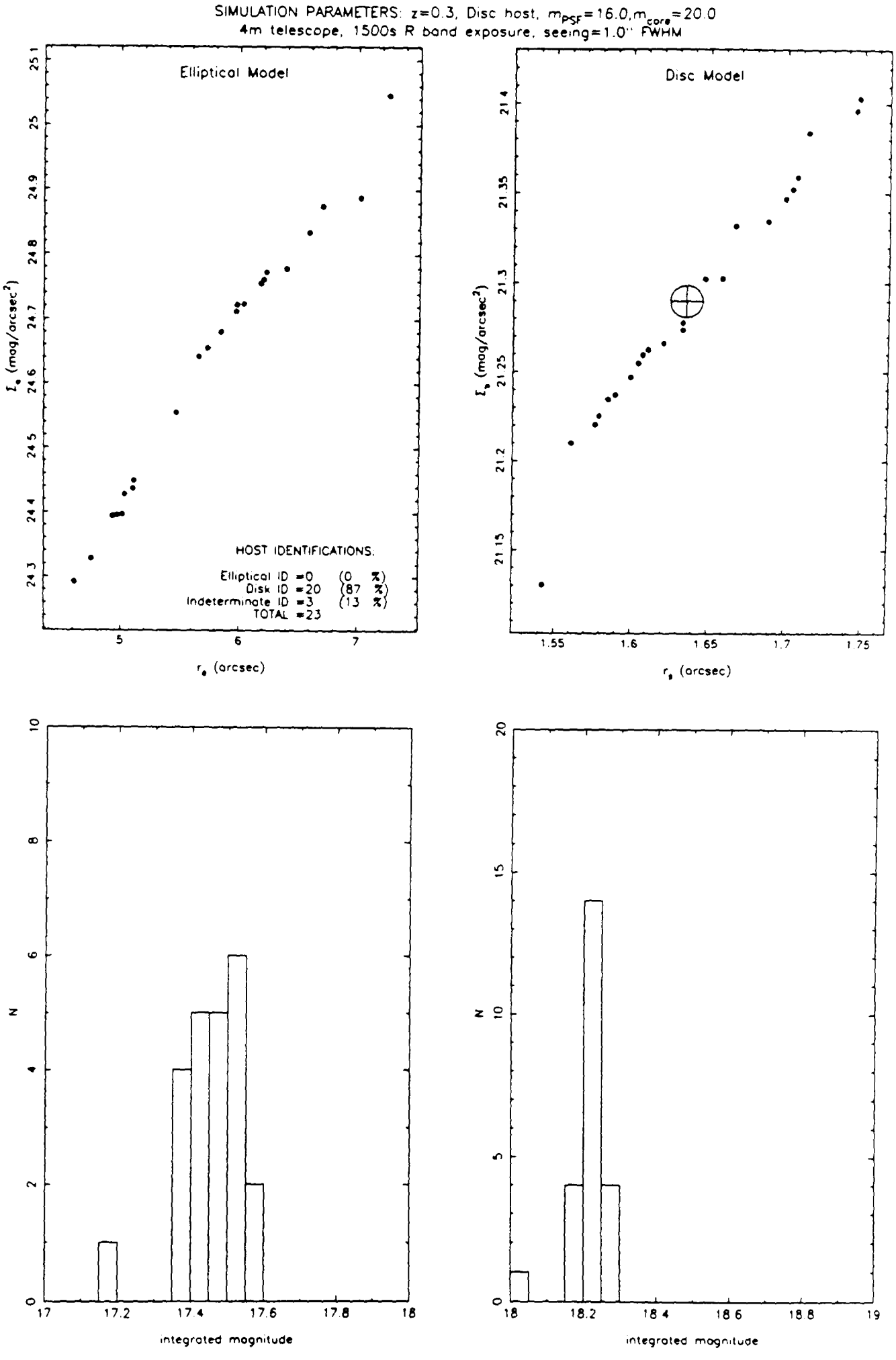

Figure 5.6 (continued)

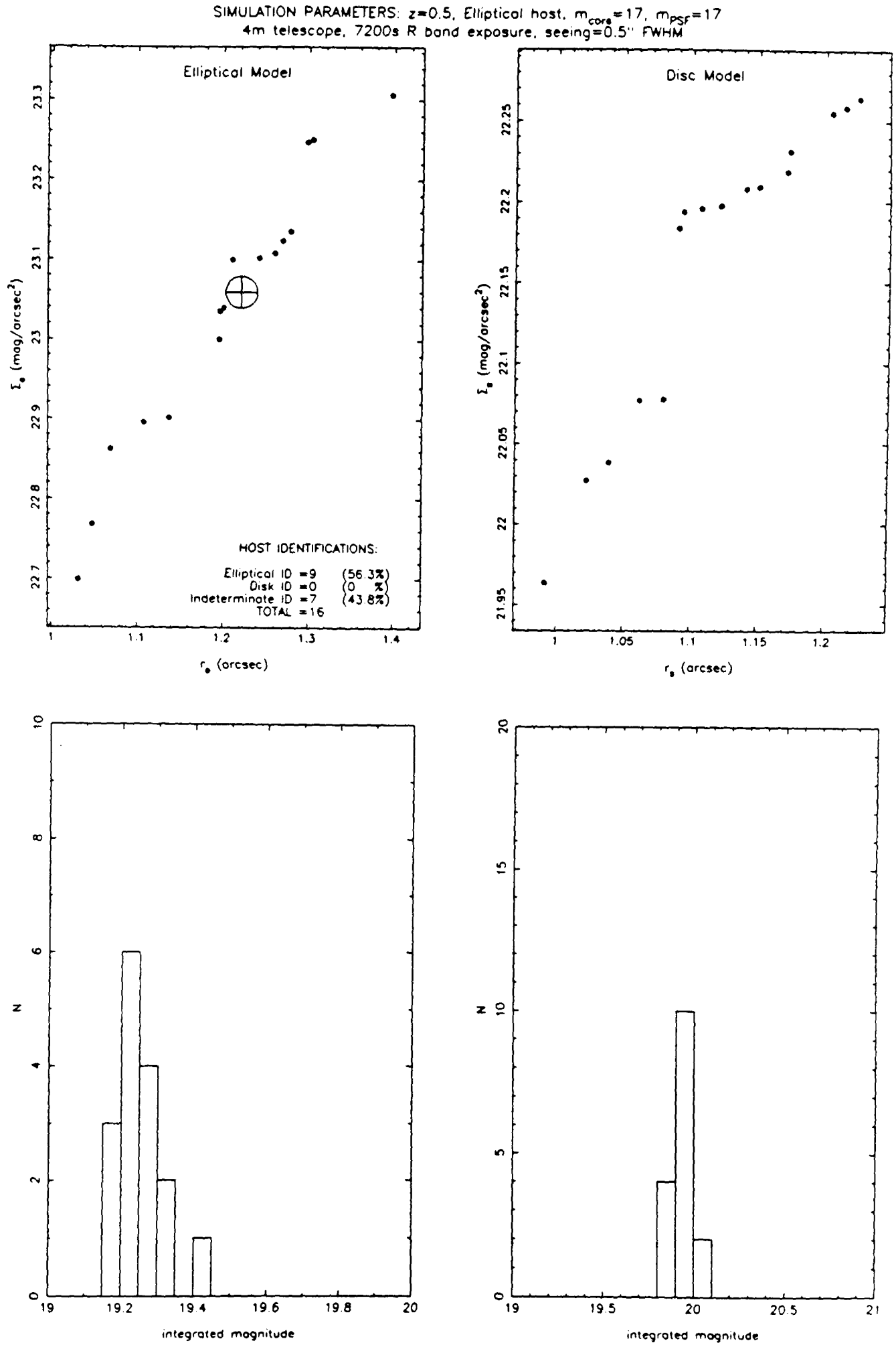

Figure 5.6 (continued)

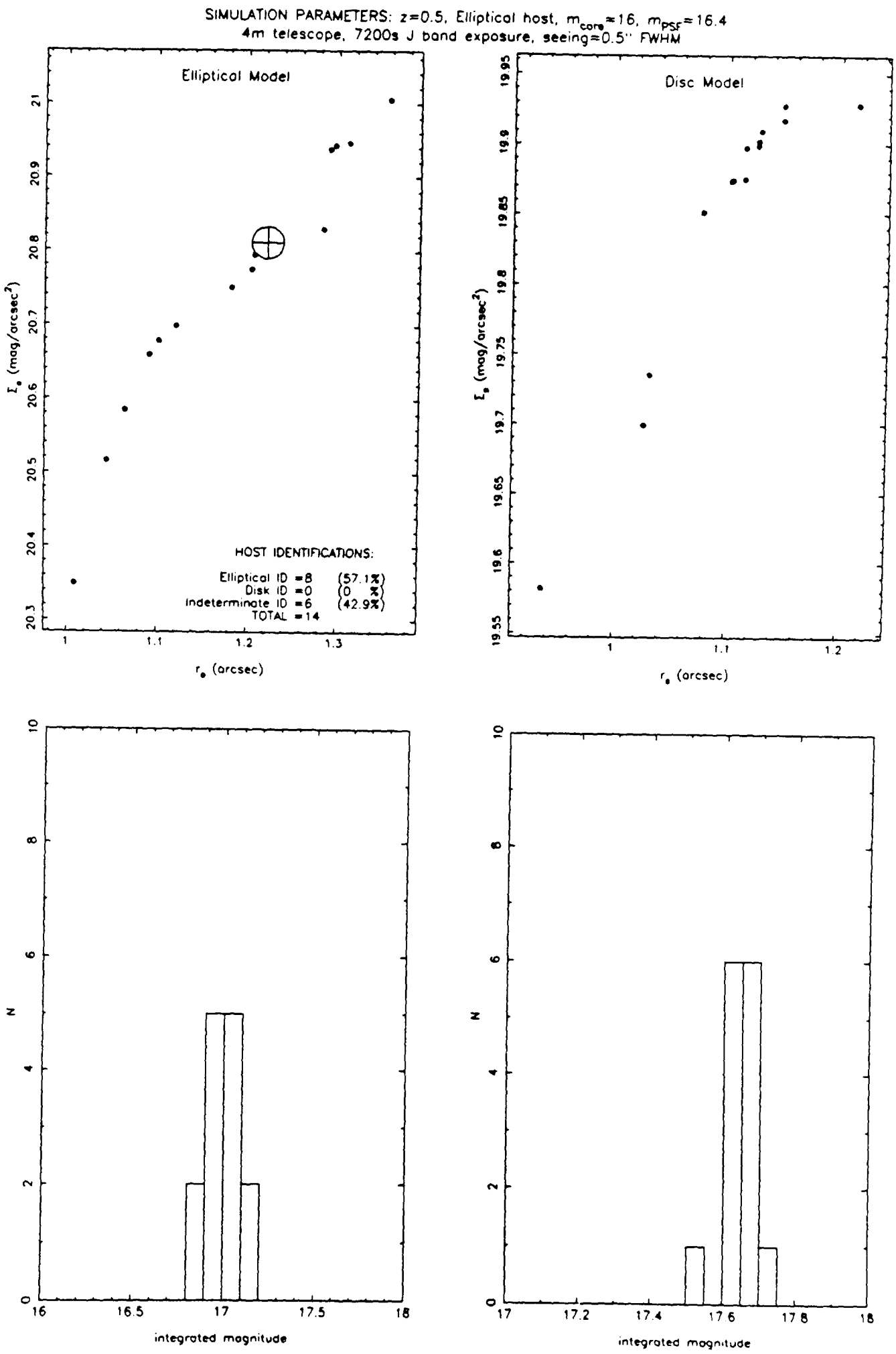

Figure 5.6 (continued)

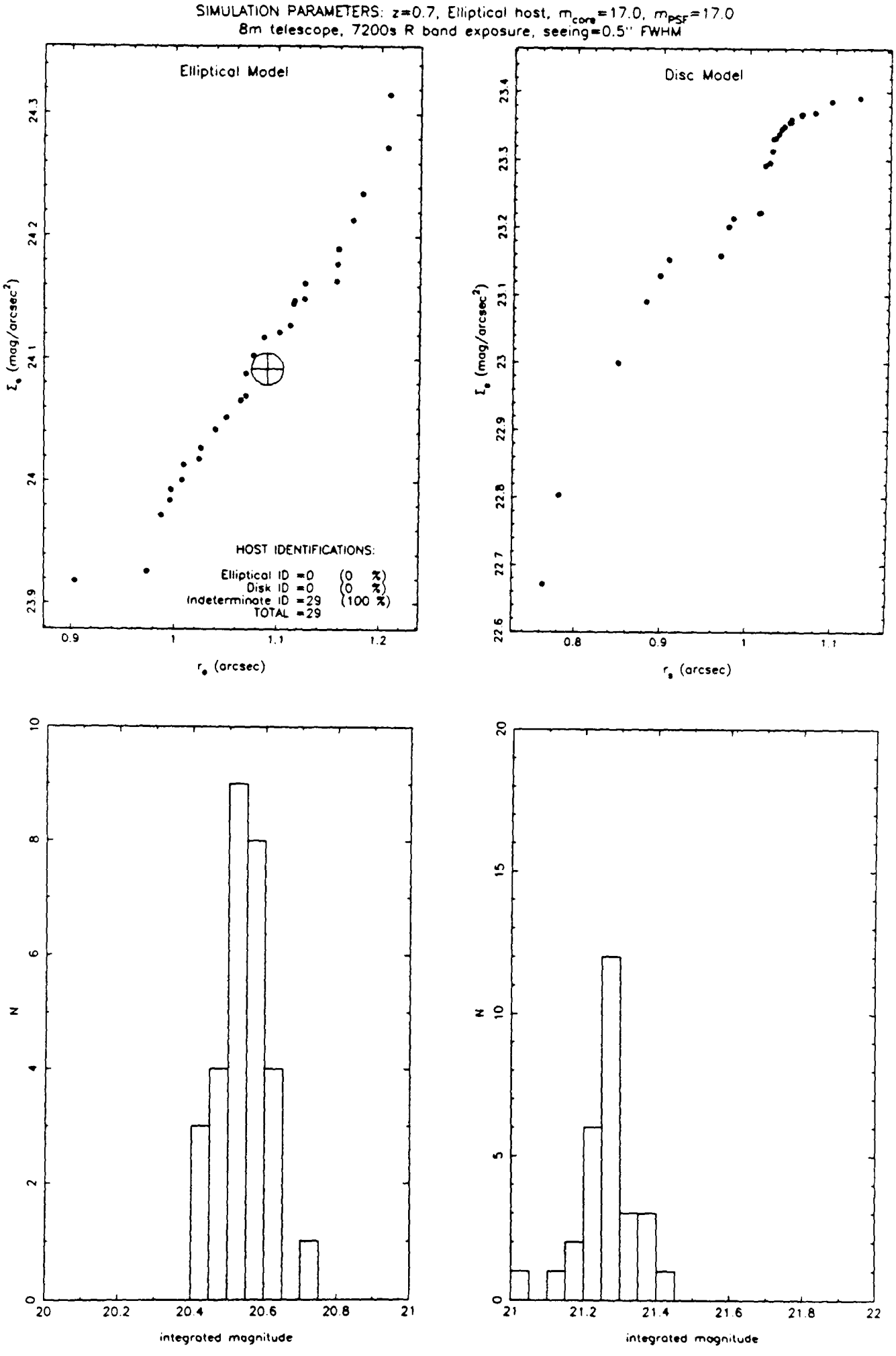

Figure 5.6 (continued)

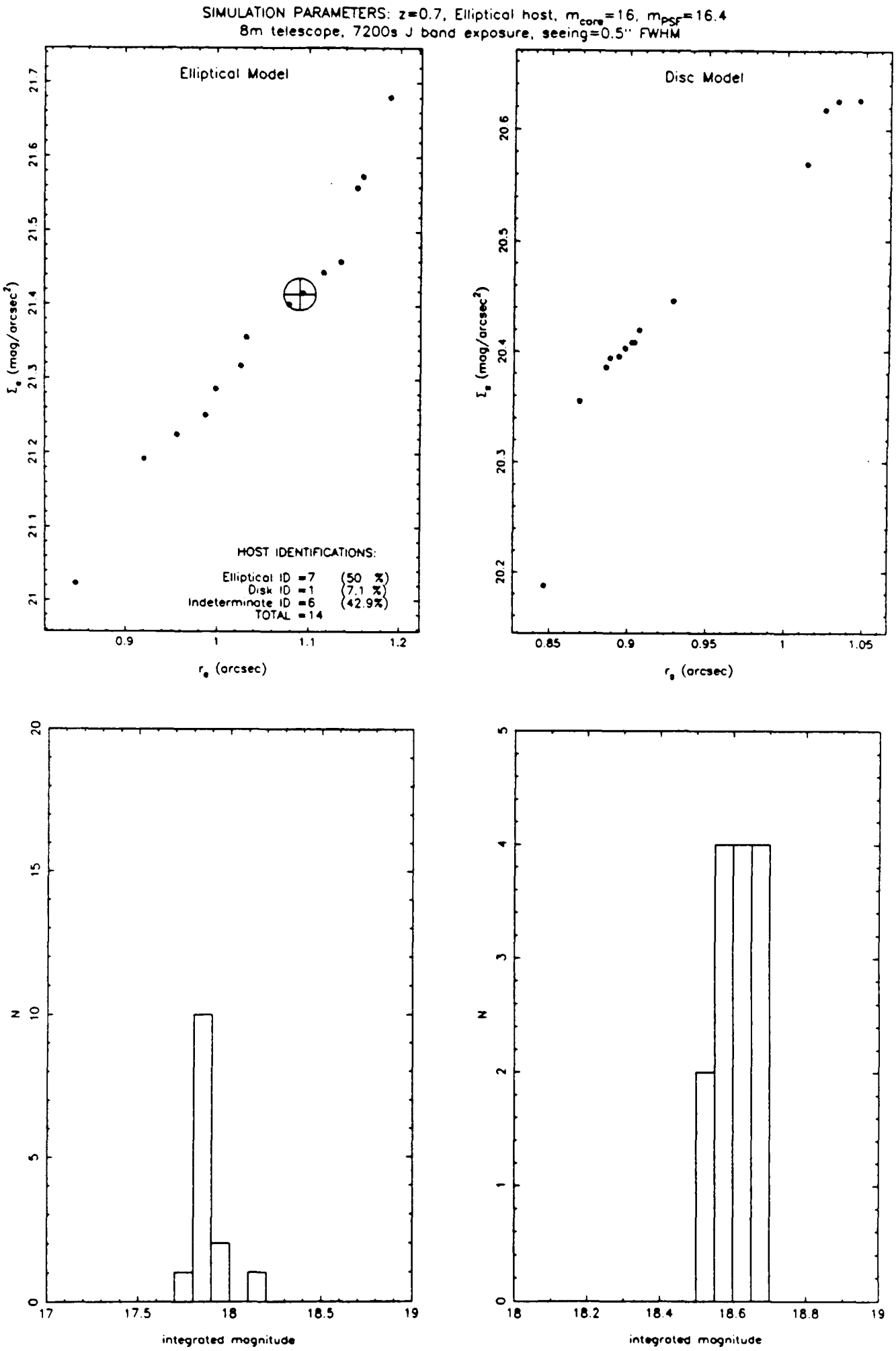

Figure 5.6 (continued)

5.4 SUMMARY

We have demonstrated that that Monte Carlo simulations are a powerful tool for quantifying the uncertainty in parameters obtained from BL Lac model fits. We have also shown that surveys of BL Lac hosts conducted with 4m telescopes with seeing conditions and exposure times comparable to those in our survey can expect to classify BL Lac hosts with reasonable completeness up to redshifts near $z = 0.3$. With superb seeing, very long exposures, and bright PSF reference stars, 4m telescopes can achieve 50% completeness out to redshifts near $z = 0.5$. With similarly long exposures and equally superb seeing, 8m telescopes operating in the infrared can expect to achieve similar results at redshifts as high as $z = 0.7$.

Chapter Six

CONCLUSIONS

What have we learned about BL Lacs as a result of the work described in the thesis? From the survey work presented in Chapter 3, we have found that:

(1) Some BL Lac objects reside in disc host galaxies.

(2) The absolute magnitudes of BL Lac hosts are consistent with those of bright FR I radio galaxies.

(3) BL Lac cores are centred on their underlying hosts.

The third statement is quite a strong one, since this conclusion is essentially incompatible with lensing models for BL Lacs. On the other hand, (1), (2), and (3) are broadly compatible with the "unified scheme" of Browne [1983], provided that at least a small percentage of FR I radio galaxies are discs.

From the modelling described in the later chapters of this thesis, we can add to these conclusions the following:

(4) Under observing conditions similar to those experienced by us during the course of this work, similar surveys can expect to reliably classify hosts out to redshifts between $z = 0.2$ and $z = 0.3$ (depending on the core brightness). Near these limiting redshifts, we expect typical errors of around $\pm 15\%$ on on the characteristic radii returned by fitting procedures, and typical errors of around ± 0.3 mag/arcsec^2 on the characteristic surface brightnesses of the host models.

(5) The next generation of large telescopes, with active/adaptive optics and enhanced infrared capability, seem set to increase by an order of magnitude the number of AGN with observable host galaxies. The prospects for future imaging studies look bright.

Worthwhile avenues of investigation have been opened up by the work presented in this thesis, and much interesting work awaits to be done. For example, what is the relationship between OVV/HPQ quasars and BL Lacs? Chapter 1 of this thesis suggested that there are substantive differences between these categories of AGN, but how are these related to the host galaxy? Do BL Lacs reside in clusters, and if so what role does the clustering environment play in triggering the active nucleus? We hope to collect enough background calibration fields to allow us to learn more about this is in the near future. What are the differences between X-ray-selected and radio-selected BL Lacs? Is there any direct evidence for the existence of disc FR I radio galaxies? Are the disc BL Lacs S0s? What are the colours of the underlying hosts?

I hope this thesis has helped us to understand a little more about the nature of BL Lacs and their underlying host galaxies, but there is clearly a long way to go before we finally penetrate the mystery surrounding these objects.

REFERENCES

Abraham, R. G., M^{c}Hardy, I. M., & Crawford, C. S., 1991. *Mon. Not. R. astr. Soc.*, In press.

Angel, J. P. R., & Stockman, H. S., 1980. *Ann. Rev. Astron. Astrophys*, **18**, 321.

Arp, H. C., 1975. *PASP*, **87**, 545

Barthel, P. D., 1989. *Astrophys. J.*, **336**, 606.

Baxter, D. A., Disney, M. J., & Phillips, S., 1978. *Mon. Not. R. astr. Soc.* , **228**, 313.

Beichmann, C. A., Neugebauer, G., Soifer, B. T., Wooten, H. A., Roellig, T., & Harvey, P. M., 1981. *Nature*, **293**, 711.

Bendinelli, O., Parmeggiani, G., Zavatti, F., and Djorgovski, S., 1990. *Astron.J*, **99**, 3..

van den Bergh, S., 1960. *Astrophys. J.*, **131**, 215.

van den Bergh, S., 1972. *Astrophys. J. Lett.*, **171**, L31.

van den Bergh, S., 1976. *Astrophys. J.*, **206**, 883.

Bevington, P. R., 1969. *Data Reduction and Error Analysis for the Physical Sciences*, McGraw-Hill Book Co., New York.

Blandford, R. D., 1991. In *Active Galactic Nuclei*, eds. Blandford, R., Netzer, H., & Woltjer, L. Springer-Verlag.

Blandford, R. D. & Rees, M. J., 1978. *Pittsburgh conference on BL Lac objects*, ed. Wolfe. University of Pittsburgh Press.

Blandford, R. D. & Koñigl, A., 1979. *Astrophys. J.*, **232**, 34.

Bregman, J. N., Lebofsky, M. J., Aller, M. F., Riecke, G. H., Aller, H. D., Hodge, P. E., Glassgold, A. E. & Huggins, P. J. 1981. *Nature*, **293**, 714.

van Breugel, W., 1982. *Astron. Astrophys.*, **110**, 225.

Browne, I. W. A., 1983. *Mon. Not. R. astr. Soc.*, **204**, 23P.

Browne, I. W. A., 1989. In *BL Lac Objects*, eds Maraschi, L., Maccacaro, T. & Ulrich, M.-H. Springer-Verlag.

Bruzual, G. A. & Kron 1980. *Astrophys. J.*, **241**, 25.

Bruzual, G. A., 1983. *Astrophys. J. Suppl.*, **53**, 497.

Burbidge, G. & Hewitt, A., 1987. *Astron. J.*, **92**(1), 1.

Burstein, D., and Heiles, C., 1978. *Astrophys. J.*, **225**, 40.

Cawson, M., 1983. PhD Thesis, Cambridge University.

Colla, G., Fanti, C., Fanti, R., Gioia, I., Lari, C., Lequeux, J., Lucas, R., & Ulrich, M.-H. 1975. *Astron. Astrophys.*, **38**, 209.

Colla, G., Fanti, C., Fanti, R., Gioia, I., Lari, C., Lequeux, J., Lucas, R., & Ulrich, M.-H. 1975. *Astron. Astrophys. Suppl.*, **20**, 1.

Condon, J. J., Hicks, P. D. & Jauncey, D. L. 1977 *Astron.J*, **82**, 692.

Eckart, A., Witzel, A., Biermann, P., Johnston, S. R., Schalinski, C., & Kuhr, H., 1987. *Astron. Astrophys. Suppl.*, **67**, 121.

Falomo, R., 1989. In *BL Lac Objects*, eds Maraschi, L., Maccacaro, T. & Ulrich, M.-H. Springer-Verlag.

Falomo, R., 1991. *Astron. J.*, in press.

Fanti, R., Gioia, I., Lari, C., Lequex, J., & Lucas, R., 1973. *Astron. Astrophys.*, **24**, 69.

Filippenko, A. V., Djorgovski, S., Spinrad, H., & Sargent, W. L. W., 1986. *Astron.J*, **95**, 307.

Forman, W., Jones, C., Cominsky, L., Julien, P., Murray, S., Peters, G., Tananbaum, H., and Giacconi, R., 1978, *Ap. J. Suppl.*, **38**, 357.

Fraix-Burnet, D., Golombek, D., and Macchetto, F. D., 1991. *Astron.J*, **102**, 562.

Freeman, K. C., 1970. *Astrophys. J.*, **160**, 811.

Gavazzi & Trincheri, 1989. *Astrophys. J.*, **342**, 718.

Gear, W. K., 1991. *Nature*, **349**, 676.

Ghisselini, G., Maraschi, L., Tanzi, E., & Treves, A., 1986. *Astrophys. J.*, **310**, 317.

Halpern, J. P., Impey, C. D., Bothun, G. D., Tapia, S., Skillman, E. D., Wilson, A. S., & Meurs, E. J. A., 1986. *Astrophys. J.*, **302**, 711.

Hammer, F., 1990. In *New Windows to the Universe*, eds. Sanchez, F. & Vasquez, M. Cambridge University Press.

Hoessel, J. G., and Schneider, D. P., 1985. *Astron. J.*, **90**(9), 1648.

Hoskins, D. G., Murdoch, H. S., Hazard, C. & Jauncey, D. L., 1972. *Aust. J. Phys.*, **25**, 559.

Hoyle, F., Burbidge, G. R., & Sargent, W. L. W., 1966. *Nature*, **209**, 751.

Hughes, P. A., Aller, H. D., & Aller, M. F., 1985. *Astrophys. J.*, **298**, 301.

Hughes. P. A., & Miller, L., 1991. In *Beams and Jets in Astrophysics*, ed. Hughes, P. A. Cambridge University Press.

Hutchings, J. B., Crampton, D., & Campbell, B., 1984. *Astrophys. J.*, **280**, 41.

Hutchings, J. B. & Crampton, D., 1990. *Astron. J.*, **99**(1), 37.

Hutchings, J. B., 1987. *Astrophys. J.*, **320**, 122.

Hutchings, J. B., Janson, T., & Neff, S., 1989. *Astrophys. J.*, **342**, 660.

Hutchings, J. B., and McClure, D., 1990. *PASP*, **102**, 48.

Impey, C., & Neugebauer, G. 1988. *Astrophys. J.*, **333**, 666.

Impey, C., 1989. In *BL Lac Objects*, eds Maraschi, L., Maccacaro, T. & Ulrich, M.-H. Springer-Verlag.

Jannuzi, B. T. & Green, R. F., 1989. In *BL Lac Objects*, eds Maraschi, L., Maccacaro, T. & Ulrich, M.-H. Springer-Verlag.

Jedrzejewski, R. I., 1987. *Mon. Not. R. astr. Soc.*, **226**, 747.

Jenkins, C. J., 1981. *Mon. Not. R. astr. Soc.* , **196**, 987.

Kinman, T. D. 1978. *Pittsburgh conference on BL Lac objects*, ed. Wolfe. University of Pittsburgh Press.

Koo, D. C., 1985. *Astron.J*, **90**, 419.

Kormendy, J., 1982. *Morphology and Dynamics of Galaxies*, 12th Advanced Course of the Swiss Society of Astronomy and Astrophysics (Saas-Fe Course 1982).

Kühr, H., & Schmidt, G. D., 1990. *Astron. J.*, **99**(1), 1.

Lilly, S. J. & Prestage, R. M., 1987. *Mon. Not. R. astr. Soc.* , **225**, 531.

Maccacaro, T., Gioia, I. M., Schild, R., Wolter, A., Morris, S., & Stocke, J.,1989. In *BL Lac Objects*, eds Maraschi, L., Maccacaro, T., & Ulrich, M.-H. Springer Verlag.

Madejski, G. M., & Schwartz, D. A. 1989. In *BL Lac Objects*, eds Maraschi, L., Maccacaro, T. & Ulrich, M.-H. Springer-Verlag.

Malkan, M. A., Margon, B., and Chanan, G. A., 1984. *Astrophys. J.*, **280**, 66.

Maraschi, L., Ghissellini, G., Tanzi, E. G., & Treves, A., 1986. *Astrophys. J.*, **310**, 325.

Marscher, A. P. & Gear, W. K. 1985., *Astrophys. J.*, **298**, 114.

Marscher, A., 1991. In: *Variability of Active Galactic Nuclei*, eds. Miller, R. H., & Witta, P. Cambridge University Press.

McCaughrean, M. J. & McClean, I. S., 1987. In *Infrared Astronomy with Arrays*, eds. Wynn-Williams, C. G. & Becklin, E. E. Published by the University of Hawaii, Institute for Astronomy, Honolulu.

McHardy, I.M., Marscher, A. P., Gear, W. K., Muxlow, T. M., Lehto, H. J., & Abraham, R. G. 1990. *Mon. Not. R. astr. Soc.* , **246**, 305.

McHardy, I.M., 1990. In *Proceedings of the 23rd ESLAB Conference on Two Topics in X-ray Astronomy.*

McHardy, I. M., Abraham, R. G., Crawford, C. S., Ulrich, M-H., Mock, P. C., & VanderSpeck, R. K., 1991. *Mon. Not. R. astr. Soc.* , in the press.

Mihalas, D., & Binney, J., 1981. *Galactic Astronomy*, Freeman & Co., New York.

Miller, J. S., French, H. B., & Howley, S. A., 1978. *Pittsburgh conference on BL Lac objects*, ed. Wolfe. University of Pittsburgh Press.

Miyaji, T., Wilson, A. S., & Peŕez-Fournon, I., 1991. *Astrophysical Journal.* In press.

Moffat, A. F. J., 1969. *Astron. Astrophys.*, **3**, 455.

Moles, M., del Olmo, A., Masegosa, J, and Perea, J. D., 1988. *Astron. Astrophys.*, **197**, 1.

Morris, S. L, Stocke, J. T., Gioia, I. M. Schild, R. E., Wolter, A., Maccacaro, T., Della Ceca, R., 1991. *Astrophys. J.*, In the press.

Muxlow, T. & Garrington, S., 1991. In *Beams and Jets in Astrophysics*, ed. Hughes, P. A. Cambridge University Press.

Narayan, R. & Schneider, P., 1990. *Mon. Not. R. astr. Soc.*, **243**, 192.

Nottale, L., 1986. *Astron. Astrophys.*, **157**, 383.

Orr, M. J. L. & Browne, I. W. A., 1982. *Mon. Not. R. astr. Soc.* , **200**, 1067.

Owen, F. N., and Laing, R., A., 1989. *Mon. Not. R. astr. Soc.*, **238**, 357.

Owen, F. N., O'Dea, C. P., and Keel, W. C., 1990. *Astrophys. J.*, **352**, 44.

Ostriker, J. P., & Vietri, M., 1985. *Nature*, **318**, 446.

Ostriker, J. P., & Vietri, M., 1990. *Nature*, **344**, 45.

Padovani, P. & Urry, C. M., 1990. *Astrophys. J.*, **356**, 75.

Padovani, P. & Urry, C. M., 1991. *Astrophys. J.*, **368**, 373.

Pence, 1976. *Astrophys. J.*, **203**, 39.

Person, Frogel & Aaronson, 1979. *Astrophys. J. Suppl.*, **39**, 61.

Pickles, A. J., 1985. *Astrophys. J.*, **296**, 340.

Polatidis, A. G., 1989. Thesis, University of Manchester.

Prestage, R. M. & Peacock, J. A., 1988. *Mon. Not. R. astr. Soc.* , **230**, 131.

Riecke, G. H., Lebofsky, M. J. & Kinman, T. D., 1979. *Astrophys. J. Lett.*, **232**, L151.

Remillard, R. A., Tuohy, I. R., Brissenden, R. J. V., Buckley, D. A. H., Schwartz, D. A., Feigelson, E. D., and Tapia. S., 1989. *Astrophys. J.*, **345**, 140.

Sadler, E. M., Jenkins, C. R., and Kotanyi, C. G., 1989. *Mon. Not. R. astr. Soc.*, **240**, 591.

Schwartz, D. A., Brissenden, R. J. V., Tuohy, I., Fiegelson, E. D., Hetz, P. L., & Remillard, R. A., 1989. In *BL Lac Objects*, eds Maraschi, Maccacaro, & Ulrich. Springer Verlag.

Schweizer, F., 1979. *Astrophys. J.*, **233**, 23.

Smith, E. P., Heckman, T. M., Bothun, G. D., Romanishin, W, and Balick, B., 1986 *Astrophys. J.*, **306**, 64.

Stickel, M., Fried, J. W., & Kühr, H., 1988.*Astron.Astrophys.Lett.*, **206**,L30

Stickel, M., Fried, J. W., & Kühr, H., 1989. In *BL Lac Objects*, eds Maraschi, Maccacaro, & Ulrich. Springer Verlag.

Stickel, M., Padovani, P., Urry, C. M., Fried, J. W., and Kühr, H., 1991. In Press (to appear in the Astrophysical Journal).

Stocke, J. T., Morris, S. L., Gioia, I. M. Maccacaro, T., Schild, R., & Wolter, A., 1989. In *BL Lac Objects*, eds Maraschi, Maccacaro, & Ulrich. Springer Verlag.

Tagliaferri, G., Stella, L, Maraschi, L, Treves, A. & Morini, M., 1989. In *BL Lac Objects*, eds Maraschi, L., Maccacaro, T. & Ulrich, M.-H. Springer-Verlag.

Tennant, A. F. 1991. *The QDP/PLT User's Guide*, NASA.

Ulrich, M-H., 1989. In *BL Lac Objects*, eds Maraschi, L., Maccacaro, T. & Ulrich, M.-H. Springer Verlag.

Ulvestad, J. S. & Antonucci, R. R. J., 1986. *Astron.J*, **92**, 6.

Véron-Cetty, M.-P., & Woltjer, L. J., 1990. Astron.Astrophys. **236**, 69.

Wagner, S. J., 1991. In *Variability of Active Galaxies*, Proceedings of the Heidelberg Meeting, Springer-Verlag.

Wall, J. V., Pearson, T. J. & Longair, M. S., 1980. *Mon. Not. R. astr. Soc.* , **193**, 683..

Weedman, D. W., 1986. *Quasar Astronomy*, Cambridge Astrophysics Series, Cambridge

University Press.

Weinberg, S., 1972. *Gravitation and Cosmology.* Wiley and Sons, New York.

Westerlund, B. E., Wlerick, G., Garnier, R., 1982. *Astron. Astrophys.*, **105**, 284.

Wolter, A., Gioia, I. M., Maccacaro, T., Morris, S. L., and Stocke, J. T.,1991. *Astrophys. J.*, **369**, 314.

Woltjer, L. & Setti, G., 1982. In *Astrophysical Cosmology*, eds. Brück et al., Pont. Acad. Sci. Scripta Varia.

Woltjer, L., 1991. In *Active Galactic Nuclei*, eds. Blandford, R., Netzer, H., & Woltjer, L. Springer-Verlag.

Woolf, N. J., 1982. *Ann. Rev. Astron. Astrophys*, **20**, 367.

Worrall, D. M., 1989. In *BL Lac Objects*, eds Maraschi, L., Maccacaro, T. & Ulrich, M.-H. Springer-Verlag.

Zensus, J. A., 1989. In *BL Lac Objects*, eds Maraschi, L., Maccacaro, T. & Ulrich, M.-H. Springer-Verlag.

Zombeck, M., 1982. *Handbook of Space Astronomy and Astrophysics*, Cambridge University Press.

ACKNOWLEDGEMENTS

On the personal front, I'm convinced that writing a thesis is an essentially selfish enterprise, and I thank all my friends who have put up with me throughout the whole thing. Big thanks to fellow/former grad students Richard Payne, Susan Mallett, Dean Johnson, Jeremy Drake, John Woods, and everyone else for all the laughs. Big thanks also to Tony Lynas-Gray and Ivan Bishop for being generally stout coves with the computers and with the buying of rounds, to Harry Lehto for being uniquely Harry, and to Paul Callanan for being such an overall swell Irish dude, plus such a pal (ditto for Steve Maddox, except for he's not Irish). Special thanks to Will Saunders for being my polar-opposite on most things, yet a great guy and office-mate nonetheless, and to Chris Jeffrey for always being so cheerful.

On the professional front (and still on the personal front, since they're kind of also in the drinking-buddy category, but technically aren't really supposed to be, I guess), I thank Ian McHardy, Roger Davies, and Carolin Crawford. Ian is responsible for getting this project off the ground and keeping me on the straight and narrow as my supervisor, often by E-mail and expensive phone calls after he moved to Southampton. I'd be here forever if I thanked Ian for all that I owe him, so please just assume that I thank him for absolutely *everything*. I will single out the biggest thing, though, which is the enthusiasm and support that helped make working on this project such a lot of fun. Roger took over as supervisor after Ian left, and I have to say I was darn impressed by how the world's busiest man always found the time to read my manuscripts and thesis chapters, and how useful and productive I found our discussions to be. Carolin was a great collaborator on this project, was always in there with the science, corrected my perfect Canadian into perfect English ("...no no, one shouldn't use 'dude' in a technical paper"), brought really decent tapes along with her during observing runs, and figured out about the secret

elevators in "Super Mario Land" during the flight home after one of our meetings with Bill (the Bill Herschel Telescope). Many thanks also to George Efstathiou for letting me be a part of Oxford Astrophysics, and to Geoff Smith who I think accepted me here in the first place. Big thanks as well to F. W. Dalby and Jim Booth, who got me started in research back at UBC, and who are probably as surprised as I am as to where it all led.

On the mega-personal front, these acknowledgements are in serious danger of being rendered illegible by all the sappy emotional stuff that pours out of me whenever I think about how much I owe to my family (especially my Mom and Abuelita Adela, and my brother Al), and to my friend Colette Foran. My Mom helped to bankroll this little enterprise (oh yeah, thanks also to Her Majesty's Government for helping out with the ORS Award and other money), but mostly she helped out with love. How much I owe Colette can't really be stated here, mostly because there's so much of it, but also because this would end up sounding like an episode of *Dynasty*. I owe an enormous debt to Julie Weadock, but all I'm going to say here is that she's a tremendous woman and friend whose major character flaw is that she's crazy enough to want to hang around with me. Thank you so much, Julie, for teaching me about England, about you, and about myself.

Finally, to fully complete the sappy display that this has become, I'd like to dedicate this thesis to the memory of my grandfather, Alfonso Blanco Garcia. I don't know if Abs ever understood why I never wanted to be a lawyer or businessman, but he was still the best grandfather that anybody ever had, and I miss him a lot.